Innovations in ambient mass spectrometry imaging

INNOVATIONS IN AMBIENT MASS SPECTROMETRY IMAGING

FROM IONIZATION TO DETECTION

Pieter C. Kooijman

Cover and layout: P.C. Kooijman
Printed by: Ridderprint
ISBN: 978-94-6458-516-2

INNOVATIONS IN AMBIENT MASS SPECTROMETRY IMAGING

FROM IONIZATION TO DETECTION

PROEFSCHRIFT

ter verkrijging van de graad van doctor aan de Universiteit van Maastricht,
op gezag van de Rector Magnificus, Prof. dr. Pamela Habibović
volgens het besluit van het College van Decanen,
in het openbaar te verdedigen op dinsdag 13 september 2022 om 16.00 uur

door

Petrus Christian Kooijman
Geboren op 1 september 1989 te Woerden

Promotor
Prof. dr. R.M.A. Heeren

Copromotor
dr. S.R. Ellis (University of Wollongong, Australia)

Beoordelingscommissie
Prof. dr. M. Honing (voorzitter)
Prof. dr. M.E. Kooi
Prof. dr. J.A.W. Haring
Prof. dr. M.W.F. Nielen (Wageningen University & Research)
Dr. C.R. Anderton (Pacific Northwest National Laboratory, Richland, WA, US)

This work was performed in the M4I research program financially supported by the Dutch Province of Limburg as part of the "LINK program. The research received funding from the Netherlands Organisation for Scientific Research (NWO) in the framework of the Technology Area COAST of the Fund New Chemical Innovations as part of the PolyImage project.

Voor de wetenschappers die na mij komen

TABLE OF CONTENTS

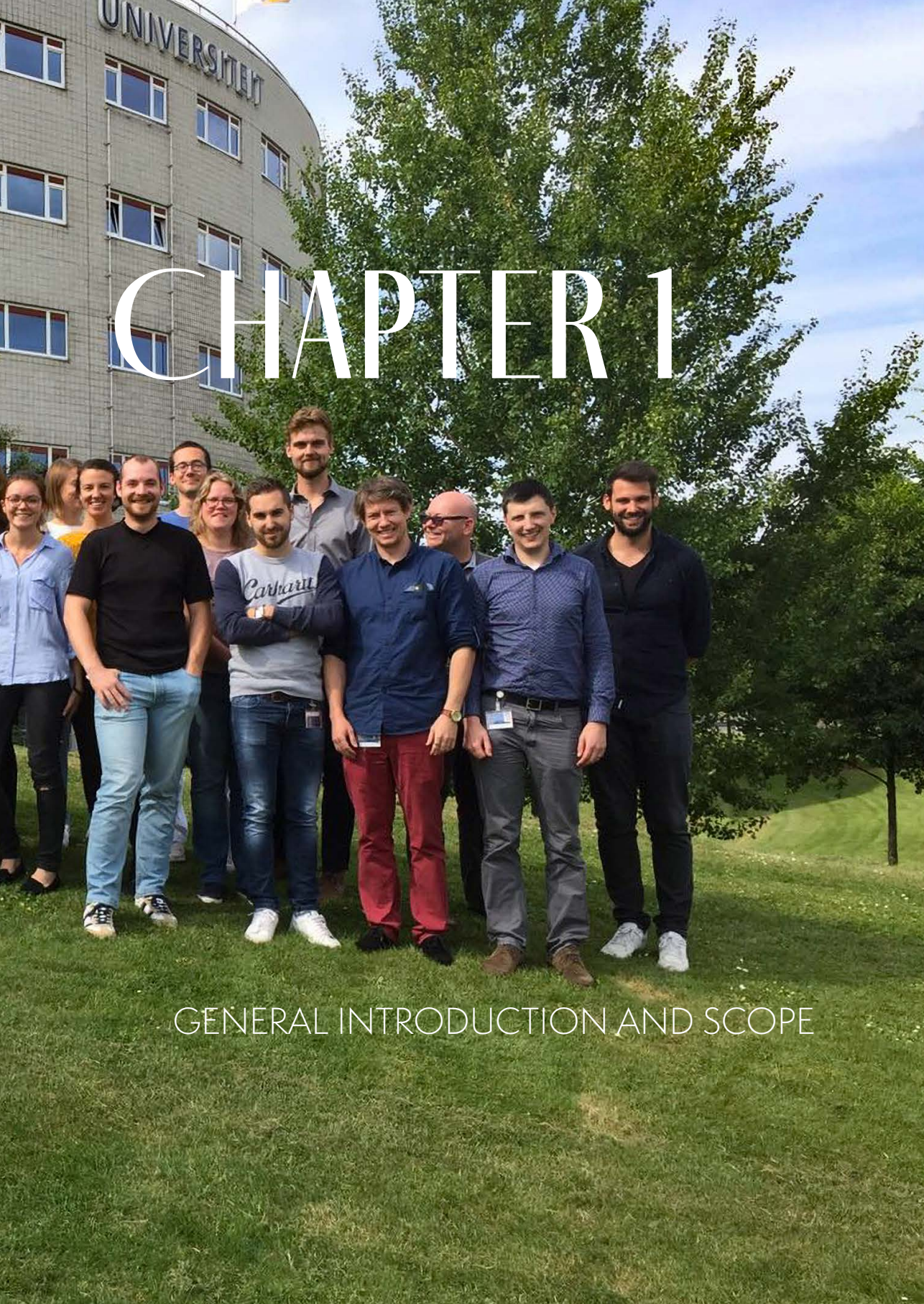

CHAPTER 1

GENERAL INTRODUCTION AND SCOPE

As a PhD candidate at Maastricht University and as part of the TA-COAST PolyImage research project, my research efforts have been directed towards technological and methodological breakthroughs for the analysis of complex sample surfaces under real native conditions. To this end, several ambient mass spectrometry imaging techniques have been explored and improved upon. The inherit benefits and challenges of ambient mass spectrometry techniques. In this chapter I will briefly introduce the field of ambient mass spectrometry imaging.

As shall be explained below, ambient mass spectrometry techniques have some specific inherent benefits and challenges. The aim for this thesis research was to introduce technological innovations to the field of ambient mass spectrometry imaging, with the intent to increase its relevance in the analytical industry. We have focussed on laser ablation electrospray ionization mass spectrometry imaging (LAESI-MSI) and biological samples of interest.

Chapter 1.1 provides a basic - i.e. laymen - introduction to key aspects of ambient mass spectrometry imaging required to understand the rest of this thesis. **Chapter 1.2** then presents the scope of scientific content of this thesis and illustrates how the different chapters fit together.

1.1. GENERAL INTRODUCTION TO AMBIENT MASS SPECTROMETRY IMAGING

The term "ambient mass spectrometry imaging" can be best explained by dissecting it into its components:

Ambient: *"of the surrounding area or environment"*. In connection to MSI this indicates that the extraction and ionization of the analyte molecules is performed under atmospheric pressure, in conditions like those in which the sample is commonly found.

Mass spectrometry: determination of the structure and/or quantity of molecules in a sample, based on measurements of mass-to-charge ratios. Mass spectrometry is done by: 1) bringing the molecules of interest to the gas phase, 2) placing a positive or negative charge on them (ionization), 3) sorting them by their mass-over-charge (m/z) ratio (separation) and 3) registration of the m/z value and signal intensity for each ion species (detection). This results in a mass spectrum: a plot of intensity versus m/z ratio.

Mass spectrometry imaging: sequential localized extraction of analyte molecules from a surface - via laser, ion beam, thermal or liquid extraction method - followed by or combined with ionization, and mass analysis. The resulting dataset can then be reconstructed into ion intensity images, wherein each extraction location is represented as a single pixel and the pixel colour represents the intensity of the ion at that location.

If these breakdowns are too cryptic for you, don't worry, I'll explain it here. The first step in any mass spectrometry technique is making sure that the molecules of interest are in the gas phase, i.e. unbound by other molecules. Molecules that are still bound to other molecules cannot be accurately "weighed". Getting molecules from the liquid or solid phase to the gas phase can be done in many ways and I'll highlight some now.

- Electrospray creates a fine mist in which all solvent molecules quickly evaporate, releasing the analyte molecules.
- Laser irradiation pumps energy into a small area to the point that the molecules there are "shaken" loose from their solid surface. The result could be described as an explosion, with molecules as flying debris.
- Ion beams collide with a solid surface where their kinetic energy knocks molecules and clusters of molecules loose.

Molecules in the gas phase cannot be analysed by mass spectrometry unless they contain a charge. Ionization is the art of placing one or more positive or negative charges on a molecule. This can be achieved by the addition or removal of an electron or an ionized species such as a proton or sodium atom. Once a molecule has a positive or negative charge it is susceptible to electric and magnetic fields and can therefore be manipulated and controlled.

The optimal method of ionization is greatly dependent on the chemical properties of your target molecule and therefore no "universal" ionization method exists. The most relevant ionization methods for this thesis are atmospheric pressure chemical ionization (APCI), electrospray ionization (ESI), matrix-assisted laser desorption/ionization (MALDI) and secondary ion mass spectrometry (SIMS) (the latter two are explained later in this chapter). In APCI the molecules are already in the gas phase (via various ways) and are brought in contact with unstable, highly energetic ions. If it is energetically favourable to transfer the charge of these ions to the analyte molecules ionization will occur. This is performed close to the mass spectrometer inlet, to make sure that analyte ions are efficiently captured in the mass spectrometer upon ionization. ESI creates a fine mist from a solution containing the analyte molecules and some additives. By careful combination of nebulizing gas, temperature and an electric field between the solution emitter and mass spectrometer a mist is created in which the solvent evaporates quickly, bringing the analyte molecules in close contact with charged particles. Again, if it is energetically favourable, analyte molecules become charged (i.e., become ions), while entering the gas phase. ESI is generally more sensitive than APCI, especially for polar analytes. As biological molecules are often polar, ESI is the most widely used ionization method in mass spectrometry.

Ionization occurs in front of (or just inside) the mass spectrometer inlet, which introduces the ions to the mass spectrometer vacuum. This vacuum is essential for all of mass spectrometry. Many types of mass spectrometers exist today, with widely

varying separation principles. Each of these separation principles has its benefits and drawbacks, but all have in common that separation and detection occurs under (high) vacuum. This is a prerequisite, for all mass spectrometers rely on moving ions during separation. Under atmospheric pressure the probability of collisions between the ions and stationary gas molecules would be too great, resulting in loss of sensitivity and mass resolving power. As a rule of thumb there is a relation between the distance an ion travels during separation and the separation quality (also referred to as "mass resolution"). Therefore, high resolution mass spectrometers require ultra-high vacuum. This is one of the reasons why high-resolution mass spectrometers are not the standard yet: extremely high vacuum requires expensive components.

Allow me to briefly introduce one of the most widely used mass spectrometer types (TOF) and elaborate a bit on two types of high-resolution mass spectrometers (FT-ICR and Orbitrap) that we used for experiments described in later chapters.

Time-of-flight (TOF) mass spectrometers are some of the most widely used, and easiest to explain, mass spectrometer types. The ions are accelerated into a high vacuum tube (commonly 1-2 meters long) simultaneously, as a tightly packed group (see Figure 1.1). An electric field gradient (suitable for negative or positive ions) is asserted between the introduction zone and the end of the "acceleration zone". Influenced by this electric field the ions accelerate, with their final velocity determined by their mass-to-charge ratio. When each ion reaches the end of the acceleration zone it maintains its velocity along the field free region and eventually hits the detector at the end of the tube. Each ion impacting the detector triggers a cascade of electrical charges, which is recorded by the detector electronics. The time that it takes an ion to move across the flight path to the detector is directly related to the mass-to-charge ratio of that ion. Properly calibrated, a TOF instrument performs extremely fast (in the order of microseconds) and quite accurate mass measurements.

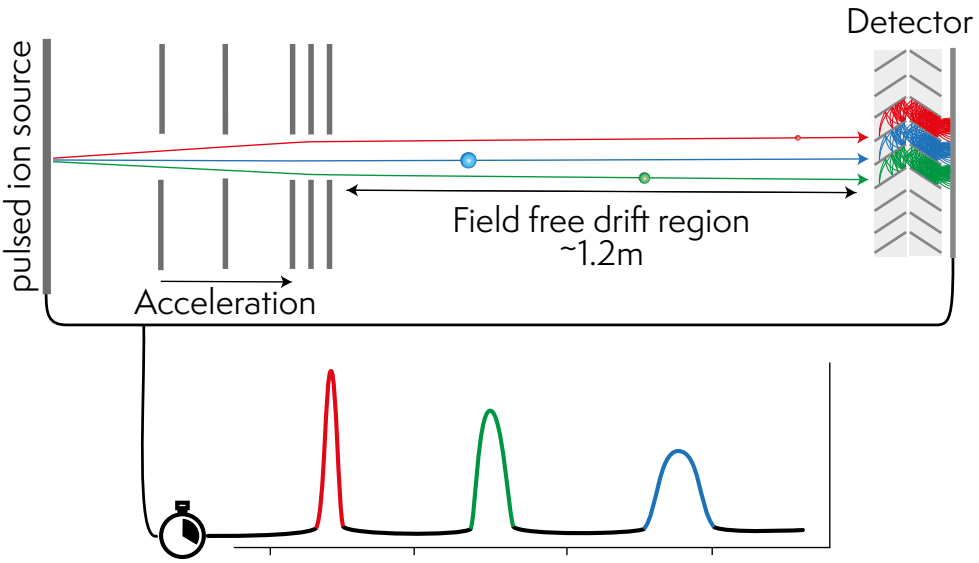

Figure 1.1: *Principle of time-of-flight mass spectrometry; (blue) heavy ions, (green) medium ions, (red) light ions. All ions are accelerated simultaneously: light ions reach the detector sooner than heavy ions. Via calibration with known masses arrival times can be converted into m/z values.*

Fourier-Transform Ion Cyclotron Resonance (FT-ICR) mass spectrometer is quite a mouthful, and for good reason. This is the most precise, slowest and inherently most expensive type of mass spectrometer. This type of mass spectrometer uses the fact that ions contained inside a uniform magnetic field exhibit a circular motion: the "cyclotron motion". FT-ICR mass spectrometers use a cylindrical superconducting magnet with an "ion trap" in its centre. Ions are introduced along the z-axis of the magnet and trapped in place: by an axial magnetic field in the x and y direction, and by an electrostatic field in the z direction. As the ions are kept within the strong magnetic field they start to exhibit the cyclotron motion – a circular orbit around the magnet z-axis. An excitation pulse then enlarges this axial orbit to a radius of a few centimetres. As each cluster of ion species sheers along the ion trap walls, they induce a small charge to the detection electrodes on opposing sides of the trap (see Figure 1.2). The resulting potential plot for every cluster of ion species is sinusoidal, reflecting the frequency at which the cluster orbits the axis (the cyclotron frequency). The frequency of the cyclotron motion is specific for each ion species, as it can be accurately described based on the ion mass, the charge on the ion and strength of the magnetic field. However, as all ion species are recorded simultaneously the recorded signal is a complex mixture of frequencies from all ion species in the trap, a so-called transient. To break this transient down into its substituents, i.e. find the frequency of every cluster of ions, FT-ICR uses Fourier transformation. By a method of mathematical frequency matching the relative contribution of every possible

frequency within the pre-set range is calculated. This results in a frequency spectrum, which is then converted into an *m/z* spectrum, as the magnetic field strength is known. The precision of the Fourier transformation results is linearly correlated to the length of the transient, i.e. the time spent recording the orbit of the ion clusters. A longer recording equals a higher resolution. Typical scan times are around 0.1-1 second, up to 10 seconds for exceptional cases.

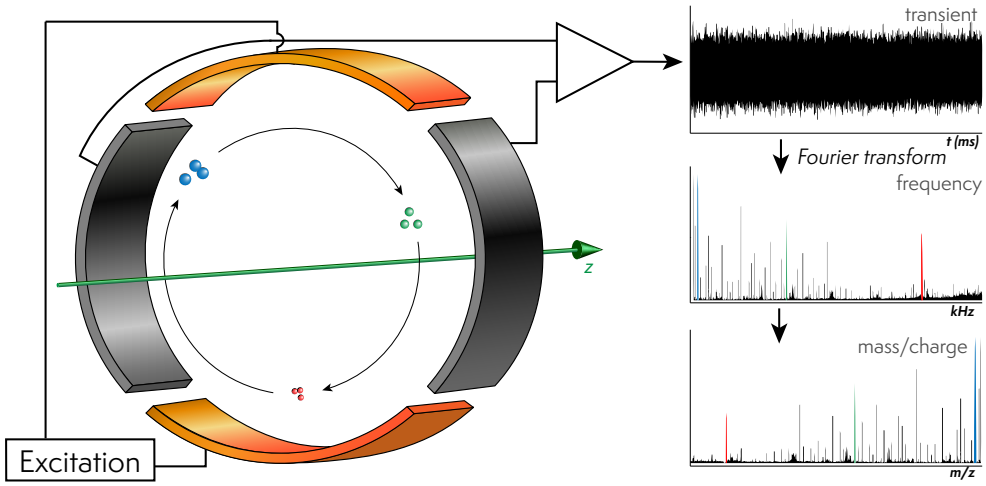

Figure 1.2: *Principle of FT-ICR mass spectrometry; (blue) heavy ions, (green) medium ions, (red) light ions. Light ions circle centre of the magnetic field (z) at a higher frequency than heavy ions, creating an oscillating potential difference between the detector plates. The resulting complex signal (transient) is processed to produce the m/z spectrum.*

Orbitrap mass spectrometers are relatively new, with its first commercial introduction in the mid-2000s.[1] Many of the results presented in this thesis are acquired on Orbitrap mass spectrometers, e.g. Chapters 3 and 4. Like FT-ICR, Orbitrap analysers rely on Fourier Transform signal processing to extract high resolution *m/z* ratios from the recorded signal. Unlike FT-ICR however, Orbitrap mass spectrometers do not use a powerful, expensive magnetic field. Instead, Orbitrap mass spectrometers use an electrostatic field to trap ions in an orbit around a shaped axis (see Figure 1.3). The frequency at which ion species oscillate from one side of the trap to the other (along the z-axis) is indicative of their *m/z* ratio. This oscillation is captured as the potential change measured between the two outer halves of the trap, resulting in a transient signal. Similar to FT-ICR, as the ions are not lost during detection, a longer measurement results in higher mass resolving power. Orbitrap scans can therefore be rather slow, up to multiple seconds. In general, FT-ICR can deliver higher mass resolving power than Orbitrap systems, though in practise the Orbitrap mass resolving power is sufficient for most analytical problems.

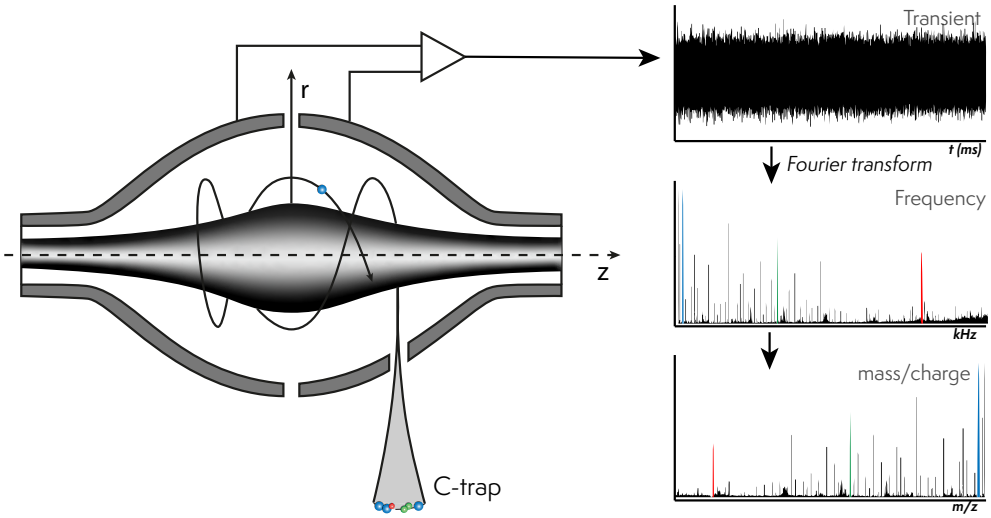

Figure 1.3: *Principle of Orbitrap mass spectrometry; the ions are collected in the C-trap and pulsed into the electrostatic trap where they orbit the central axis due to a static potential. The m/z ratio of each ion species then determines the frequency at which they oscillate along the z- axis (left-to-right in this figure). The two halves of the Orbitrap mass spectrometer detect the change of potential as ion species move along the z-axis, which results in a transient signal. Fourier transform, similar to its implementation in FT-ICR mass spectrometry, then resolves mass spectrum. Based on the patent application of Makarov et al..*[2]

All mass spectra contain *m/z* values, rather than mass values, because a singly charged ion and a doubly charged ion with twice the mass behave identically in an electric/magnetic field. They are therefore indistinguishable by *m/z* ratio. Separating such isobaric compounds is done by careful interpretation of the spectrum, for example by observation of isotope or fragmentation patterns.

Mass spectrometry imaging combines the separation techniques described above with selective extraction of sample material (by laser, ion-beam or solvent-spray, commonly). The extraction positions are pre-defined in a raster pattern and probed sequentially, as shown in Figure 1.4. These positions (sometimes referred to as voxels or pixels) are between 250 µm and 50 nm in diameter, depending on the technique and experimental requirements. The extracted material is then ionized (by charge-transfer from other particles, mostly) and analysed as described above. The resulting dataset contains mass spectra for every position on the raster. After the experiment, intensity images can be created for any mass spectral feature (usually one peak), where the pixel colour or brightness represents the feature intensity, normalised for the whole image. A typical experiment results in a dataset of many images (anywhere between 1 and 50,000), with as many pixels as extraction locations (typically 10,000-100,000). A major benefit of mass spectrometry imaging over other imaging techniques is the possibility to simultaneously image many molecules in an untargeted and unlabelled manner. This makes MSI ideal to screen for relevant, thus far unknown molecules.

Many MSI techniques are introduced and explained in **Chapter 2**, but I'll highlight some of the most important here. Matrix-assisted laser desorption ionization (MALDI) is the most common MSI technique. MALDI uses a UV laser to desorb thin sectioned samples covered by an ultraviolet light absorbing coating (i.e. matrix). This matrix assists the desorption and ionization of the sample molecules. MALDI is relatively sensitive, fast and is typically performed with a 10-50 µm spatial resolution. Single cell analysis is therefore just about possible with MALDI.

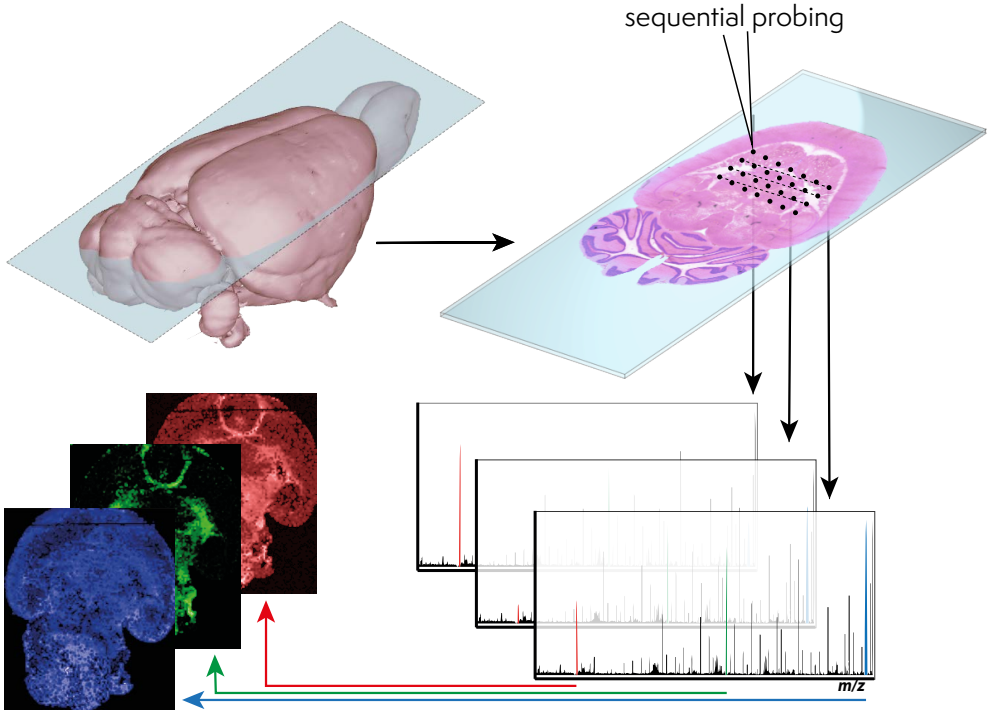

Figure 1.4: *The basic principle of a typical mass spectrometry imaging experiment. Flat sections are cut from the object of interest; each section is probed (e.g. by laser, solvent spray or ion beam) in a sequential, rasterized manner; the mass spectra from all probing positions are collected; the image of any m/z ratio can be plotted and compared.*

Secondary ion mass spectrometry (SIMS) uses the impact of a tightly focussed beam of ions to desorb molecules from a target surface. The ionization step is generally less efficient than MALDI, and the spatial resolution is much higher (approx. 100 nm). The sensitivity suffers from both these aspects and is significantly lower than in MALDI. Due to the harshness of ion beam impact larger molecules tend to be more difficult to measure with SIMS as they undergo fragmentation during analysis. However, the spatial resolution of SIMS is far superior to all other MSI techniques. Single cell and elemental analysis are therefore major applications of SIMS.

Desorption electrospray ionization (DESI) mass spectrometry uses the ESI principle explained earlier. A charged solvent spray (without analytes this time) from an ESI emitter is directed at a sample surface, where it desorbs soluble sample molecules and partially ricochets towards the mass spectrometer inlet. The charged spray droplets are also drawn towards the MS inlet by the electric field. DESI is versatile and has the most simple, compact, and inexpensive setup of any MSI technique. DESI is a soft desorption/ionization technique and suitable for a wide variety of (biological) compounds. DESI is naturally more sensitive for highly soluble compounds, so care should be taken to choose a solvent that suits the analyte of interest. DESI MSI is generally considered to be somewhat slower, less sensitive and have a lower spatial resolution than MALDI MSI.

Laser ablation electrospray ionization (LAESI) mass spectrometry is also based on the ESI principles but decouples the desorption and ionization steps. Desorption is performed by infrared laser ablation of the sample directly underneath the electrospray - between the electrospray emitter and the mass spectrometer inlet. Ionization then occurs by mixing the ablated sample material with the electrospray droplets.

Ambient *mass spectrometry imaging* differs from regular mass spectrometry imaging in that the extraction step is performed at atmospheric pressure. For regular mass spectrometry imaging (e.g., MALDI, SIMS) the sample is placed in a vacuum chamber to avoid interference between the analyte molecules and neutral gas molecules. This has positive consequences on sensitivity, contamination, and mass discrimination, amongst others. However, not all samples are amenable with vacuum, most notably liquid-containing samples or samples that are difficult to fit within the strict thickness and size requirements of vacuum-based MSI sources. Liquid-containing samples (e.g., biological tissues) are therefore often desiccated prior to analysis. Ambient mass spectrometry techniques such as DESI and LAESI can analyse samples without desiccation or other - potentially disruptive or misleading - sample preparation methods. Larger, non-sectioned and even liquids or emulsions can more readily be imaged through ambient MSI than vacuum based MSI. Typical samples for ambient mass spectrometry are plant materials, gels and bacterial colonies, where non-ambient techniques tend to focus on synthetic materials and animal or human tissues. However, due to recent technological advances some ambient techniques (e.g., DESI) now rival non-ambient techniques for non-niche applications.

1.2. SCOPE AND OUTLINE

Ambient mass spectrometry imaging is a relatively novel offshoot in the field of analytical chemistry. It is relatively young, with many novel technologies striving to become a household name in the field. In **Chapter 2** we describe the field of mass spectrometry imaging of biomaterials, and the current position of ambient mass spectrometry imaging techniques within this field. Many examples of mass spectrometry imaging applications are shown and an outlook for future applications is given.

As noted before, for this thesis we have chosen to focus on the LAESI MSI technique. Thanks to the separate ablation and ionization steps in LAESI we can independently optimize both. In most other MSI techniques these steps cannot be separated, and there is always a trade-off. In addition, laser irradiation is a more aggressive desorption technique which implies a less selective desorption of analytes than DESI, for instance. The infrared laser interacts with OH stretch vibrations, so all water-containing and many other samples work well with LAESI. The sensitivity of ESI for polar compounds translates to LAESI, which theoretically makes it an ideal match.

LAESI has certain drawbacks though. For one, the sensitivity of LAESI cannot rival electrospray ionization. This is mostly due to inefficient: 1) gas-phase liberation of analyte molecules, 2) mixing of the ablated analyte material and the electrospray plume and 3) capture of analyte molecules in the mass spectrometer inlet. In addition, the relatively low sensitivity for less polar compounds of ESI also translates to LAESI.

We address these drawbacks in **Chapter 3**. We present a novel ionization source design that incorporates a second ionization mode (APCI) in the same probe as ESI, without loss of the original functionality. The probe can be rapidly switched between the modes, to best suit the analyte properties. The combination of infrared laser ablation and APCI we coined "LA-APCI". In addition to improved sensitivity for less polar compounds, our LA-APCI approach has an inherently more robust ionization principle when combined with laser ablation. In this chapter we investigate if our design results in improved sensitivity and repeatability. We then present a time series imaging study performed by LA-APCI on fungicide metabolism in plant leaves.

ESI ionization is often lauded for its "soft" ionization character (i.e., molecules tend not to fragment) and the possibility to introduce multiple charges to a molecule. These characteristics make ESI particularly suitable for the intact analysis of large, fragile molecules such as protein complexes. In fact, these analyses have recently become a research field of their own, called "native MS". In **Chapter 4** we take on the challenge to analyse intact non-covalently bound protein complexes by LAESI-MS. Can these large, fragile biological complexes survive laser irradiation and ionization at atmospheric pressure? We tested a range of biomolecules, from hemoglobin to human IgG, and compared the results with the current golden standard, nano-ESI.

If we have now successfully progressed the field of ambient mass spectrometry imaging – in terms of analyte compatibility and sensitivity – we have inevitably made the resulting mass spectra more complex. As more molecules are detected, the job of separating them and assigning their structure becomes increasingly difficult. To meet this challenge, we have dedicated **Chapter 5** to mass spectrometer improvements. We add advanced data recording and processing techniques to an existing FT-ICR system to push the boundaries of mass resolution in an imaging experiment. Can mass spectrometry imaging resolve the complexity of the lipidome?

The impact of the technological and methodological advancements presented in this thesis are discussed in **Chapter 6**, with emphasis on societal, industrial, and personal aspects. Here, we reflect on how academic research can strengthen the world around us, and vice versa.


1

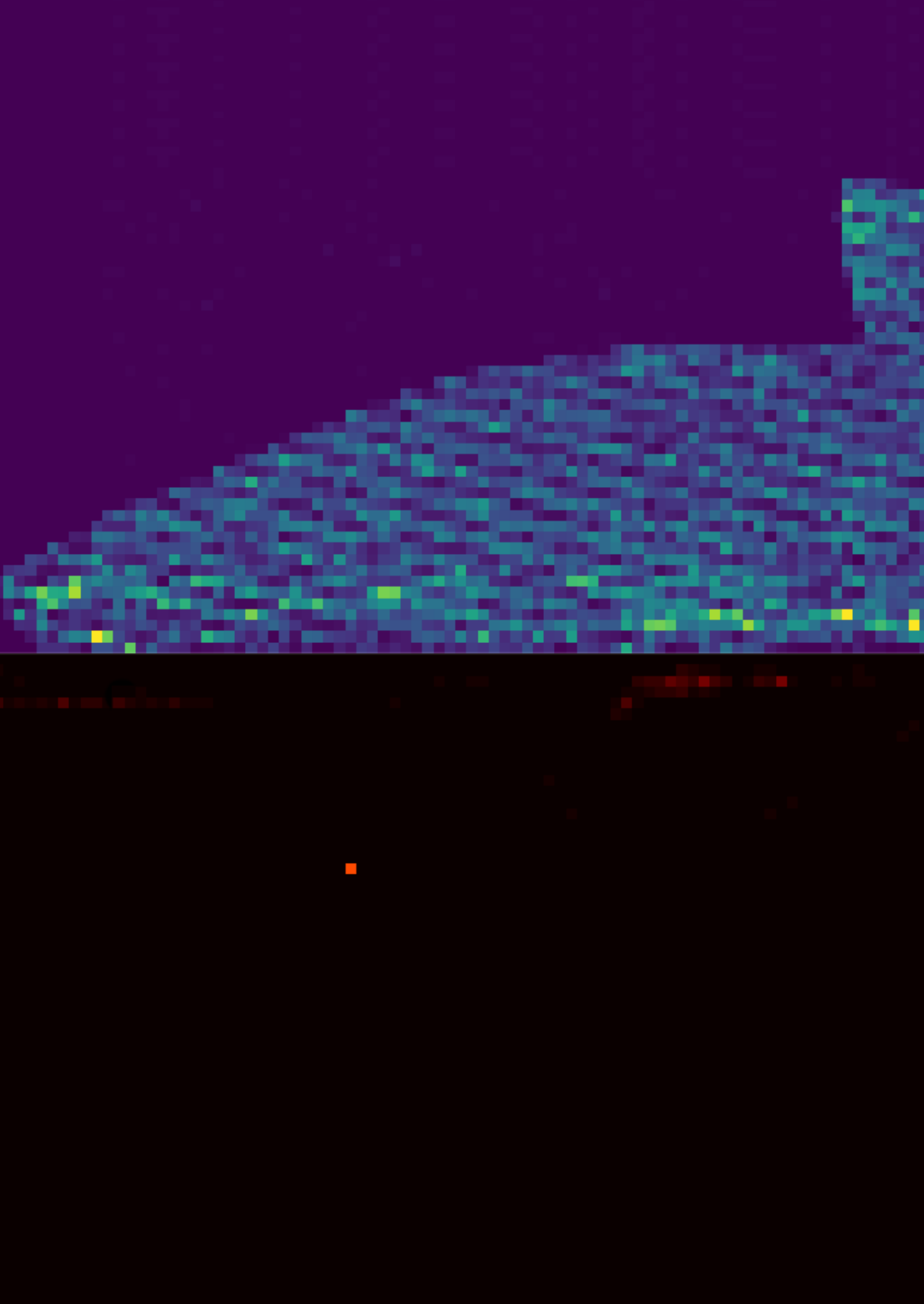

CHAPTER 2

INTRODUCTION TO MASS SPECTROMETRY IMAGING

Based on

Visualizing molecular distributions for biomaterials applications with mass spectrometry imaging: a review

Martin R. L. Paine[¥], Pieter Kooijman[¥], Gregory L. Fisher, Ron M. A. Heeren, Facundo M. Fernández, Shane R. Ellis

Journal of Materials Chemistry B 5.36 (2017): 7444-60

2.1. INTRODUCTION

Interactions at the surface of biomaterials have a major impact on their in vivo performance and physiological response of the host. Therefore, detailed characterization of surface properties, both physical and chemical, is required to engineer new materials and increase their biocompatibility.[3,4] Many analytical techniques have been routinely employed to characterize the surface properties of biomaterials including but not listed to; X-ray photoelectron spectroscopy (XPS),[5] atomic force microscopy (AFM),[6] Auger electron spectroscopy (AES),[7] contact angle methods,[8] vibrational spectroscopy (e.g., Raman and Fourier transform infrared spectroscopy),[9] near edge X-ray absorption fine structure (NEXAFS)[10] and energy dispersive x-ray spectroscopy (EDX).[11] An informative comparison between these and MS based approaches is provided in a review by Senoner and Uger.[12] Of the aforementioned techniques, detailed elemental and topographical information of the surface can be obtained, but this information usually relates to one or a few chemical species, lacking specific chemical information at the molecular level. The exception being vibrational spectroscopy, which is able to provide non-specific chemical profiling, complementary imaging techniques are typically required when broadband molecular information is required from both the substrate and the biological material that interacts with the substrate.

Mass spectrometry imaging (MSI) enables visualization of a broad range of chemical species in a single experiment with high molecular specificity and the ability to structurally characterize detected molecules. As many materials chemistry applications have traditionally required analysis of inorganic or covalently bound materials with high (<1 μm) spatial resolution, secondary ion mass spectrometry (SIMS) has been a mainstay for chemical imaging of materials in many disciplines as it is particularly well suited for such analyses.[12-15] However, as research into biomaterials and their associated biomolecular interactions has emerged, so too has the demand for new MSI methods enabling detection and characterization of many classes of labile biomolecules. With the development of alternative ionization methods and rapid improvements in MSI instrumentation, both in terms of mass analyser and sampling/ionization technologies, massive gains in mass-resolving power, speed and sensitivity have been achieved. These dramatic improvements have positioned MSI as a unique resource within a growing number of analytical characterization facilities. In particular, the use of MSI for the investigation of biological tissues has flourished, providing a wealth of information on the spatial distribution of pharmaceuticals, metabolites, lipids, peptides, and proteins from practically every type of organic substrate.[16-18] The increased usage of MSI for biomolecular investigations has resulted in successful methodologies for a broad family of compound classes, making the translation to inorganic or non-biological substrates a logical step. Thus, emerging fields such as biomaterial development, where changes in surface composition and

structure of synthetic materials placed inside the body (e.g., biomimetics or biomedical devices) affect a biological response are primed for interrogation by MSI. As a surface sampling technique, MSI is well equipped to probe biomaterials that encompass the interface between synthetic substrates and biological tissue.[19,20] Characterizing the biomaterial surface properties (i.e., chemical composition, structure, orientation) and understanding the biological effect these properties have by measuring the spatial distribution of biomolecules on these surfaces is paramount to the development and successful implementation of biomaterial technology.

The ability to perform MSI for a particular application depends largely on the type of desorption/ionization source employed of which there are three major categories; secondary ion mass spectrometry (SIMS), matrix-assisted laser desorption/ionization (MALDI), and various ambient mass spectrometric methods. Each technique can produce ions in both positive- and negative-ion mode (broadly referring to detection of basic and acidic compounds, respectively), however their method of operation varies significantly leading to different populations of ions detected. SIMS represents the most energetic desorption technique, capable of ablating covalently or ionically bound material and penetrating into the depth of the substrate, making it well suited for elemental and inorganic analyses. MALDI is a softer desorption technique, capable of desorbing and ionizing loosely bound inorganic material and a wide range of biomolecules (proteins, peptides, lipids, and metabolites). Ambient techniques generally represent the softest desorption techniques and are best suited to delicate substrates (particularly those not vacuum stable) and labile organic molecules in the 50-2000 Da range. Therefore, alternative MSI techniques such as MALDI and ambient methods may be more effective in biomaterial applications where broader chemical detection is required or when probing delicate substrates.

In these following paragraphs, we highlight the broad array of MSI techniques currently available for molecular detection by showcasing their reported use in biomaterial applications, as well as broader materials science applications to illustrate the potential of these techniques for future research. The discussion includes concise descriptions of the processes underpinning each technique, current developments in instrumentation technology, and key applications that exemplify the benefit of MSI for biomaterial surface analysis. Finally, a perspective on the role of new MSI approaches at the intersection of biomaterial analysis is provided.

2.2. SECONDARY ION MASS SPECTROMETRY (SIMS)

SIMS was the first MS technique employed for imaging and arguably the one most familiar to materials scientists.[13,21,22] SIMS utilizes the release of charged (ionized) material from a substrate upon impact of an electrostatically focused high-energy primary ion beam (traditionally of monoatomic sources such as Au^+, Ga^+ and In^+). As the high-energy (10-40 keV) primary ions impact the surface, a collisional cascade is initiated in the top few monolayers of the sample, leading to the ejection of secondary particles consisting of sputtered neutral molecules, ions, molecular fragments (of both neutrals and ions), and electrons.[23,24] The secondary ions generated, typically protonated/deprotonated ions, cationized adducts or radicals, are then detected based on their mass-to-charge ratio (*m/z*), typically using time-of-flight (TOF) mass spectrometry. For SIMS analyses, samples are typically mounted in a high vacuum sample chamber, must be as flat as possible and be mounted onto conductive substrates to minimize the effect of surface charging which can significantly hamper both spatial and mass resolution as well as sensitivity. For insulating samples these are often prepared as thin section (approx. 1-20 µm) and mounted onto conductive substrates such as silicon, steel or indium-tin oxide coated (ITO) slides. It should be noted that charge compensation can enable analysis of insulating samples by actively neutralizing surface charge and such capabilities are available on commercial systems.

The primary advantage of SIMS over other MSI techniques is the ability to restrict the analysed area down to <100 nm, with features resolved by several beam diameters, providing by far the highest spatial resolution of any MSI approach. As many (bio)materials applications require sub-micron resolutions SIMS thus provides unique advantages not available with other approaches described below. Combined with the energetic desorption/ionization process SIMS is particularly well-suited for analysis of inorganic materials and materials bound to surfaces via chemical bonds. However, compared to softer desorption/ionization techniques like MALDI and DESI, SIMS imparts significantly more internal energy to desorbed molecules, resulting in substantial molecular fragmentation. In some cases this feature can be highly advantageous, e.g., for analysis of elements, covalently-bound surface materials and for detection of molecules that have been covalent bonded to certain atoms that serve as a chemical tag. The high sensitivity of SIMS for elemental imaging is in part due operation in the so-called "dynamic-SIMS" mode. In dynamic SIMS high ion doses (>10^{13} ions.cm^{-2}) are used to produce ions from a large fraction of the entire surface. Due to the high ion doses detection of only small molecular fragments and elements originating from the surface is possible due to accumulation of surface damage. The high spatial resolution and sensitivity offered by dynamic SIMS has recently been exploited in a unique approach termed Nano-SIMS. In this approach a caesium or oxygen primary ion beam is used which can be focused down to approx. 50 nm.[25] The unique MS design allows up to seven *m/z* channels to be continuously

monitored whereby *m/z* information is obtained via angular separation in a magnetic sector analyser. Detectable ions are either elements or diatomic fragments such as CH^-.[25-28] Examples of materials chemistry applications include the analysis of ^{13}C-enriched Resveratrol coated Fe_3O_4 coated nanoparticles whereby Resveratrol was detected via the enriched ^{13}C signal in areas where it was localized[29] and the localization of isotope-labelled lipids and selected proteins simultaneous through the use of fluorinated gold immunolabels[30]. By virtue of its high sensitivity and abundance precision Nano-SIMS has also found been widely used to study dynamic chemical changes in biological systems.[31,32] For instance, via incorporation and monitoring of stable isotope enrichments (in these cases ^{15}N enriched thymidine), it has been possible to pinpoint stem cell generation in mice hippocampi[33] and relatively quantify the different origins of new cardiomyocytes[34]. Similarly, laser ablation inductively coupled plasma (LA-ICP) mass spectrometry provides a highly complementary approach to element imaging with SIMS. Several authors report the use LA-ICP-MS to study the biological uptake of nanoparticles[35,36] and the in vivo degradation of metallic implants[37-39]. Although it does not offer as high spatial resolution by virtue of the use of a laser to desorb material it offers excellent quantitative abilities enabling absolute surface concentrations of elements to be determined with high precision (typically 5-15% RSD).[40-42]

In many cases, especially in untargeted (bio)molecular investigations, information on molecular distributions is required. In this case, the methods described above do not suffice, and traditionally an approach known as static SIMS is utilized. In static SIMS the ion dose is maintained below 10^{13} ions.cm^{-2} which ensures less than 1% of the surface is impacted by a primary ion. Thus, surface damage is minimized and the probability of detecting larger *m/z* species having *m/z* values up to 2000 is greatly enhanced. It should be noted that with the advent of softer cluster ion sources (see below) it is also possible to acquire intact molecular information at ion doses above the static limit due to the drastically reduced surface damage of these large primary ions.[43] Although still detection of intact labile molecules having molecular weights above 500 Da can be a challenge characteristic molecular fragments are often detectable under such conditions using traditional ion beams. For example, lipid analyses mostly result in the detection of lipid fragment ions (i.e., the phosphatidylcholine head group ion at *m/z* 184 in positive-ion mode or free fatty acids in negative-ion mode) rather than the intact lipid itself, complicating result interpretation.[13,27,44]

Driven by the increasing need to detect larger molecules, primarily for biomolecular analysis, recent SIMS developments have heavily focused on the development of softer ionization sources that greatly minimize fragmentation and surface damage.[45] In particular larger, polyatomic sources such as C_{60}^+ [43,46-49], SF_5^+ [50-52] and Au_n^+ [48,53-55], gas cluster beams such as Ar_n [56-58] and recently water cluster beams[38] have revolutionized SIMS and brought it into the realm of true molecular analysis. In

these cluster ion sources a single primary ion can have a mass of up to 100,000 which greatly reduces fragmentation and sub-surface damage, thereby enabling both softer ionization and sputtering (see below).[59] It must be noted that large cluster beams do not generally offer the ≤100 nm[45] spatial resolution of atomic or small cluster sources (e.g., Bi_3^+). The current state of the art of cluster sources can achieve focused spot sizes down to several micrometres for gas cluster ion beams and in some cases as low as 300 nm for C_{60} ion beams.[60,61] It should be noted that despite the tremendous advances made in molecular detection with SIMS over recent years, as reflected in the discussion below many applications still centre on detection of elements of elemental/small molecular markers of larger molecules.

A second key advantage of SIMS over other MSI techniques is the exploitation of the gradual removal of material by the primary ion beam to enable 3D analysis (i.e., depth profiling).[62,63] In such an approach a cluster ion beam is often used to sputter away several monolayers or more of material while minimizing surface damage and modification, after which the freshly exposed surface is imaged using SIMS. This process can be repeated using sequential sputter/analysis cycles and enable 3D chemical reconstruction of heterogeneous materials. Crucially, the achievable depth resolution can be as low as several nanometres,[64,65] providing almost a monolayer by monolayer representation of the material. In the sections below, we highlight a diverse array of applications of SIMS-MSI in materials chemistry with specific emphasis on biomaterials and their interactions. For comprehensive reviews on biological tissue imaging applications of SIMS-MSI the reader is referred to a series of reviews published on this topic.[27,44,66-74]

Synthetic polymers

SIMS-MSI has found widespread use for studying polymeric materials in a diverse array of applications.[75] For example, using a 5 keV Ar_{2000}^+ beam for sputtering and a Bi_3^+ beam for mass analysis, the composition of spin-cast polymer multilayers contacting alternating layers of polystyrene (PS) and polyvinylpyrrolidone (PVP) on silicon substrates has been studied.[76] Polymer signals were identified by the characteristic $C_7H_7^+$ and $C_6H_{10}NO^+$ signals for PS and PVP, respectively and incorporated PS layers as thin as 45 nm could be resolved. A similar approach has also been employed using C_{60}^+ for sputtering instead.[77] 3D-SIMS has also provided valuable insight into surface topographies of poly(bisphenol A-co-decane ether) films. SIMS could, for the first time, reveal the presence of hollow interior structures on the surface of these polymers when prepared with either chloroform or THF solvents. These hollow droplets were found to have a thickness of several hundred nanometres and were sandwiched between the two polymer layers.[78] As another example it was recently shown how polyelectrolyte multilayer composite films could be synthesized and exposed to a mineralization process. The quality of polymeric nucleating agents was

assessed in terms of calcium carbonate mineral infiltration efficiency by SIMS depth profiling with a combination of a Bi^+ beam for analysis and a cluster Ar_n^+ beam for sputtering.[79] With respect to biomaterials Jung et al. have deployed 3D-SIMS to study the spatial distributions of the biopolymers cellulose and lignin in tension wood as a model for biomass using a Bi_3^+ beam for analysis and an O_2^+ beam for sputtering.[80] Finally, in a recent publication by Goor et al., the reactions of incorporated materials within a supramolecular assembly were studied with 3D-SIMS-MSI (Figure 2.1).[81]

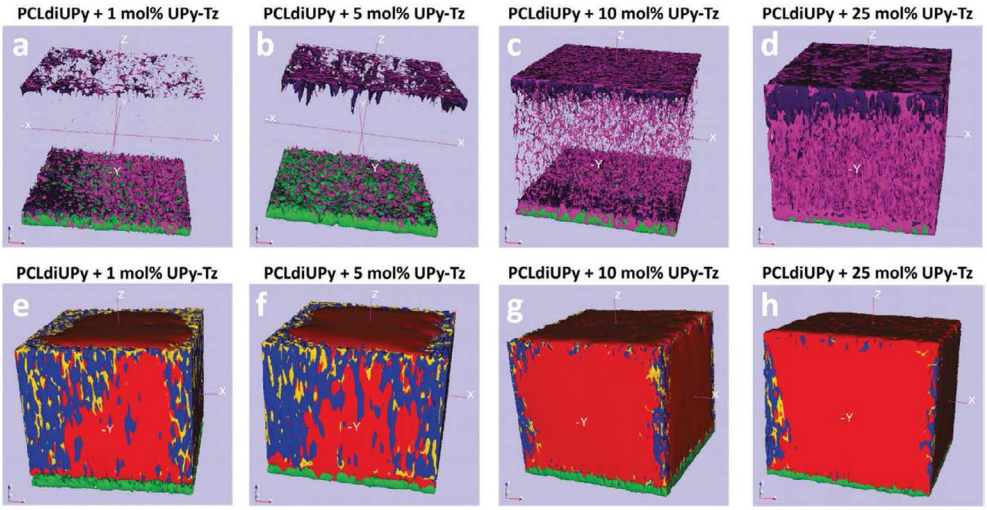

Figure 2.1: *A 3D-reconstruction of increasing concentrations of mixed-in guest molecules (UPy-Tz) within a UPy thin film using SIMS-MSI where clickchemistry to an iodine containing model compound was performed on the surface. The ion distributions of relevant mass fragments are depicted in different colors: iodine (purple, TCO fragment), fluorine (pink, from UPy-Tz), m/z 124 (red, UPy-fragment), m/z 150 (blue, UPy-fragment), m/z 113 (yellow, PCL-fragment), InO2 (green, from glass slide substrate). The films have a thickness of 100–150 nm. Dimensions of depth profile area are 100 µm x 100 µm. Figure reproduced and adapted from ref. 79.*

An ureidopyrimidinone (UPy)-based matrix serving as a thermoplastic elastomer was mixed with reactive UPy-tetrazine (UPy-Tz) additive. The UPy-Tz provides supramolecular intercalation into the UPy to generate a functionalized surface. To assess which UPy-Tz concentration resulted in the most surface-localized functionalization an area of 100x100 µm was imaged with a Bi_3^+ beam following each C_{60}^+ sputter cycle. At low UPy-Tz concentrations the fluorine signal (specific signal to UPy-Tz model compound) was localized at the surface of the material. At higher concentrations UPy-Tz-related signal was also observed throughout the bulk material, but with higher intensity always on the surface. Proof of successful click-reaction was provided by the surface-exclusive detection of iodine following the click-reaction of trans-cyclooctene iodine with intercalated UPy-Tz. Combined with the homogenous distributions throughout the film of UPy and monomers of the polycaprolactone (PCL, also part of the elastomer), localized chemical analysis in 3-dimensions using SIMS

was able to directly visualize differences in surface and bulk reactivity as relevant for functionalization of supramolecular materials.[81] The authors conclude that such materials and functionalization reactions may find use in regenerative medicine where in-vivo functionalization may be exploited to elicit the required materials-tissue/cell interactions.

Nanoparticles

The ability to track nanoparticles within cells is attracting much interest in the analytical field due in part to the development of nanoparticles capable of delivering therapeutics intracellularly.[82-87] SIMS has proven a useful tool for studying such materials and their interactions.[12,84,86,88-93] In a recent study, Hua et al. described an innovative microfluidic/sputtering approach allowing SIMS imaging of individual cells in a hydrated environment.[94] This was used to study the effect of ZnO nanoparticle uptake in C10 cells with sub-micron resolution. Nanoparticle uptake was visualized by the characteristic Zn^+ signal while nanoparticle containing cells were observed to exhibit elevated Ca^+ and decreased Na^+ and K^+ signals which were attributed to altered intracellular Na^+ and K^+ transport induced by ZnO nanoparticle uptake.

By using a C_{60}^+ source for both sputtering and analysis both organic and inorganic materials can be imaged in 3D in a single experiment. For example, this was shown by Angerer et al. for the 3D MSI of a titanium dioxide nanoparticle engulfed by a unicellular eukaryote, Tetrahymena pyriformis. They were able to visualize the incorporation of nanoparticles inside food vacuoles of the eukaryote.[85] Another powerful example of 3D TOF-SIMS on polymer nanoparticles is given by Rafati et al.[95] The surface heterogeneity and relative localization of the poly(lactic-co-glycolic) acid (PLGA) backbone, polyvinyl acrylate (PVA) surfactant, and protein lysosome (model therapeutic) were visualized to gain understanding in the effect of polymer microsphere fabrication parameters and revealed that the lysosome was primarily distributed around surface pores in the microsphere.

Multimodal approaches with SIMS and fluorescence or transmission electron microscopy (TEM), for example, have proven especially useful to track nanoparticles in biological matrices.[30,96] Several studies have reported cytotoxicity assessment of nanoparticles with TOF-SIMS, such as Fe_3O_4 nanoparticles[97] or polymeric nanoparticles combined with fluorescence microscopy[98]. Recently, the delivery of cytotoxic drugs was evaluated by polymeric oxaliplatin nanoparticles through monitoring of the time-dependent spread of both the nanoparticle carrier and the Pt(II)-based anticancer drug in-vivo. The combined fluorescence microscopy, TEM and SIMS approach discovered the oxaliplatin NPs are taken up in intracellular vesicles. The consecutive break-down of the carrier material stimulates release of the cytotoxic drug, confirming the targeted delivery mechanism.[99]

Tissue engineering/cell culture

Tissue engineering is a young, thriving field of study clearly in need of imaging techniques with the ability to differentiate biological responses based on changes in local molecular composition. For example, SIMS has been deployed to study the homogeneity of cell populations based on their molecular phenotype[100] and shed light on the biological pathway changes related to culturing conditions[101]. SIMS can also be applied to evaluate the potential of tissue engineering stem cell lines. For instance, the osteogenic differentiation capabilities of human embryonic stem cell-derived mesodermal progenitors (hES-MPs) were studied and compared to human mesenchymal stem cells (hMSCs), one of the most documented cell types for tissue engineering purposes.[102-105] Using 3D-SIMS-MSI depth-profiling and 3D-mapping, distinct biomineralization patterns were shown, with hES-MPs yielding higher hydroxyapatite signal than hMSCs after six weeks but lower after 3 weeks of osteogenic stimulation.[105]

As TOF-SIMS offers exciting opportunities to correlate surface chemistry to biological response it is well suited to guide substrate development for proliferation and differentiation control.[106-108] Such an approach has been utilized to assess the cell proliferation effect of hydrogel substrate additives[109,110], naturally derived extracellular matrices[111-113] and surface geometries[114]. Current state-of-the-art substrates tend to have complex compositions and geometries, which require more specific and sensitive methods to verify. Bongo et al. showed their PEDOT(TOS):gelatine composite films were able to support cell growth while retaining the beneficial electrical conductivity and mechanical properties of the original polymer substrate.[115] The authors used a nano-SIMS instrument to reveal the distribution of carbon, nitrogen and sulphur and demonstrate the homogeneous gelatine incorporation in the film.

Implants

Successful implant integration in the surrounding tissue is of vital importance to patient health, but much remains unknown about the mechanics of implant-tissue interaction. In an effort to shed light onto these effects the interaction area between bone and a titanium implant has been imaged with TOF-SIMS, revealing distinctive molecular and elemental species for bone, implant, and interaction area.[116,117] Gonzalez et al. studied a bioactive coated Ti-NB-Hf alloy implant material using Bi_3^+ beam and showed this material had a significantly increased osteoblast adhesion. In another study the distribution of the immunosuppressant rapamycin in a coronary stent coating (poly(lactic-co-glycolic acid)) was studied to determine the effect of the coating application method on drug elution behaviour.[118] 3D TOF-SIMS analysis showed a high degree of heterogeneity in the rapamycin concentration throughout the sample, with the most homogeneous areas providing the most gradual elution. It was therefore concluded that the coating application method has a major effect

on the early drug elution behaviour and therefore deserves thorough optimization. Supramolecular materials such as biodegradable hydrogels are considered promising drug delivery carrier candidates. Ureidopyrimidinone (UPy) cross-linked poly(ethylene glycol):polycaprolactone (PEG:PCL) hydrogels implanted under the renal capsule of rats have been analysed with Au^+ SIMS, through relative distributions of endogenous compounds (lipids, and cholesterol) and the implanted polymer (PEG).[119] Interestingly, it was observed that the PEG-related signal was co-localized in the tissue with cholesterol sulfate, suggesting the occurrence of cellular infiltration in the polymer. This study demonstrates the vast potential of SIMS to study foreign-body response mechanisms and can help monitor material-tissue interactions, for example in drug-delivery applications.

Advances for chemical identification using SIMS

The use of axial TOF analysers for SIMS requires the primary ion beam to be pulsed on the order of several nanoseconds to obtain reasonable mass resolution. However, this introduces both speed and sensitivity constraints due to the limited duty cycle resulting from the fact that only one ion packet may be injected into the analyser per TOF event. For example, a 2 ns pulsed beam operating at 10 kHz and a maximum flight time of 100 µs means only 0.002% percent of the time is spent generating ions. To overcome these limitations and enable continuous ion generation several groups have developed SIMS instrumentation employing orthogonal TOF analysers.[120-122] Through decoupling of the mass analysis and ion generation such systems can take particular advantage of cluster ion beams. Their ability to generate intact molecular ions at higher ion doses with reduced surface damage makes them ideal to operate in continuous (DC) mode. That is, the beam is effectively generating ions 100% of the time resulting in significantly reduced analysis times.[69] It should be noted that these orthogonal TOF analysers have less efficient transmission than axial TOF analysers, sacrificing part of the theoretical gain in sensitivity and time.

Recent advances in SIMS have also enabled confident structural identification of detected molecules using tandem mass spectrometry (MS/MS).[120,122,123] Although such capabilities have long been available for MALDI and ESI-based instruments they were for long lacking for SIMS. Such approaches are critical for identifying unknown surface modifications and unresolved isobaric ions. To date, such technologies have been employed mostly for biomolecular characterization from tissues and cells.[120,124] However, the structural assignment of detected molecules is also of high importance for materials characterization. Most of the ions generated in conventional tandem MSI approaches are discarded, only the fragments of the selected precursor are detected. To overcome this disadvantage a parallel TOF tandem MS system based on an axial TOF design was recently developed.[123,125] In this design the addition of a collision cell and second TOF analyser was capable of recording both MS and MS/MS spectra

simultaneously, thus providing both fragment ion (MS/MS) detection of a selected monoisotopic *m/z* range and broadband (MS) detection of the remaining ions. The increased chemical specificity enabled by MS/MS imaging was demonstrated for heat treated polyethylene terephthalate (PET).[126] Figure 2.2 shows the total ion and *m/z* 149 images of which the latter is a known SIMS fragment of PET. The *m/z* 149 image, along with other images of ions in the full-MS spectrum, reveal the presence of polymer crystals, but these *m/z* signals also arise from the surrounding substrate resulting in ionic signal observed across the full sampling area. However, when imaging in MS/MS mode using the ethylene terephthalate trimer ion (*m/z* 577) as the precursor, the same PET-characteristic fragments are also produced upon collision-induced dissociation. Importantly, these are now detected in the absence of isobaric interferences as the MS/MS detector is only detecting the *m/z* 149 that originate from the polymer-related precursor. With the use of tandem MS imaging the background interference is eliminated and the polymer crystals are observed with higher contrast at a measured lateral resolution of < 200 nm while composition of the crystals was unequivocally found to be ethylene terephthalate trimers.

With the increased ion yields for larger molecules when using cluster sources the intrinsically moderate mass resolution of a TOF analyser begins to become a limitation. It is widely known that in the analysis of complex mixtures, multiple ions are produced with the same nominal mass but different elemental composition and thus exact mass. Although high resolving power instrumentation is widely available and compatible with MALDI and various ambient ionization methods, this has not been the case for SIMS. In an effort to resolve the complexity of biological surfaces using SIMS Smith et al. have orthogonally coupled a C_{60}-SIMS source with a Fourier transform ion cyclotron resonance mass spectrometer (FT-ICR MS).[127] FT-ICR provides at least an order of magnitude increase in mass resolving power compared to TOF systems and was shown to provide more specific chemical information from a complex sample. For example, applying SIMS-FTICR-MSI to the analysis of a mouse brain nine different chemical features were detected within a 0.4 Da mass range. The high mass accuracy also allows elemental formula for many detected species to be rapidly assigned.[128] The main drawback of this approach, however, is the sacrifice in required speed and/or spatial resolution resulting from the longer dwell times needed per pixel to accumulate enough ions for adequate signal-to-noise (approx. 0.4 s per pixel). With current developments in the coupling of SIMS with FT-based mass spectrometers, such as the 3D nanoSIMS project,[129,130] it is expected that such approaches will soon find powerful usage for analysis of localized chemical composition in the materials sciences.

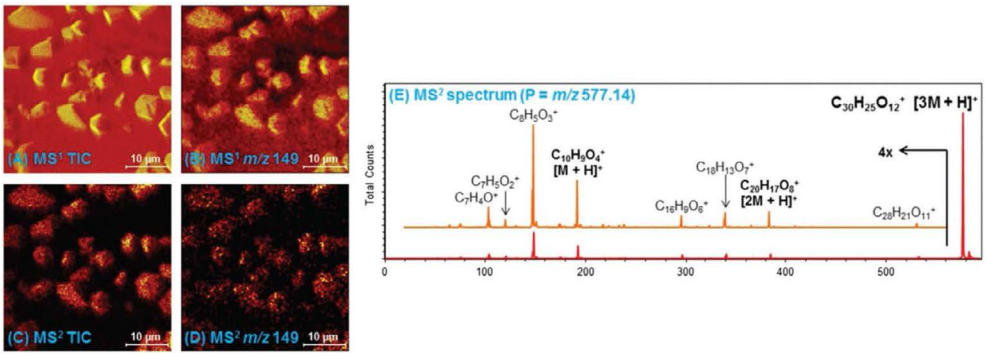

Figure 2.2: *Parallel SIMS-MS and tandem SIMS-MS/MS imaging of heat-treated polyethylene terephthalate crystals. (a) Total-ion current (sum of all signals) image in full-MS mode. (b) Distribution of m/z 149 in full-MS (MS1) mode. (c) Total-ion current (sum of all signals) image in MS/MS mode following selection and collision-induced dissociation (CID) of m/z 577 corresponding to the ethylene terephthalate trimer ion. (d) Distribution of m/z 149 in MS/MS mode revealing significantly less background and higher contrast images of the polymer crystals. (e) Corresponding MS/MS spectrum revealing structure-specific fragments arising from the polyethylene terephthalate ion after (CID). Figure adapted from ref. 126.*

2.3. MATRIX-ASSISTED LASER DESORPTION/IONIZATION (MALDI) AND DIRECT LASER DESORPTION/IONIZATION

The discovery of matrix-assisted laser desorption/ionization (MALDI) in the late 1980s was pivotal in the birth of macromolecular MSI (i.e., intact molecular detection).[131-133] For the first time, MALDI enabled the direct detection of many different molecular classes from solid substrates, including large fragile biomolecules such as intact proteins, with minimal fragmentation. Although today MALDI is used almost exclusively for organic molecules, analysis of inorganic materials is also possible,[134,135] while direct laser desorption (i.e., without the matrix) can also be employed for inorganic materials.[136] In MALDI, the sample is first mixed with an organic matrix having strong absorption at the typical wavelength used for desorption (337 or 335 nm). After mixing, the analyte molecules are co-crystallized with the matrix to form co-crystals. Typically, the sample is then loaded into a vacuum stage varying anywhere from 1 mbar to 1×10^{-7} mbar for analysis depending on the instrument design. In efforts to simplify sample analysis MALDI analysis at atmospheric pressure is also possible[137,138] but less commonly used, in part due to the lower sensitivity resulting from the difficulties in transferring ions from atmospheric pressure into the intermediate vacuum region of the mass spectrometer. MALDI typically requires flat (roughness in low micrometre scale), thin (typically 4-20 μm) samples to ensure equal irradiation conditions across the sample and to help minimize charge build up. Surface charging is only a major issue for axial-TOF analyser (the most widespread analyser for MSI) and its negative effect is typically ameliorated by mounting the sample on a conductive substrate (typically ITO coated glass slides) onto which the high ion acceleration voltage is applied. Orthogonal mass analysers (i.e., those with ionization and mass analysis regions decoupled) can

accept insulating substrates without reducing MS performance. Upon irradiation by a pulsed UV laser in initiated and the majority of the energy is absorbed by matrix molecules. Analyte ionization occurs through a series of gas-phase reactions initiated by photoionized matrix molecules and ultimately charge transfer to the analyte with protonated/deprotonated or alkali-adducted (i.e., $[M+Na]^+$) ions typically observed. Unlike SIMS, MALDI is not strictly a surface analysis technique due to the matrix solution extracting molecules from within a volume of the sample surface and its relatively large sampling depth (approx. several micrometres per sampling position when multiple laser shots are accumulated). When corrected for sampling volume, it has been reported that under favourable conditions SIMS can be up to several orders of magnitude more sensitive than MALDI.[139,140] However, unlike SIMS, the MALDI process is soft and minimal fragmentation is observed resulting in significantly more interpretable chemical information from complex surfaces.

As MALDI enables localized analysis, the extension to imaging was first taken in the mid-90s[141] and has since been the key driver in the development of MSI, particularly for biomolecular imaging in tissues.[70,142-144] Owing to its high sensitivity, significant commercial development and ability to detect the most diverse array of molecular classes of any MSI technique, MALDI is currently the most common method for MSI. For MSI applications the matrix is typically applied using either a pneumatically assisted spray, sublimation (for some small molecule applications) or controlled droplet deposition such as via piezoelectric printing. For all applications it is essential to ensure a homogenous coverage of matrix with minimal analyte delocalization on the surface. The application of the matrix presents the greatest source of error in the reproducibility of MALDI measurements. MALDI spatial resolution is determined by the size of the matrix crystals and the laser beam diameter on the surface and is currently at-best 5-10 μm in commercial instruments and as low as 1 μm in prototype systems.[145-147] It should be noted resolutions ≤10 μm typically requires matrix application via sublimation which can compromise analyte extraction, and thus sensitivity, relative to spray-based approaches.[116] To-date almost all MALDI-MSI applications have focused on biological tissue imaging and for these the reader is referred to relevant reviews.[70,142,143,148] The extension of MALDI-MSI to materials chemistry applications remains, in our view, a dramatically underexploited field. Below we outline recent examples where MALDI-MSI has provided valuable insight into the localized chemical changes occurring during the processing and preparation of various materials.

MALDI has found widespread use for the chemical analysis of polymeric substrates.[118, 119] These capabilities have recently begun to be extended to visualizing localized chemical changes occurring on polymeric materials designed for a variety of applications. For example, Crecelius et al. have applied MALDI-MSI to visualize chemical changes within polystyrene (PS) films exposed to ultraviolet (254 nm) light.[149]

Polymer films were prepared by mixing PS solutions (PS, Mn, SEC = 4760 g/mol, Mw, SEC = 5000 g/mol) with toluene, matrix (trans-2-[3-(4-tert-butylphenyl)-2-methyl-2-propenylidene]malononitrile) and AgTFA dissolved in THF and spin coating this mixture onto indium-tin-oxide coated (ITO) slides. Shaped masks were then placed onto the films prior to UV irradiation for different times. Comparison of areas exposed to UV light revealed the gradual loss of polymer signals with exposure time which were attributed to polymer cross-linking upon photo-generation of backbone radicals. The ability to monitor surface modification upon light irradiation opens up the possibility of studying the chemical changes occurring on photoresists and performance coatings.[150] A negative photoresist (Novolac) containing 10% w/w benzophenone photo-activator was used and a wiring diagram imprinted onto the surface with UV light. The substrate was imaged with a resolution of 100 µm, and polymer signals characteristic of the Novolac resin monitored. Of significance was a decrease of the undodecamer and tridecamer polymer signals in areas exposed to UV light. This loss in signal correlated with areas of lithographic imprinting and again was attributed to photo-induced polymer crosslinking, thus demonstrating the capability of MSI to study the chemical changes induced by lithographic structuring such as that used in PCB board manufacture.

Polymer MSI has also been applied to study their heterogeneous biotic and abiotic degradation of polycaprolactone diol in water.[151] After incubation in biotic (artificial stream) and denitrifying (liquor from a waste water treatment facility) solutions the polymer materials were sectioned and studied with MALDI-MSI. Whereas the chemical composition following aerobic (biotic) conditions was only slightly altered, the sample exposed to denitrifying conditions revealed evidence for significant polymer degradation (loss of signal intensity) and oxidation. Degradation was observed to occur more heterogeneously throughout the polymer material when exposed to denitrifying conditions, thus further demonstrating the power of MSI to study localized degradation processes of polymers and other substrates.

Ultrahigh molecular weight polyethylene (PE-UHMW) is a widely used material for replacing the acetabular cup of hip and knee joints. Despite this popularity, it suffers from relatively short lifetime with replacement often needed every 5-10 years.[152,153] Oxidation of the polymeric material has been recognized as a major contributor to this short lifetime. An interaction of the PE-UHMW with the surrounding biological environment consisting of synovial fluid is an important contributing to polymer modification. In this light, Fröhlich et al. have recently applied MALDI-MSI to study adsorption of lipids from the synovial fluid onto the polymer surface and its correlation with surface modification.[154] Following incubation of PE-UHMW in synovial fluid, the polymeric material was analysed with both MSI (spatial resolution of 10-150 µm) and SEM. After incubation, polymer surfaces were roughened and adsorption of biological materials could be observed with SEM. MSI allowed the localization and structural

identification of adsorbed lipids such as PC, PE and cholesterol directly from the substrates. Chemical specificity of MSI was increased by performing MS/MS imaging whereby characteristic fragment masses are detected and visualized. Localization of lipids was found to correlate with the presence of roughened substrate features. Given the strength of MSI to detect many molecular species simultaneously, detection of the polymer substrate itself was also possible. Interestingly, oxidized PE-UHMW was detected by *m/z* spacing of 74, indicative of PE-UHMW hydroperoxide, and was also found to be localized in areas of high lipid adsorption. Combined, application of MALDI-MSI to joint replacement materials provided the first evidence of preferential adsorption of lipids from synovial fluid onto roughened and oxidized surface areas. Oxidation can be rationalized by presence of reactive oxygen species in synovial fluid which can have detrimental effects on implant lifetime. Given the lubricating nature lipids play in both native and artificial joints, MSI provides a promising tool to help develop new joint materials that promote positive interactions with the surrounding biological environment. The same authors have also reported on the use of MALDI-MSI for localization of proteins adsorbed onto PE-UHMW incubated with synovial fluid.[154] On flat samples homogenous protein distributions were observed, while preferential adoption onto roughed or folded areas was observed. In line with the lipid results, this suggests that in vivo damaged regions are more susceptible to protein adsorption which may alter implant properties. In related applications concerning the localized interactions of biomolecules with biodegradable materials MALDI-MSI has also been deployed to study lipid and protein adsorption onto thermoplastic polyurethane grafts for vascular replacements.[155,156] For example, in one study by Fröhlich et al. the diffusion of cholesterol into the synthetic vessels wall was observed

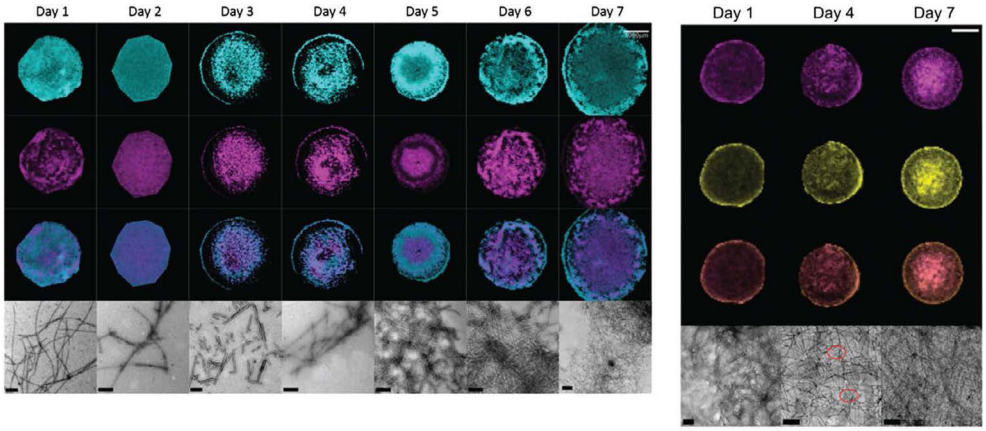

Figure 2.3: *(Left) Time-series MALDI-MSI images of a two component peptide mixture (IKHLSVN in cyan and IKFLSVN in magenta) from day 1-7. (Right) Time-series MALDI-MSI images of a two component peptide mixture (IKFLSVN in cyan and IKYLSVN in yellow) after 1, 4 and 7 days. Both MALDI-MSI datasets show the self-assembly process of the fiver mixtures. TEM images of the corresponding mixtures are provided below the respective MSI images. Reproduced from ref. 157.*

and tentatively attributed to the favourable thermoplastic polyurethane pore size facilitating small molecule diffusion.[156]

Insight into the self-assembly behaviour of mixed peptide fibres has also been recently obtained with MALDI-MSI.157 Self-assembling peptides (peptide 1= IKHLSVN, peptide 2 = IKFLSVN and peptide 3= IKYLSVN) were mixed into various two component systems and deposited onto ITO slides where they aged over time. After matrix application peptide fibre distributions were imaged using high resolution FTICR-MSI. Mixture A (peptide 1, Figure 2.3, cyan) and peptide 2 (Figure 2.3, magenta) was found to initially form long fibres with a relatively homogenous distribution of the two peptides (days 1-2). This state was hypothesized to be only kinetically stable. During days 3-4 the fibrils became smaller and this was correlated with fibre rearrangement and segregation of the individual peptides. This process was observed until day 7 whereas a thermodynamic steady state is reached and only segregated, individual fibres are observed. In contrast, peptide mixture 2 (peptide 2 and 3) initially formed a thermodynamically stable system whose morphology did not change significantly over time. MALDI-MSI revealed that both peptides were homogeneously distributed. TEM analysis revealed intermixed flat ribbon and twisted structures which were assumed to each correspond to single component fibre. Differences between the mixtures were attributed to the different hydrophobicity and non-covalent interactions. Unlike optical imaging techniques require labelling which can interfere with the self-assembly process, direct MSI analysis permits analysis of the unmodified peptides and study of their self-assembly behaviour into organized kinetically and thermodynamically favoured structures.

Carbon nanomaterials are attracting much interest for a diverse array of applications, including biomedical applications where they are loaded into the body. In such applications it is critical to understand how they are metabolized and in what organs they accumulate. Recently, laser desorption/ionization (LDI) has been applied to directly visualize the sub-organ accumulations of carbon nanotubes (CNTs), single-layer graphene (GO) and carbon nanodots (CD) after injection into mice.[158] In this approach direct LDI of dosed tissues (i.e., without the application of a MALDI matrix) was used to directly detect carbon nanomaterial by virtue of their low mass carbon cluster signals (e.g., Cn-, n=1, 2, 3, 4, 5, etc.). Carbon nanomaterials could be rapidly detected in various tissue such as kidney, spleen, lung, liver, brain and heart tissue. For example, Figure 2.4 shows results obtained from mice spleen revealing preferential accumulation of CNTs in the marginal zone of the spleen with subsequent lower concentrations observed in the red and white pulp, respectively. Quantitative MSI using dosed tissue homogenates for signal calibration was also performed and after calibration maximum signal could be calculated to be approx. 8 pg/20 µm pixel for CNTs in the spleen. Calculated detection limits were 0.02, 0.04 and 0.10 $\mu g.ml^{-1}$ for CNTs, GO and CDs, respectively. Quantitative results revealed the largest

uptake of CNTs and GOs in the lung, while CDs preferentially accumulated in the spleen. The extension of this method demonstrated the selective accumulation of drug loaded CNTs into a tumour, thus providing a powerful tool for targeted drug

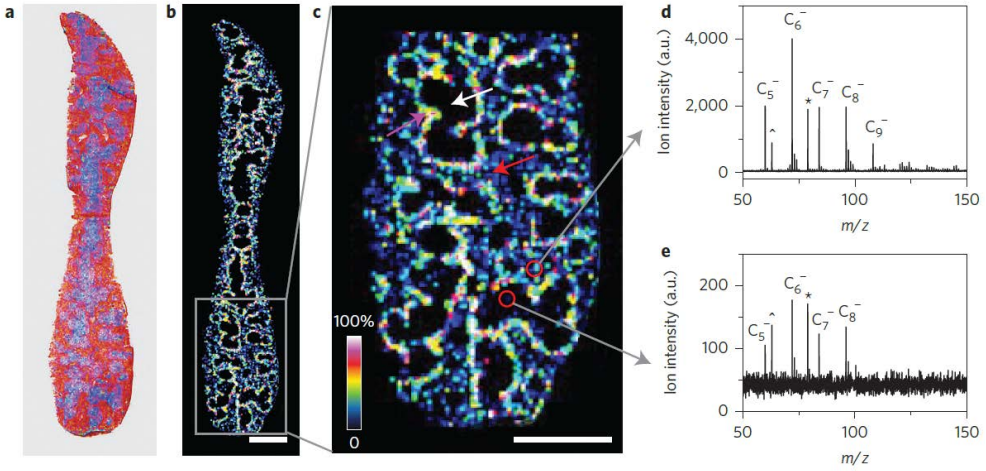

Figure 2.4: *Mapping of sub-organ distributions carbon nanotubes (CNTs) in mice spleen using direct laser desorption/ionization (LDI). (a) Optical image of the spleen tissue. (b) Ion distribution of CNT-specific m/z 72.0 throughout the spleen. (c) Expanded region of (b) revealing accumulation of CNTs in the red pulp of the spleen. Representative LDI mass spectra acquired from red and white pulp regions (d and e, respectively). Scale bars are 2 mm. Reproduced from ref. 158.*

delivery applications. In another application LDI-imaging of inkjet-printed patterns of functionalized gold nanoparticle has also been demonstrated.[159]

The above examples highlight a diverse array of materials-chemistry-focused MALDI-MSI applications. However, when compared to applications to biological tissues, these relative numbers are quite low. Nonetheless, we believe that the unique ability of MALDI-MSI to detect most molecular classes, combined with the extensive ability of high performance commercial instruments offering both high spatial resolution (10 μm) and high mass resolution, should make it a powerful approach for many researchers and industries where understanding the localized chemical composition, its changes to external factors, and interaction with the surrounding environment is key for material design and performance. It can be expected such approaches will increase in popularity in the near future.

2.4. AMBIENT MASS SPECTROMETRY IMAGING

Over recent years much work in the MSI field has focused on making a broader range of samples accessible. An important requirement for the methods discussed above is the requirement that the samples be placed in vacuum. As a result, many samples (such as those containing water) cannot be analysed in conditions that closely mimic their natural state. These requirements have spawned the field of ambient MSI

methods, that although generally possess lower resolution (typically approx. 50-300 µm), enable MSI analysis of samples in the open environment without any sample pre-treatment (e.g., matrix application). The following section will briefly discuss different MSI techniques that although have very few reported applications to biomaterial analysis to-date, have the potential to be very useful, possessing some unique qualities that are not shared by SIMS or MALDI. These techniques may be complementary to SIMS and MALDI analyses or employed for certain applications where SIMS or MALDI are not applicable, such as non-vacuum compatible samples.[160-168] These ambient MSI techniques can be highly adaptable, allowing optimization for different sample shapes and sizes with minimal effort.

Solvent-based techniques

One of the most popular ambient MSI techniques is desorption electrospray ionization (DESI) due to its simplicity and relative ease of operation.[160] For DESI, charged solvent droplets impact the surface creating a very thin fluid layer where analyte extraction and subsequent desorption occurs.[160,169] The spatial resolution achievable with DESI imaging is generally around 150 µm, however with optimized hardware and experimental parameters resolutions as low as 35 µm have been reported.[170-172] DESI-MS imaging offers lower spatial resolution than MALDI or SIMS due to the spray based desorption/ionization but is particularly useful for samples that are bulky, irregularly shaped, or require enhanced extraction of analyte from the substrate.[173] DESI-MSI has been applied mostly to biological tissue analysis,[163] although various other substrates such as TLC plates, rocks containing heterogeneous mineral deposits, bulk polymers and polymer coatings, and organic materials have also been studied.[174,175] For example, in the analysis of thermoset polymer-based coatings the performance of formulated antioxidants could be measured in situ without any sample pre-treatment (Figure 2.5).[175] Another example showcasing the broad applicability of DESI-MS is the surface analysis of biocompatible polymers ex vivo, providing insight into their interactions with living tissue. Suder and co-workers employed DESI-MS to investigate the plaque deposits on a polyethylene terephthalate vascular graft that was removed from a patient after 2 years serving to replace part of the femoral artery. Imaging cross sections of the plaque deposits revealed changing lipid profiles associated with atherosclerotic plaque formation and saturation of the polymer surface by endogenous lipids. These results demonstrate that DESI-MS is an ideal analytical approach for biomedical applications where artificial and biological materials interface due to its selectivity and relatively soft method for probing the sample.

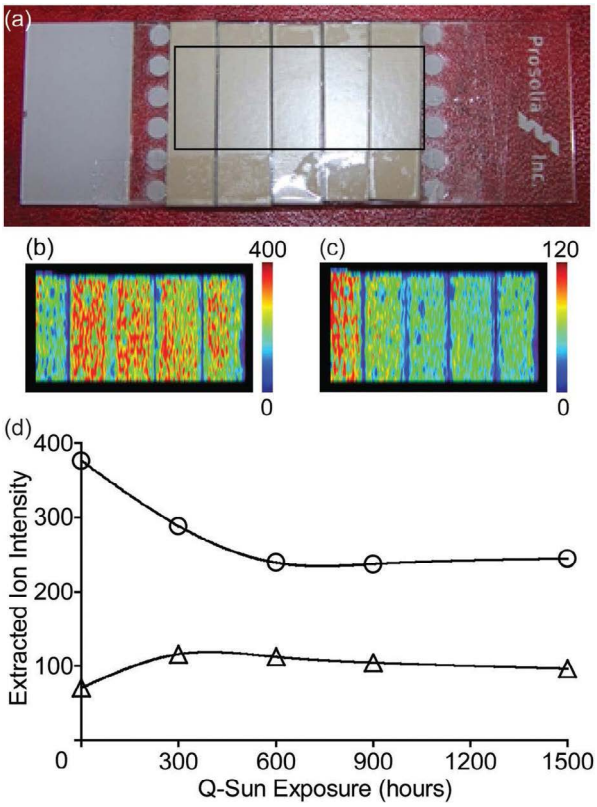

Figure 2.5: *(a) A photograph of a double draw-down panel consisting of two polyester-based paint formulations, a green pigmented coating containing no HALS (left) and a brown pigmented coating (right) containing TIN123 (2% wt of resin solids). (b) A representative extracted ion chromatogram (XIC) of the m/z 737.5 ion corresponding to $[M+H]^+$ ion of TIN123 acquired across the panel left-to-right using DESI-MS. (c) A photograph of coil coated metal samples cut from panels that were exposed to 0 (far left), 300, 600, 900, and 1500 hrs (far right) of Q-Sun artificial weathering and affixed to a microscope slide, and the resulting false color images of the extracted ion intensities (ion counts) at (b) m/z 737.5 and (c) m/z 609.5 by 2D DESI-MSI. (d) Extracted ion chromatograms integrated over 50 mm^2 for each exposure interval (0, 300, 600, 900 and 1500 hrs) for the ions at m/z 737.5 (open circle, o) and m/z 609.5 (open triangle, Δ). Reproduced and adapted from ref. 175.*

Alternative solvent extraction-based techniques have been developed that differ from DESI by decoupling the extraction and ionization steps.[176-180] These techniques have yet to be exploited for any true biomaterials applications but have potential use in the field including; liquid micro junction solid sampling probes (LMJ-SSP) in their various forms, nano-DESI, and liquid extraction surface analysis (LESA). The first two involve a continuous flow of solvent in contact with the surface, desorbing analytes at the point-of-contact followed by aspiration through an electrospray emitter. In comparison, LESA uses discrete amounts of solvent contained within a pipette tip to create a temporary liquid micro junction with the surface.[181-183] LESA is well equipped for applications where sample carryover interferes with continuous imaging

experiments but does limit the spatial resolution to >0.5-1 mm.[184] These liquid micro junction techniques would be excellent candidates for the analysis of delicate gels and nanofabricated materials that are not amenable to lasers, heat, or pneumatically-assisted sprays. For example, hydrogel scaffolds containing cell cultures or organoid assemblies, or where the surface integrity needs to be highly maintained for further analyses after MSI. For example, LESA-MS has been applied to study the deposition of tear lipids on worn contact lenses demonstrating the ability of such techniques to study the molecular processes associated with biofouling of polymeric surfaces.[185]

Laser desorption-based techniques

Laser desorption/ablation-based techniques are becoming increasingly popular for ambient MSI due to their high spatial resolution (down to 10 µm sampling spot size) and ability to be coupled to solvent sprays and plasma plumes for enhanced ionization. Three major techniques have been reported for MSI that combine laser ablation (LA) with an electrospray ionization source; laser ablation electrospray ionization (LAESI or MALDESI)[186], electrospray-assisted laser desorption ionization (ELDI)[187], and laser electrospray mass spectrometry (LEMS).[188] For these techniques the experimental setup is the same, differing only in the type of laser employed to ablate material that is then entrained within the electrospray plume flowing on-axis towards the MS inlet (see Figure 2.6).[189,190]

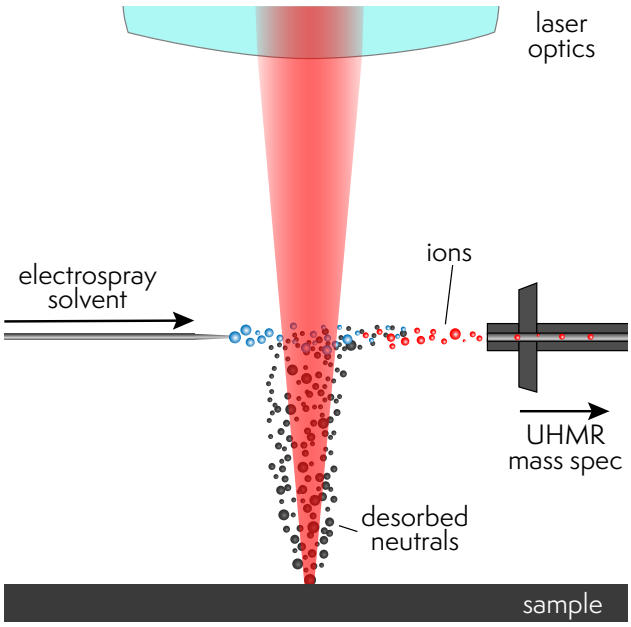

Figure 2.6: *Schematic overview of LAESI, ELDI and LEMS desorption techniques. Potential is applied between the electrospray needle and the mass spectrometer inlet, and a constant flow of solvent is sprayed from the needle tip. The laser (type dependent on technique) ablates material from the sample surface, which is entrained in the electrospray plume to be analysed in the mass spectrometer.*

An LMJ-SSP coupled with transmission laser ablation has been employed for the detection of insoluble surface components such as small oligomers of polyaniline and elemental analyses from thin metallic films.[191] This ambient imaging technique represents an ideal method for surface analyses where changing distributions of soluble analytes correlate with insoluble, heterogeneous polymer or metal substrates as this technique, theoretically, could be able to characterize both sample and substrate in a single acquisition.

As an alternative to solvent-based ionization, laser desorption-based ambient MSI can incorporate a plasma-based ionization step. Techniques involving corona, dielectric barrier or glow discharge ionization have been demonstrated for MS imaging under various acronyms.[192-195] Commonly, the sample ablation and ionization steps occur simultaneously, by intersecting the sample ablation plume with charged gas molecules while the laser is probing the surface. LA-FAPA decouples these steps.[193] Application demonstrators have included food stuffs, ink, pharmaceuticals and counterfeit detection.

Thermal desorption-based techniques

A recent innovation by Van Berkel and co-workers has led to the development of a thermal desorption (TD) imaging technique that provides the highest spatial resolution for ambient MSI currently reported.[196,197] The technique combines atomic force microscopy (AFM) with MS where a hybrid sampling probe provides co-registered topographical, band excitation nanomechanical[198], and chemical imaging of a surface.[199,200] By heating the AFM tip to 350 °C, thermal desorption coupled with ESI or atmospheric pressure chemical ionization (APCI) can be applied to surfaces with a spatial resolution corresponding to 2.0 µm x 2.5 µm pixel sizes.[199,200] The technique has been applied to printed inks, bacterial colonies on agar plates, and phase-separated polystyrene/poly(2-vinylpyridine) polymer blend thin films. For the polymeric samples, chemical compositions of valley and plateau regions within the surface were identified by co-registering topographical measurements and band excitation images with mass spectral chemical images (Figure 2.7a-d).[201] Figure 2.7 also shows a schematic representation of the AFM-MS setup designed by Van Berkel and co-workers and is an excellent example of the relative ease that ambient MS affords for ad hoc instrumentation. The AFM-MS technique also demonstrates the capability of simultaneous multimodal imaging data acquisition, providing added layers of information to each voxel in the dataset through co-registration of multiple data images.

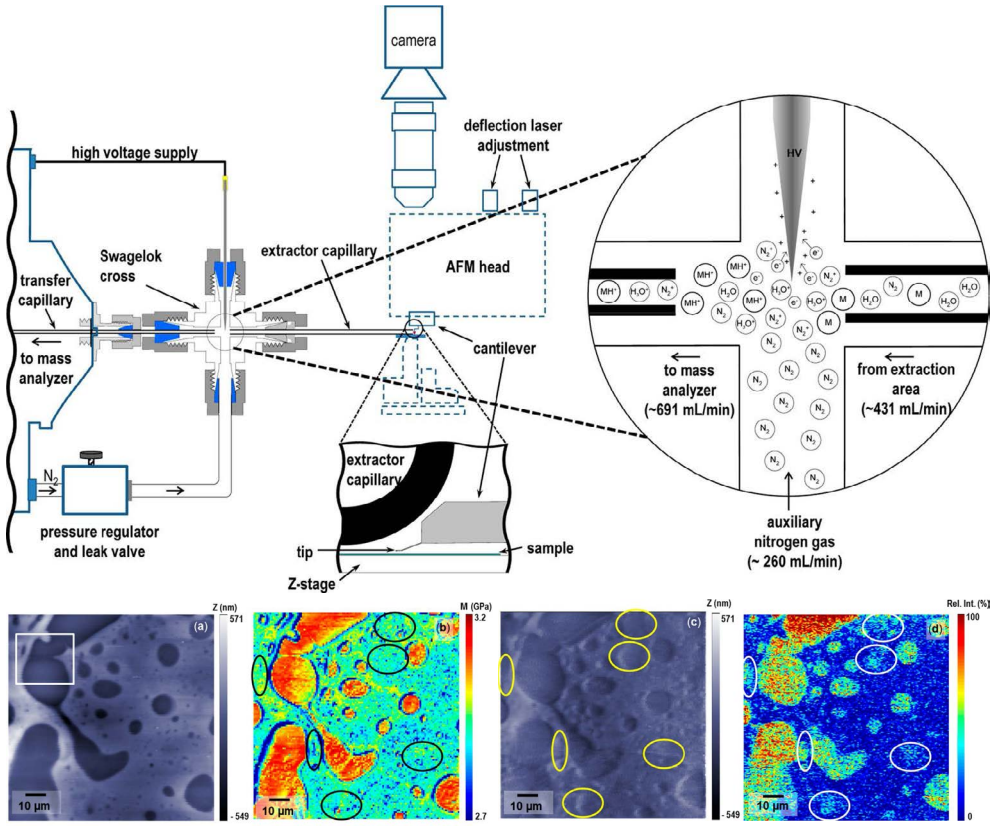

Figure 2.7: *Schematic illustration of the combined AFM-MS experimental setup with an enlarged view showing the details of the inline APCI and ion molecule chemistry and an enlarged view of the AFM nano-TA probe positioned approx. 0.3 mm away from the sampling capillary. Co-registered AFM (a) pre-pyrolysis topography image, (b) BE elastic modulus image, (c) post-pyrolysis topography image, and (d) mass spectrometry chemical image for m/z 106, obtained from an approx. 500 nm thin film of phase-separated polystyrene/poly(2-vinylpyridine) blend. The colour scale for the topography goes from dark to light, which is proportional to an increase in relative surface height. Highlighted ovals in panels (b), (c), and (d) indicate areas where the AFM topography, elastic modulus, and mass spectrometry images differ in terms of the presence of P2VP. Reproduced from ref. 201.*

2.5. CONCLUSIONS

The growing use of MSI for (bio)materials chemistry analyses is evidenced by the number of excellent applications detailed in this review. However, there is scope for MSI to be an even greater resource in the field of biomaterials research. Via this review we have not set out to provide a comprehensive review of all reported applications of MSI in the materials sciences, but rather have endeavoured to convey the unique opportunities alternative techniques offer to materials chemistry investigators. By highlighting the broad chemical sensitivity, specificity, and structural elucidation capabilities afforded by mass spectrometry and its complementarity with other surface imaging techniques we hope to illustrate the usefulness of MSI

approaches available to the materials science community. The ability to analyse many different molecules in a single experiment is particularly important for understanding the biological response to synthetic materials in vivo as it is always a complex array of metabolites, lipids, and proteins that are associated with phenotypic changes.

Ambient MSI techniques in particular are poised to see an increase in usage as there is no requirement for samples to be under vacuum, allowing the surface analysis of delicate substrates such as hydrogels and soft biomimetics – two substrates that are the foci of many emerging biomedical applications. The sampling probes used in many ambient MSI techniques are also very gentle, especially solvent-based methods such as nano-DESI, allowing the interrogation of delicate surfaces while leaving them physically unperturbed. Smart drug delivery systems comprise another emerging field of research, for example, nano- and micro-particles as drug carriers, in which SIMS imaging is uniquely capable to investigate, being able to monitor spatial distributions of inorganic particles within biological tissue as well as changes to select biomolecules within a single experiment, all at sub-micro spatial resolution. Further development of SIMS instrumentation and sample preparation including; alternative primary-ion beams more amenable to detecting labile molecules intact, increased MS/MS capabilities, and development of metal- and matrix-enhanced SIMS[202,203] for increased sensitivity and cryogenic preparation/analysis will undoubtedly result in greater use of the technique, not only for biomaterials but for many other imaging applications.

As for MALDI-MSI, due to its widespread popularity and strong commercial development for biological imaging applications we believe it is also well suited for biomaterials applications. Commercially available MALDI-MSI instrumentation is now able to provide a combination of both high spatial- and mass-resolution and major advancements are coming from increases in speed of acquisition and enhanced ionization methods. One notable advancement is the development of MALDI post-ionization that enables up to a two order of magnitude increase in sensitivity for certain molecules.[204] In addition, transmission geometry MALDI provides an avenue to increase spatial resolution to approx. 1 μm for UV transparent subtrates.[205] Such resolution can enable, for example, studying molecular interactions between cells and materials at the subcellular level. Perhaps the largest disadvantage of MSI at the moment is the complications in acquiring quantitative MSI data, i.e., absolute analyte quantities per unit area or volume. Such quantitative information is essential for many biomaterials applications yet is currently difficult to acquire with MSI. With careful experiment design, however, quantitative MSI data can be acquired and much progress has been made for this increasing in-demand capability over recent years through the development of various normalization strategies.[206]

In summary we strongly believe the MSI techniques outlined represent a diverse and useful set of tools for characterizing the molecular composition and

responses of (bio)materials and they should see a growing usage in the biomaterials chemistry field in the near future.

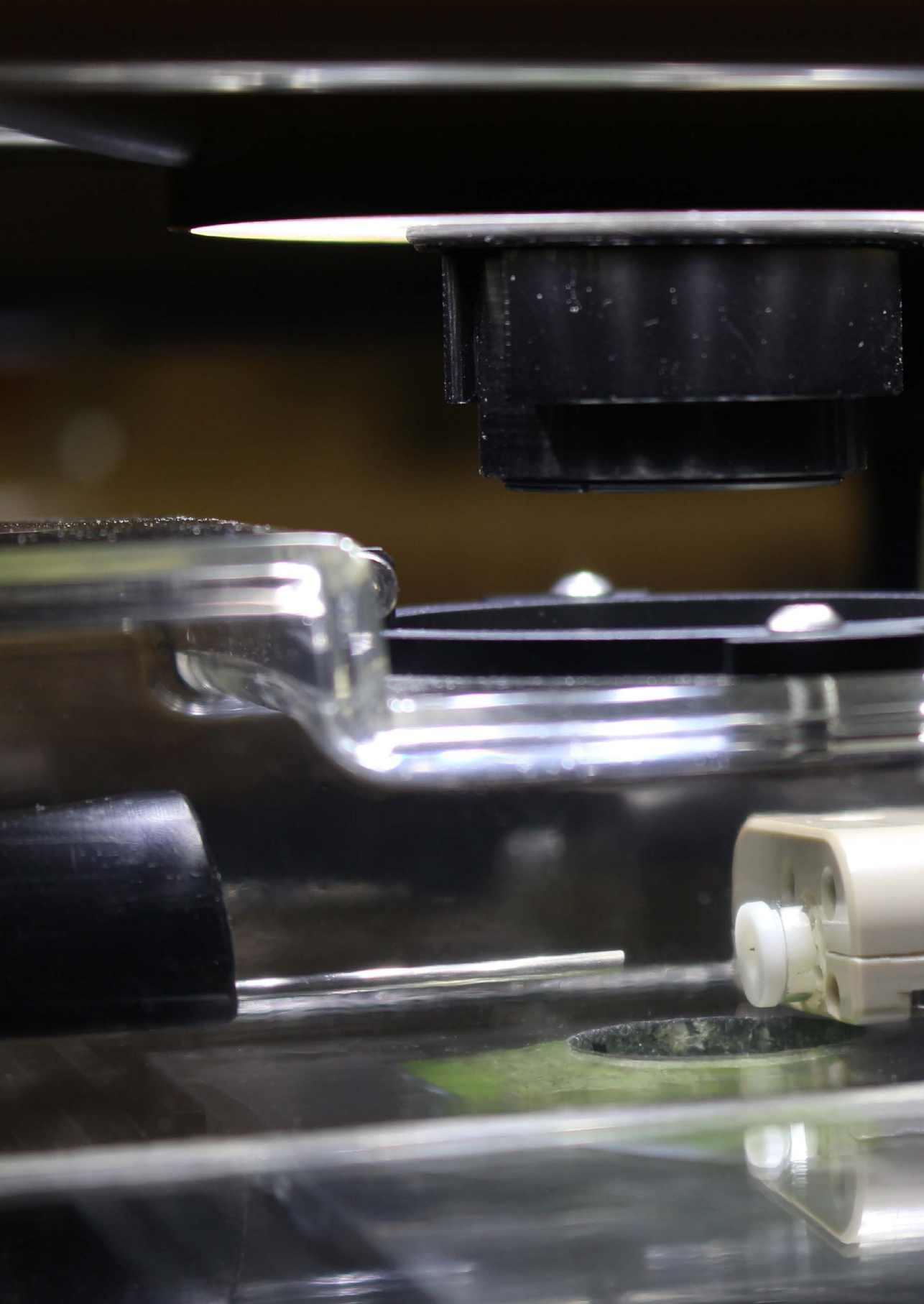

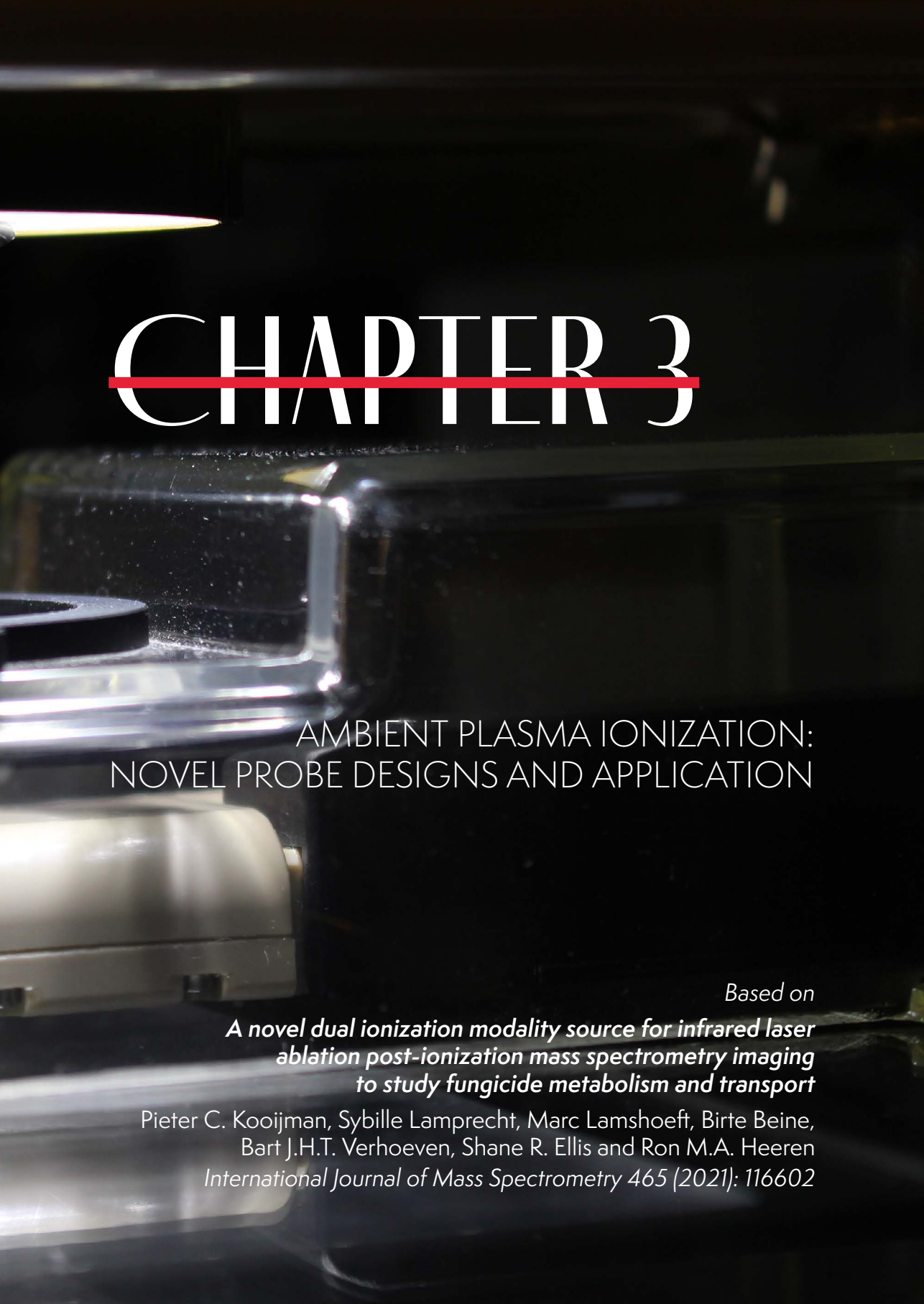

CHAPTER 3

AMBIENT PLASMA IONIZATION: NOVEL PROBE DESIGNS AND APPLICATION

Based on

A novel dual ionization modality source for infrared laser ablation post-ionization mass spectrometry imaging to study fungicide metabolism and transport

Pieter C. Kooijman, Sybille Lamprecht, Marc Lamshoeft, Birte Beine, Bart J.H.T. Verhoeven, Shane R. Ellis and Ron M.A. Heeren

International Journal of Mass Spectrometry 465 (2021): 116602

ABSTRACT

We present a novel probe design for ambient laser-based mass spectrometry imaging combining electrospray ionization (ESI) and atmospheric pressure chemical ionization (APCI) in a single probe, compatible with a commercial laser ablation electrospray ionization (LAESI) instrument. Here we describe the probe design considerations and features, as well as an in-house developed data processing routine designed to extract accurate mass spectrometry imaging data from ambient laser ablation post-ionization experiments. We characterize the probe performance in both APCI and ESI mode on a selection of compounds and show improved pixel-to-pixel repeatability for LA-APCI as compared to LAESI. We apply the dual ionization probe in APCI mode in a time series experiment to monitor agrochemicals on tomato plants. We investigate the translocation of fungicide isotianil and one of its metabolites, anthranilonitrile, by mass spectrometry imaging over a period of two weeks after application on a leaf surface. LAESI-MSI shows translocation of anthranilonitrile from treated leaves towards non-treated leaves. In summary, we demonstrate that LA-APCI imaging is a valuable addition to the ambient mass spectrometry toolbox, with particular advantages for imaging experiments across a variety of compounds.

3.1. INTRODUCTION

In recent years, mass spectrometry imaging (MSI) has proven itself as a valuable tool to uncover the spatial distribution of biologically relevant compounds[70] either in a targeted[207-209] or untargeted[210-213] approach. The scope of samples and compounds compatible with MSI has grown considerably as the technology has matured. Key driving force behind these developments has been matrix-assisted laser desorption/ ionization (MALDI) MSI[214]. MALDI offers superior sensitivity for many compounds and high spatial resolution (down to approx. 1 µm).[215] MALDI relies on surface extraction of analytes through the application of an UV absorbing matrix onto the sample surface, typically a thin tissue section. For many sample types, most notably animal or human tissue sections, MALDI has proven immensely powerful[216], but for plant material it is difficult to retain morphological information in this manner. Plant material contains a significant amount of water that makes it poorly compatible with most MALDI instruments that analyse the sample in vacuo. Desorption electrospray ionization (DESI) has been shown to efficiently sample the outer surface of a plant leaf, but does not penetrate the subsurface layer[217]. An approach for the analysis of plant material is needed, capable of direct sampling both the surface as well as the subsurface layers - without need for extensive sample preparation - under ambient pressure conditions.

LAESI-MSI

Many efforts have focussed on the development of ambient infrared laser-based sampling techniques coupled with a separate ionization step. The most developed of these techniques is called laser-ablation electrospray ionization (LAESI)[186] (or infrared matrix-assisted laser desorption electrospray ionization (IR-MALDESI)[218]). This molecular imaging technique has been developed to analyse biologic surfaces in their native state in an ambient environment (i.e. at atmospheric pressure). The infrared laser ablation wavelength of 2.94 µm in these experiments is chosen to couple directly to the hydroxyl vibrations of water in biological samples. The coupling of the IR laser desorption step to ESI enables us to locally detect a wide range of compounds, including the generation of multiply charged intact proteins[219]. This is challenging with MALDI-MSI. LAESI-MS has been used in the past to perform analysis on plants[189,220,221], tissue sections[218,222] and bacterial colonies[223,224] amongst others.

Drawbacks mentioned for this technique are a relatively low throughput[219], moderate spatial resolution (commonly performed at 100-250 µm spatial resolution)[225,226] and electrospray ionization is poorly suited for the analysis of non-polar compounds[227,228]. Another inherent drawback of the commercial LAESI geometry is limited repeatability (both pixel-to-pixel and between experiments). Electrospray ionization efficiency relies on a stable and constant electrospray plume, while each laser desorption event in LAESI introduces a potential disturbance. Several

groups have optimized experimental LAESI parameters to improve the stability of imaging experiments[224,229,230].

This paper describes a new ionization probe that addresses two of these drawbacks: the analyte electronegativity range and the repeatability of measurements. The ionization probe design that we describe is somewhat similar to the design idea of the dual ESI and APCI source introduced by Cheng et al.[231]. The design has been adapted significantly to be compatible with LAESI instrumentation. The probe enables atmospheric pressure chemical ionization (APCI), based on a dielectric barrier discharge (DBD) principle, without sacrificing the ability to utilize ESI-based post-ionization. DBD relies on the generation of charged species in a noble gas plasma environment. When in contact with atmospheric gases a cascade of charge-exchange reactions leads to analyte ionization under ambient conditions. This principle works well for a broad range of compounds, being more effective in ionizing non-polar compounds than electrospray ionization.[227,228] We have performed a general characterization of the system performance, looking specifically at the instrument sensitivity for several compound classes, as well as the pixel-to-pixel repeatability of both ionization techniques.

In this work we also describe the application of the dual ionization probe in a study to visualize the distribution of the fungicide isotianil (IST), one of its metabolites and native compounds in leaves of the tomato plant (Solanum lycopersicum) over time. Isotianil is a novel fungicide belonging to the group of plant defence modulators/inducers (FRAC Group P) as it induces systemic acquired resistance in plants. Isotianil is particularly effective to control rice blast and bacterial leaf blight. It is also active against some leaf spot diseases, powdery mildews, as well as against bacterial diseases like Pseudomonas sp. and Xanthomonas sp..[232] In contrast to most plant activators, isotianil is a prodrug which is slowly converted into the active compound, DCIT-acid, and anthranilonitrile (ANT)[233] (see Figure 3.1). Isotianil supposedly remains at the deposition site on top of the leaf surface, working as a depot by slowly releasing the active compound. In search of new applications for isotianil it is of great interest to obtain information on the interaction with and distribution through target crops of the pro-drug and its metabolites. For instance, the rate of metabolization of isotianil is crop specific and of great influence on the efficacy of isotianil as a fungicide. Earlier studies to answer these questions have employed autoradiography to monitor the distribution of ^{14}C or ^{15}O radiolabelled compounds through leaves.[234] This technique is sensitive and can monitor a large sample area without sample preparation. However, autoradiography can only be applied in a targeted manner and cannot distinguish

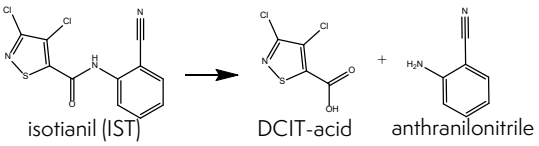

Figure 3.1: *Isotianil metabolism route to the active compound DCIT-acid and anthranilonitrile.*

between the initial labelled molecule and possible metabolites. It requires the time-consuming and expensive synthesis of radiolabelled compounds and does not provide information on endogenous compounds in the sample. MSI based approaches in the ambient environment can investigate the distribution of a variety of plant-based molecules, agrochemicals and their metabolites without the use of any radiolabels. We designed a time series MSI experiment on isotianil treated leaves using the LA-APCI mode of our novel ionization probe to investigate the translocation of IST and its metabolites over time.

3.2. MATERIALS AND METHODS

LAESI-MS system

All experiments were performed using a modified Protea DP-1000 LAESI system (Protea Biosciences, US) coupled to a Thermo Q-Exactive mass spectrometer (Thermo Scientific, Bremen, DE), unless stated otherwise in the text. The DP-1000 LAESI system was equipped with an external inlet capillary heater, set to 190 °C for all experiments, and a 2.94 µm 10 Hz IR OPO laser with a fixed focal length of 50 mm. The resulting laser spot size was approximately 200-250 µm, with a step size of 250 µm for all imaging experiments. The sample stage was cooled to 4 °C and the sample bay was continuously flushed with nitrogen gas for all experiments to maintain the sample water content during analysis[235]. The mass spectrometer was operated at a set mass resolution of 17500, *m/z* range of 100-350 and an injection time of 20 ms for the LA-APCI time series imaging experiments. The high mass resolution imaging experiments were performed with a resolution setting of 120,000 at *m/z* 200, with 820 ms injection time. The MS inlet capillary temperature was set to 190 °C, the S-lens level to 50 arb. units. For the limit-of-detection (LOD) measurements the mass range was kept at *m/z* 100-550 for all experiments.

Chemicals

Isopropyl alcohol, acetonitrile, water, HPLC-grade methanol and formic acid 99% were purchased from Biosolve B.V. (Valkenswaard, The Netherlands). Ethylene glycol, cholesterol, verapamil hydrochloride, sodium taurocholate hydrate, atrazine, anthranilonitrile were purchased from Sigma Aldrich Chemie Gmbh, Germany. Fluopyram and isotianil standards were supplied by Bayer AG, Crop Science, Germany. Argon gas (5.0 purity) was purchased from Linde Gas.

Dual modality ionization probe

The dual modality ionization probe was designed to replace the original ESI probe from the DP-1000 unit. The probe is fully interchangeable with the standard probe of the DP-1000 unit and requires no changes to experimental parameters - when operated in the LAESI mode - compared to the original probe. The dual modality

ionization probe features a radial DBD design, surrounding the coaxially placed ESI emitter. The basic concept of the new dual modality probe is shown in Figure 3.2 and an additional schematic design and photo is added in Figure S3.1. Our design deviates from the design presented by Cheng et al.[231] in several ways: (1) the addition of a metal electrospray emitter and consequential insulation between the APCI ground electrode and the electrospray emitter; (2) the miniaturisation of the whole system to fit parallel to the sample at the correct height offset; (3) the addition of a PTFE glass nozzle to focus the gas stream; and (4) the addition of thermal and electric insulation of the probe to protect the sample integrity. The dual ionization probe can be operated in two modes, either APCI or ESI. Switching between LAESI and LA-APCI mode takes approximately 60 sec, plus time for electrospray stabilization.

In APCI mode, argon gas is fed into the DBD chamber (entering Figure 3.2 from the left). An RF potential (input voltage 30 V, 30.7% duty cycle and 90.0 kHz output) was applied to the copper outer electrode by a G2000 power supply (Redline

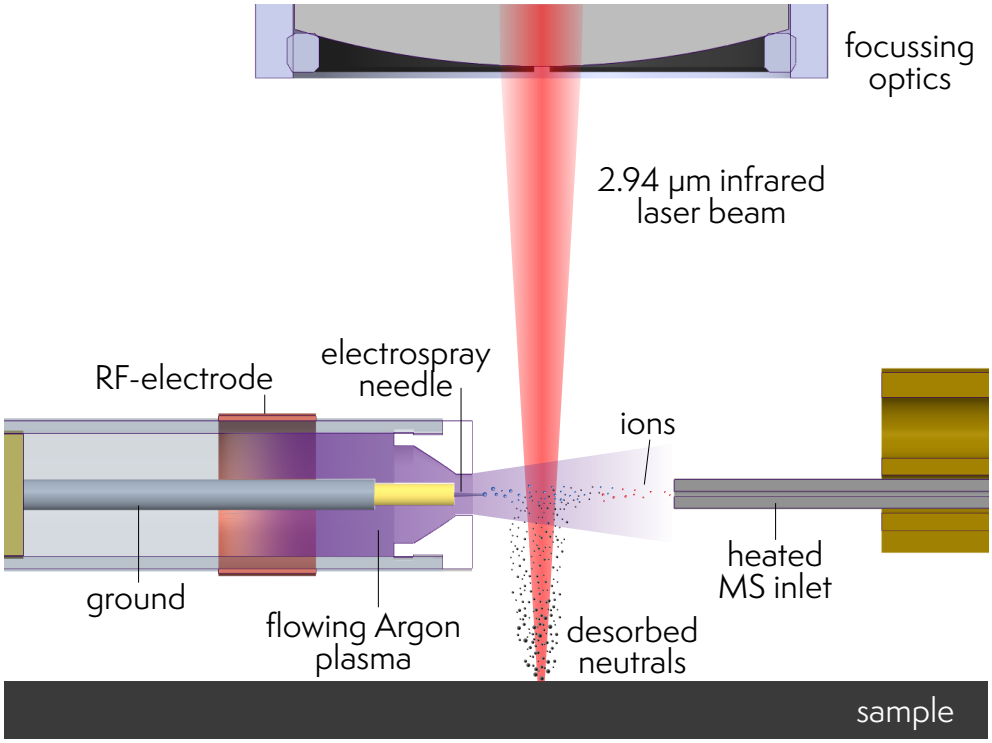

Figure 3.2: *Schematic representation of LAESI/LA-APCI geometry. The main components of the dual ionization probe are shown (left), the mass spectrometer inlet (right), the laser and focusing optics (above) and the sample (below). Upon a laser ablation event, neutral particles are released into the void between the ionization probe and the mass spectrometer inlet. Here, the neutrals receive a charge from either the electrospray nebula or the APCI gas stream. The constant electric field gradient between the ionization probe and MS inlet drives the analyte ions towards the mass spectrometer inlet.*

Technologies, Baesweiler, DE) and tuned to the lowest RF amplitude that would sustain a stable discharge (approx. 1 kV peak-to-peak in our experiments). The quartz dielectric barrier limits the discharge current to the central, grounded, stainless-steel counter electrode. A PEEK sleeve insulates the grounded electrode from the coaxially placed stainless steel Metal TaperTip emitter (320 µm o.d., 100 µm i.d., New Objective, Woburn, MA, USA). A +700 V or -700 V DC potential was placed on the emitter for MS analysis in positive or negative mode, respectively. The gas flow rate of Argon 5.0 was controlled by a flow controller (Bronkhorst, Veenendaal, NL) at 50 mL min^{-1}, which was determined to be optimal for this setup.

In ESI mode, the probe works similarly to the original LAESI DP-1000 probe (e.g. the same electrospray emitter) and has the same overall geometry. In this mode, up to 1 L min^{-1} of nitrogen sheath gas flows through the quartz tube, exiting parallel to the electrospray emitter. The optimal operational parameters for ESI mode depend on the application and are comparable to the standard DP-1000 system. We have chosen to use settings commonly used in literature[221,223,236] for the experiments shown here: 4000 V DC potential with a solvent flow rate of 1.2 µL min^{-1} 1:1 methanol/water + 1% (v/v) formic acid in positive mode. 2700 V DC potential with a solvent flow rate of 1.2 µL min^{-1} 2:1 methanol/chloroform + 0.1% (v/v) acetic acid in negative mode.

3.3. EXPERIMENTAL PROCEDURES

Source characterization

Sensitivity measurements were performed on standards following a protocol adapted from Vertes and Anderton (see Protocol S3.1) both for LAESI and LA-APCI. Most notably, 1:1 isopropyl alcohol:ethylene glycol (v:v) was used as a solvent to promote solubility of less polar compounds and reduce adverse effects from evaporation and surface tension.

Fluopyram, cholesterol, atrazine and anthranilonitrile were individually diluted in 1:1 isopropyl alcohol/ethylene glycol to form dilution series ranging from 100 µM to 50 nM. Verapamil and taurocholic acid were diluted in the same solution to form concentration series ranging from 10 µM to 500 pM, because these compounds are known to be easily detected in LAESI. The isotianil dilution series (100 µM to 50 nM) was prepared in 1:1 isopropyl alcohol/ethylene glycol, though it should be noted that isotianil proved difficult to dissolve in all IR-laser compatible solvents that we tested. All compounds, except taurocholic acid were measured in positive mode, for both ESI and APCI mode. 10 µL was spotted onto a Protea 96-well target plate for each standard and concentration. Each well was irradiated with 10 shots at 70% laser power (0.8 mJ, $\sigma \approx 1\%$) and 10 Hz in sequence from low to high concentration. The full sequence was repeated three times on the same target plate.

To determine the signal-to-noise ratio for each analyte, the average peak intensity was determined per experiment (36 scans averaged) by a custom Matlab script. The

LOD and LOQ were determined as 3 and 10 times the standard deviation of the noise, respectively. The average noise level was provided by the Xcalibur software package (Thermo Scientific Inc., San Jose, US).

Fungicide detection in plant leaves

Tomato plants were supplied and treated by Bayer Crop Science. On day 0 multiple leaves were spotted with 5 times 10 µL of fungicide formulation (Bayer AG, Monheim, DE) (250 ppm isotianil) directly the base of the leaf and left to dry. For each time point leaves were collected, individually packed in air-tight zip-lock bags and kept frozen at -20 °C until analysis. In addition, leaves were collected that were not treated, but were on the same plant as a treated leaf (which we refer to as 'distal leaves'). The sample was left to thaw while packed shortly prior to analysis. Thawed, the leaf was transferred onto a plain glass slide (top-side up) and inserted into the sample bay and kept at 4 °C. For each sample, a region containing approx. 7000 pixels was selected covering both the leaf base and the tip of the leaf. Each position was irradiated 6 times, at 5 Hz and 70% laser power (1.1 J/cm^2) followed by 2 seconds of dwell time. The sample is fully penetrated for both LAESI and LA-APCI using these settings.

The method used to prepare the samples for the high mass resolution experiments (Page 58) and Figure S3.3-Figure S3.5 is slightly different. The leaves were washed by immersion in 80% acetonitrile solution directly after harvesting. After drying the samples were mounted onto a glass slide using double sided tape. The samples were subsequently analysed immediately after mounting, alleviating the need for cryostorage and thawing.

Data processing strategy

A data processing strategy was developed in-house to handle continuously recorded, pulsed extraction imaging experiments on ion trap-based systems (e.g. FT-ICR or Orbitrap). In most post-ionization experiments, acquisition of mass spectral data occurs independent from the laser ablation event. Therefore, spectra need to be identified, assigned to a given sampling position, and extracted for data processing. We developed a spectral extraction algorithm in MATLAB (MathWorks, Inc., Natick, USA) based on the ChemomeTricks platform[237]. This algorithm relies on two key parameters: (1) a source trigger pulse recorded in parallel with the mass spectral data on an analog input channel and (2) the extracted ion chromatogram of one predefined sample related peak. The correct spectral number for each pixel is automatically determined by correlating the source trigger pulses to peaks in the extracted ion chromatogram. The spectral summation window width and image size information (step size, x/y-dimensions) are based on analysis parameters extracted from LAESI DP-1000 metadata. In addition, the algorithm determines the mass spectral bin width across the spectrum, based on the data acquisition rate, and corrects for possible

missing or erroneous triggers. The peak-picked imaging dataset is then exported to the ChemomeTricks[237] data format and imzML. All mass spectrometry images shown are plotted on a linear scale using the viridis colormap, with TIC normalization. The viridis colormap has been proposed as a 'fair', representative and colour-blind friendly alternative to other commonly used colormaps in MSI.[238]

3.4. RESULTS AND DISCUSSION

LA-APCI ionization principle

When the source is operated in APCI mode, an argon plasma is created in the chamber via a Townsend-type discharge. The argon plasma mixes with atmospheric air near the exit of the probe, upon which a charge transfer cascade ionizes laser desorbed neutrals in a manner analogous to traditional APCI approaches. The electric field gradient between the probe and the MS inlet enhances (approx. 10-fold signal increase) the sensitivity of the source by directing positively charged particles towards the MS inlet, without significantly altering the observed ions. The most abundantly observed species in APCI mode are singly protonated ions, though radical ions (approx. 3% of the singly protonated peak intensity) and ammonium adducts (<30% of the singly protonated) can also be observed.

Table 3.1: *An overview of all compounds monitored in the source characterization protocol and their respective LOD, LOQ and RSDs for LAESI and LA-APCI*

Compound	Structure	Observed species	MS spectrum		LOD	LOQ	RSD
Anthranilonitrile (ANT) M_{mi} = 118.05 gmol^{-1}	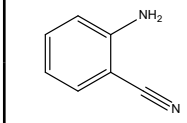	$[M+H]^+$: 119.0604	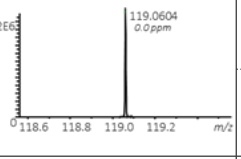	LAESI	486 nM	1.54 µM	1.08
				LA-APCI	391 nM	1.53 nM	0.434
Atrazine M_{mi} = 215.09 gmol^{-1}	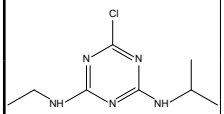	$[M+H]^+$: 216.1010 $[M]^{\bullet+}$: 215.0938	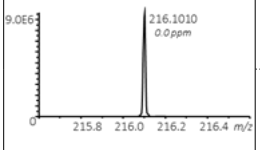	LAESI	12.2 nM	50.7 nM	0.637
				LA-APCI	46.8 nM	139 nM	0.445
Isotianil (IST) M_{mi} = 296.95 gmol^{-1}	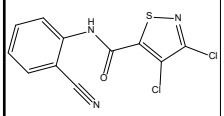	$[M+H]^+$: 297.9603	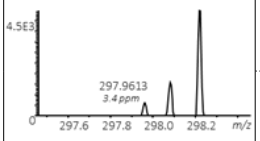	LAESI	-	-	-
				LA-APCI	-	-	-
Cholesterol M_{mi} = 386.35 gmol^{-1}	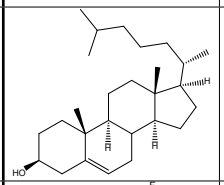	$[M-OH]^+$: 369.3516	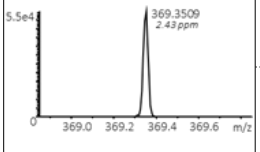	LAESI	2.47 µM	7.08 µM	1.09
				LA-APCI	22.2 µM	51.7 µM	1.23
Fluopyram M_{mi} = 396.05 gmol^{-1}	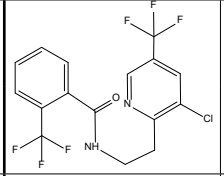	$[M+H]^+$: 397.0537	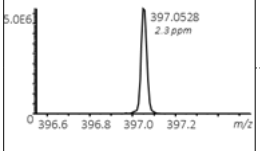	LAESI	27.0 nM	102 nM	0.516
				LA-APCI	33.0 nM	119 nM	0.494
Verapamil M_{mi} = 454.28 gmol^{-1}	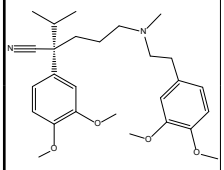	$[M+H]^+$: 455.2904	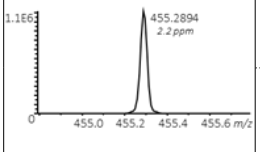	LAESI	13.0 nM	40.3 nM	0.868
				LA-APCI	29.7 nM	97.5 nM	0.558
Taurocholic acid M_{mi} = 515.29 gmol^{-1}	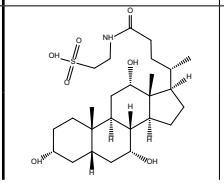	$[M-H]^-$: 514.2844	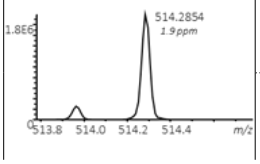	LAESI	47.0 nM	156.6 nM	0.815
				LA-APCI	52.7 nM	181.1 nM	0.805

Table 3.1 shows the compound structure, monoisotopic mass, observed species, limit-of-detection, limit-of-quantitation and relative standard deviation. The mass spectra are averages of a single measurement point of the highest concentration of each compound. All spectra shown are 1 Th wide.

Source characterization

To characterize the performance of the probe we determined the limit-of-detection, limit-of-quantitation and repeatability on seven compounds in both ESI and APCI mode. These compounds were chosen for their relevance to the fungicide distribution study (anthranilonitrile, isotianil), their bioactivity (atrazine, fluopyram, cholesterol) or because they are known for LAESI sensitivity testing (verapamil and taurocholic acid)[186,239,240]. The results are summarized in Table 3.1.

Table 3.1 shows that LAESI and LA-APCI modes have comparable sensitivity for fluopyram, anthranilonitrile and taurocholic acid. LAESI exhibited higher sensitivity for cholesterol and verapamil, and to a lesser extent atrazine. In all cases except cholesterol - in which LA-APCI sensitivity was significantly lower - the LA-APCI results have less variation (lower RSD values) than the LAESI data, thus having better pixel-to-pixel repeatability. Our observations suggest this is due to frequent disturbances of the electrospray plume by laser ablation events in LAESI experiments. Visual observations have shown ablated material and/or pressure wave effects cause the electrospray regime to alter temporarily which induces spray instabilities. This influences the ionization efficiency for subsequent laser ablation events. LA-APCI, which relies on an ionized gas flow, suffers significantly less from these effects because the generation of reactive species in the DBD chamber is not affected by ablation events. Most of the remaining variation in our LA-APCI measurements is presumed to originate from variation in the laser ablation event itself.

Calibration curves were generated for all compounds (included in Figure S3.2), except for isotianil. Isotianil dissolved poorly in all IR-laser compatible solvents that we considered for this experiment, due to its strong hydrophobic character. This characteristic also makes isotianil a prime candidate for APCI-based ionization. In this source characterization study no signal was obtained from isotianil with LAESI. We were able to obtain a spectrum with LA-APCI but only at a 100 μM concentration. This spectrum could have been produced from non-dissolved particulate matter. From the isotianil distribution studies (below) however, we have observed LA-APCI to be quite sensitive to detect isotianil on a leaf surface, in contrast to LAESI. In the following section, we will demonstrate how LA-APCI MSI can be used to monitor the isotianil distribution and the distribution of one of its metabolites on a plant surface.

Visualizing the translocation of fungicide isotianil and metabolites in tomato leaves

Next, we investigated the ability of LA-APCI-MSI to visualise the translocation of the isotianil distribution after its local application to the base of a tomato leaf. We were able to simultaneously image several endogenous molecular species combined with metabolites of isotianil. The isotianil metabolite anthranilonitrile (ANT) distribution was also subject of study. Leaves were harvested from the plant 2, 4, 7, 11 and 14 days after local application of isotianil formulation at the base of each leaf, and measured after cryostorage. The control specimen, harvested on day 0 without application of the fungicide formulation exhibited no isotianil or ANT signal. Figure 3.3 shows the translocation of isotianil and ANT during the course of this experiment. A fragment of phenylalanine (2-phenyl-ethenamine), a confirmed tomato plant endogenous amino acid[241], was monitored as a reference molecule to visualize the leaf surface (Figure 3.3c). The identity of 2-phenyl-ethenamine was confirmed through a separate experiment (data not shown). The LA-APCI images shown in Figure 3.3 took between 6 and 9 hours to acquire per leaf.

The isotianil images show that this compound is still fixed on its application site, even after 14 days. The highest TIC normalized signal intensity is visible on the first measurement day, gradually diminishing in average normalized signal intensity to 50% by day 14. This allows us to estimate the metabolic rate of isotianil in tomato leaves. Figure 3.3 shows anthranilonitrile is most abundant at the application site, with a similar pattern to that of isotianil. In contrast, Figure S3.3 shows homogenous distributions of anthranilonitrile over the entire tomato leaves. These leaves have been washed prior to analysis (see Page 50) and therefore contain only trace amounts of isotianil on the surface, with most of the isotianil still present absorbed into the leaf tissue. The leaves of Figure 3.3 have been frozen and thawed with the isotianil residue still on the leaf surface and thus contain a much higher concentration. This leads us to believe the most intense anthranilonitrile signal in Figure 3.3 is in fact a laser fragmentation product of isotianil, as opposed to a metabolite.

The anthranilonitrile signal - normalized to the TIC - in the leaf surrounding the application area rises steadily, from ~$1.5e^{-3}$ on day 2 to ~$5e^{-3}$ on day 14. Figure 3.3d shows the ratio between the anthranilonitrile and isotianil signal intensities – summed for the entire image area. This ratio shows the relative concentration of anthranilonitrile increases up to day 10, before receding at day 14. We therefore conclude that - as isotianil is converted over time - anthranilonitrile distributes throughout the tomato leaves.

Interestingly, we are able to obtain very high signal-to-noise ratios (up to S/N 3000) on isotianil desorbed from the leaf surface (Figure 3.3), in contrast to the LA-APCI LOD results. We conclude isotianil is not a suitable compound for liquid based limit-of-detection measurements in IR-laser setups. As an approximation we can use

the amount of isotianil applied as a reference to estimate the sensitivity of our setup. A single pixel of the application area should contain approximately 280 pmol of isotianil, which should theoretically yield an LOD of 450 nmol cm^{-2}.

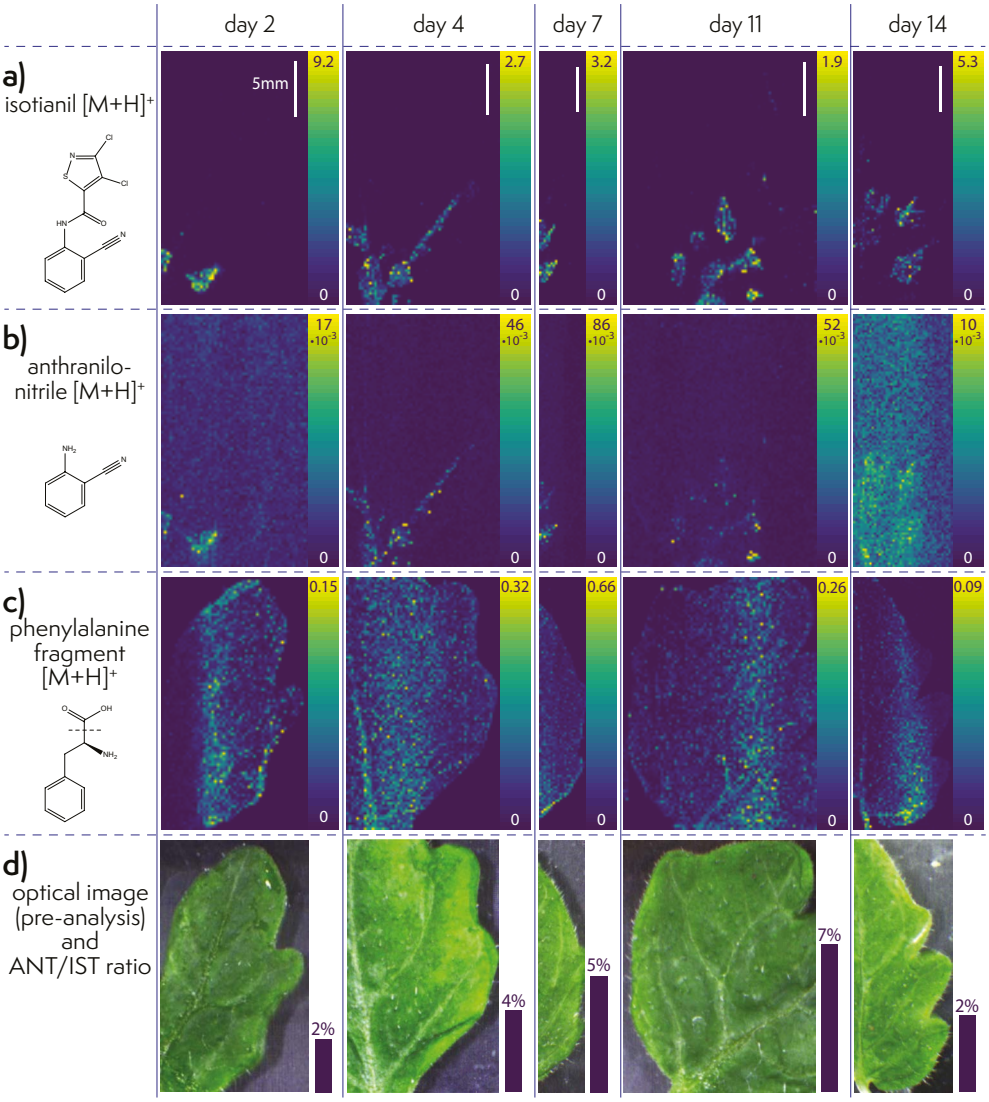

Figure 3.3: *Time series showing the distribution of isotianil (IST) (a) and its metabolite anthranilonitrile (ANT) (b) using LA-APCI mass spectrometry imaging. Leaves treated locally at the base with IST were harvested 2, 4, 7, 11 and 14 days after application and measured after cryo-storage. The control specimen, harvested on day 0, without application of the fungicide formulation exhibited no IST or ANT signal. The distribution of the phenylalanine fragment 2-phenyl ethenamine is (c) and the pre-analysis optical images (d) are added for reference. The ratio between the total summed anthranilonitrile and isotianil signals is plotted in d).*

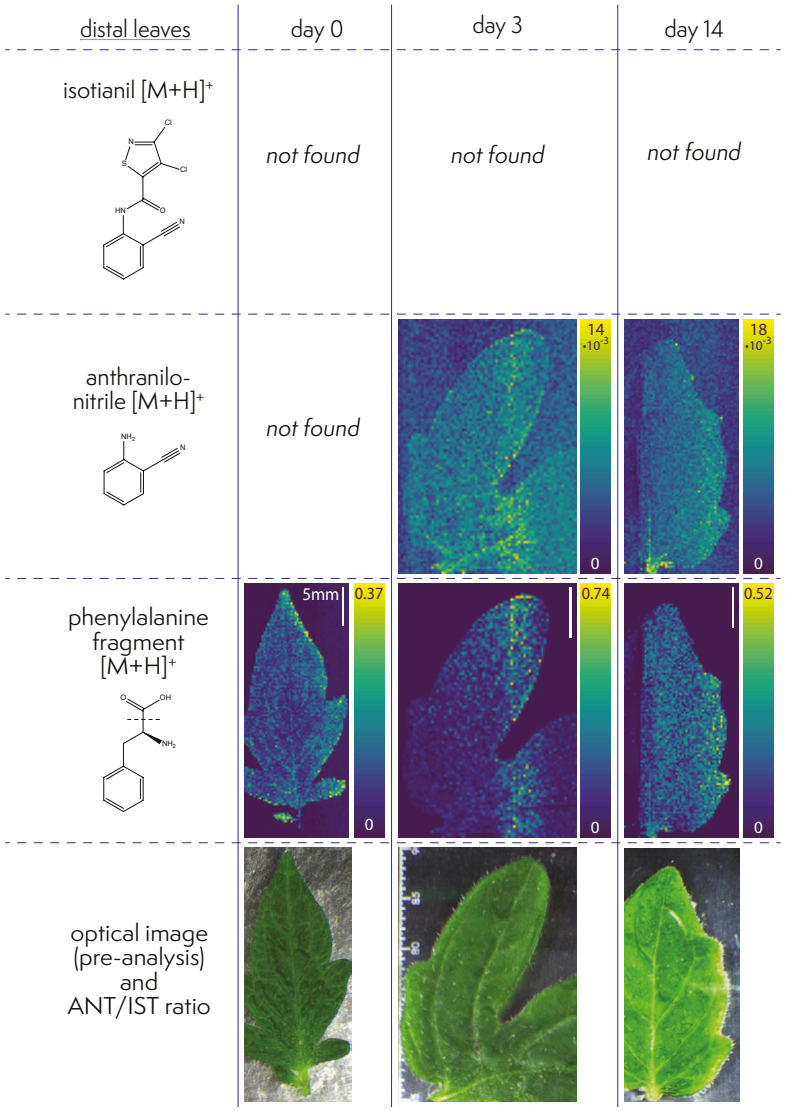

Figure 3.4: *Mass spectral images of anthranilonitrile detected in a distal leaf of a treated plant 3 and 14 days after application. Isotianil was not detected in any of samples. The leaf harvested on day 0 - before treatment of the plant - shows no signal for either isotianil or anthranilonitrile. The distribution of endogenous metabolite phenylalanine and the optimal images are added for reference. All images are plotted on a linear scale and TIC normalized.*

ANT distribution is distal leaves

So far, we investigated the translocation behaviour of IST and ANT within the leaf upon which IST was applied. For the effectiveness of a fungicide it is equally important if and how the fungicide translocates to other parts of a plant. We harvested untreated leaves from tomato plants carrying several treated leaves at three time points: day 0,

day 3 and day 14. Figure 3.4 shows the translocation of the compounds over time in these "distal" leaves. Isotianil is not detected in any of the distal leaf samples, proving that isotianil stays immobilized at the application site. Anthranilonitrile was not detected in the control sample harvested on day 0, but was detected with a TIC normalized signal intensity of ~$7e^{-3}$ and ~$11e^{-3}$ in the day 3 and day 14 samples, respectively. This is markedly higher than the signal intensity found outside the application area of the treated leaf, demonstrating translocation of anthranilonitrile from treated leaves towards non-treated leaves. Phenylalanine fragment MS images and the optical images are added for reference.

High resolution LA-APCI imaging confirms compound identity

We repeated our imaging experiment on a Thermo Orbitrap Elite system with high mass resolution to confirm our compound assignments through accurate mass measurements and MS/MS. The accurate mass measurements are shown in Figure 3.5.

Figure 3.5a is a single pixel spectrum from this experiment. LAESI spectra (and in fact most ambient desorption techniques) and LA-APCI spectra contain a significant amount of background ions. These background ions could originate from solvent contaminants, laboratory air contaminants or other sources. As can be seen in Figure 3.5b-d our single pixel spectra contain some interfering compounds, that require high mass resolution to resolve. With a mass resolution of 120,000 it is possible to create mass spectral images with high contrast, even for low intensity compounds in the presence of isobaric interferences. This comes at a price of time, taking 11 hours to record the images shown in Figure 3.5e-g. With longer total mass spectrometer scan times (in this case 1.38 seconds, with a C-trap injection time of 820 ms) the period that the C-trap is not accumulating ions can become significant (i.e. low duty cycle, see **Chapter 5**), and can coincide with laser ablation events. The periodic loss of analyte ions results in a pattern of analyte ion intensity dips. This effect is visible in Figure 3.5f as a striped pattern in embedded in the image. Nonetheless, mass spectrometry imaging can measure endogenous compounds and target molecules simultaneously, as demonstrated in Figure S3.4 for a tomato leaf and Figure S3.5 for a grapevine leaf. LA-APCI can generate high quality, crisp mass spectral images if both high selectivity (either by mass resolution, MS/MS or ion mobility) and a high duty cycle are provided, as shown in Figure S3.4 and Figure S3.5.

Combined ESI and APCI post-ionization

Finally, we investigated the possibility to perform both ESI and APCI at the same time. The combination of APCI and ESI mode was found to be feasible and generates molecular ion species characteristic for either mode simultaneously. However, the parameter range suitable for simultaneous APCI and ESI mode does not match the

optimal parameter range of either of the modes when used separately. Consequently, the sensitivity of the system in combined mode is significantly reduced. A better alternative is to perform ESI and APCI mode MSI imaging in sequence. Switching between ESI and APCI mode is relatively fast, in the order of seconds, though both ionization modes require some time to stabilize after initialization (5-10 minutes). Therefore, switching between modes in between pixels is not feasible. However, APCI and ESI mode images can be recorded in sequence on the same sample area if a larger grid size is chosen and a one-pixel offset is used between the images.

Combined ESI and APCI post-ionization

Finally, we investigated the possibility to perform both ESI and APCI at the same time. The combination of APCI and ESI mode was found to be feasible and generates molecular ion species characteristic for either mode simultaneously. However, the parameter range suitable for simultaneous APCI and ESI mode does not match the optimal parameter range of either of the modes when used separately. Consequently, the sensitivity of the system in combined mode is significantly reduced. A better alternative is to perform ESI and APCI mode MSI imaging in sequence. Switching between ESI and APCI mode is relatively fast, in the order of seconds, though both ionization modes require some time to stabilize after initialization (5-10 minutes). Therefore, switching between modes in between pixels is not feasible. However, APCI and ESI mode images can be recorded in sequence on the same sample area if a larger grid size is chosen and a one-pixel offset is used between the images.

3.5. CONCLUSION

We have designed and tested a novel ionization probe for ambient IR-laser based desorption mass spectrometry combining both ESI and APCI modalities for use in a LAESI-MS imaging platform. ESI mode proved more sensitive for some tested compounds, whereas APCI mode was more sensitive for isotianil. Overall, APCI mode has shown to have a higher pixel-to-pixel repeatability. We argue this is due to the nature of dielectric barrier discharge – suffering less from ablation event disturbances than ESI mode. This is corroborated by our observations in imaging experiments, in which LA-APCI imaging is more robust and contains significantly less instrumental variation compared to LAESI imaging experiments. We have tested our new approach for the investigation of plant-based metabolism of agrochemicals and endogenous molecules on plant leaf surfaces. We were able to visualize the translocation behaviour and metabolism of isotianil in tomato plants over time, while simultaneously monitoring endogenous compounds. The method presented here has added analytical value for agrochemical studies and ambient imaging applications in general.

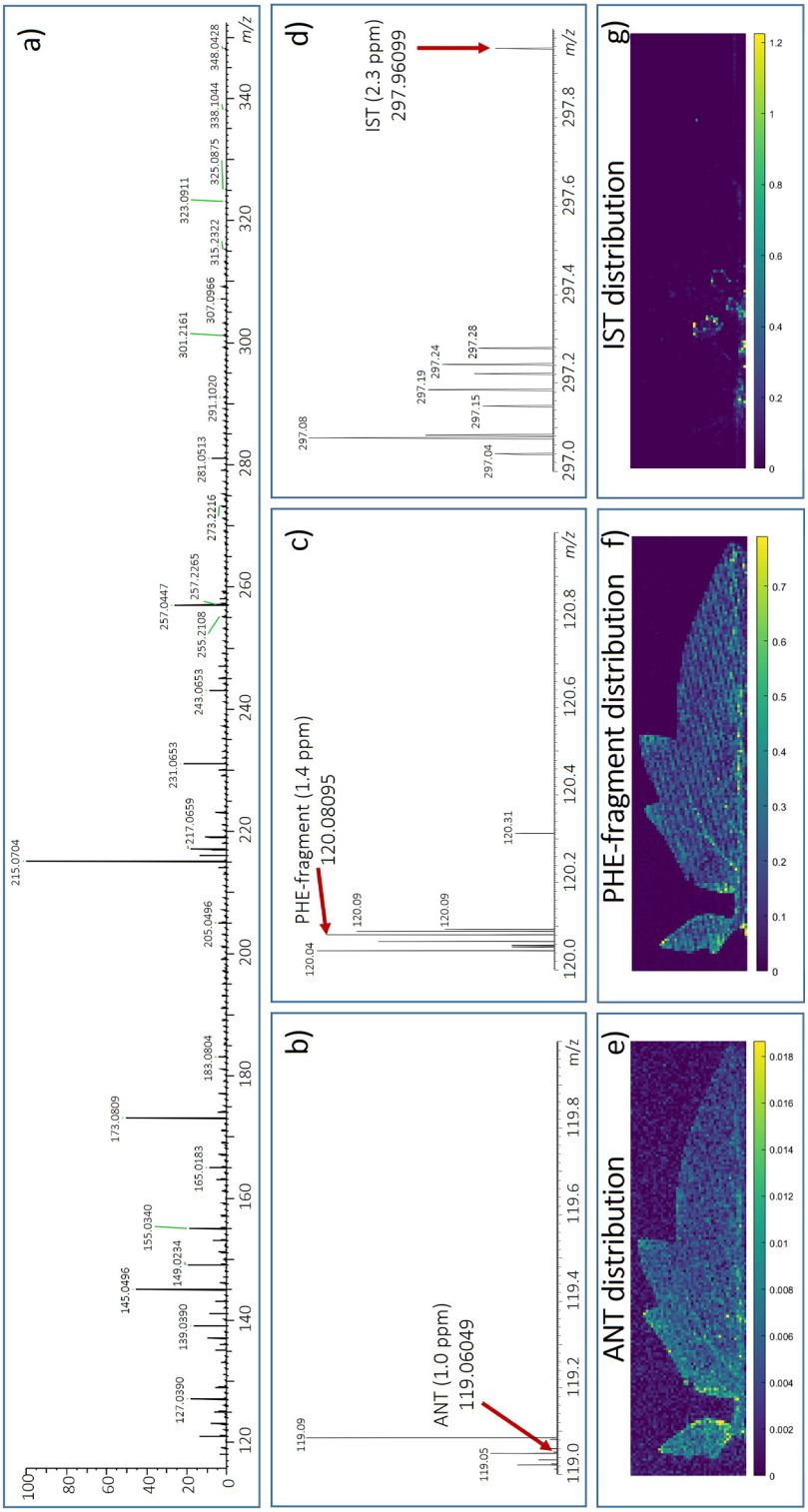

Figure 3.5: *High mass resolution Orbitrap based LA-APCI imaging experiment on an isotianil (IST) treated tomato leaf, harvested at day 9. a) Single pixel spectrum over the entire mass range 118-305 m/z. b) Anthranilonitrile (ANT) range extracted from A 119-120 m/z. c) Phenylalanine (PHE)-fragment range extracted from A 120-121 m/z. d) IST range extracted from A 297-298 m/z. Red arrows indicate the exact mass peak at which images in e), f), g) are generated, that show the distribution of ANT, PHE-fragment and IST respectively derived from the Orbitrap imaging experiment. The total imaging area is 43.3 x 11.5 mm.*

3.6. SUPPLEMENTARY INFORMATION

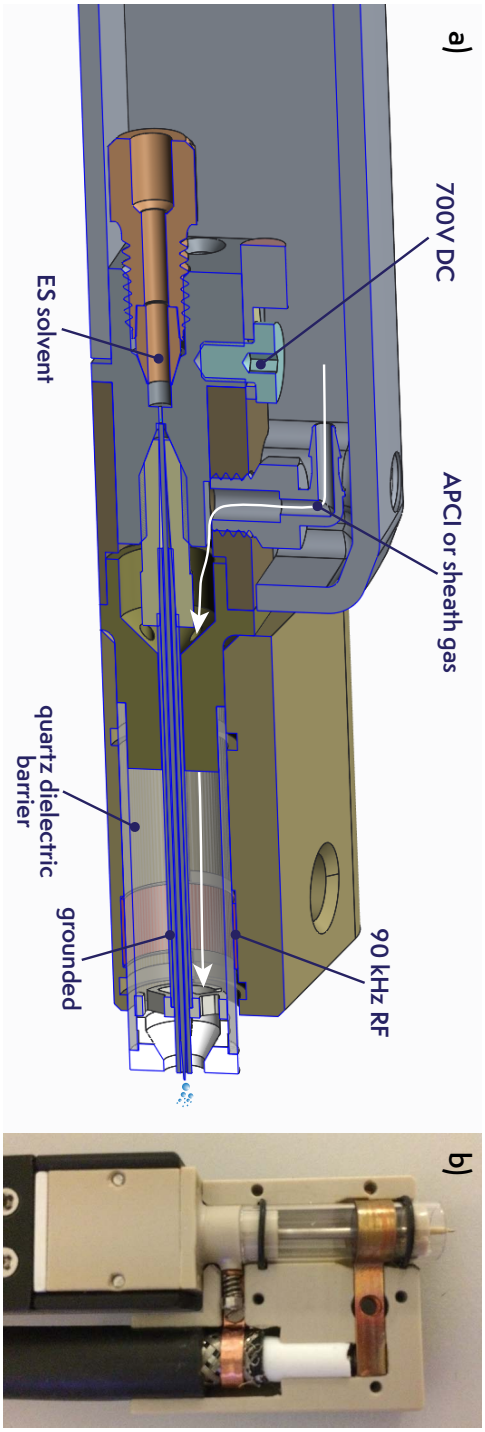

Figure S3.1: *(a) cut-through side view of the dual ionization probe design. On the left are shown the connections for electrospray solvent and DC potential and flow path of APCI or sheath gas (depending on operating mode). The copper electrode on which the RF potential is applied, the grounded counter electrode and the quartz dielectric barrier are visible on the right of (a), as well as the electrospray emitter and droplets. (b) shows the underside of the actual probe, with part of the insulation removed.*

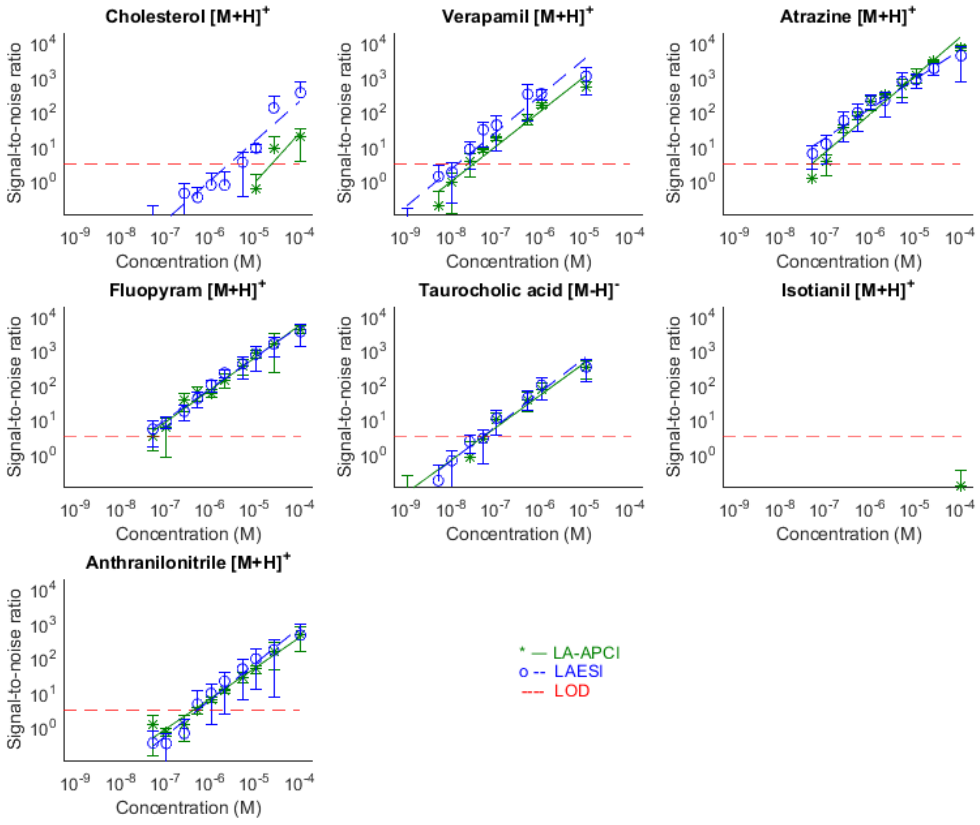

Figure S3.2: *calibration curves for all seven test compounds, recorded in both LAESI (circle, dashed) and LA-APCI (asterisk) mode. All points were sampled in three series of ten laser shots. Plotted as concentration against signal-to-noise ratio in a double logarithmic scale with an LOD threshold plotted at a S/N ratio of 3. For fluopyram, anthranilonitrile and taurocholic acid the observed LOD values for LAESI and LA-APCI do not significantly differ. LAESI is more sensitive than LA-APCI for cholesterol and verapamil, and to lesser extent atrazine. We were not able to create suitable calibration curves for isotianil, due to its insolubility in IR-laser compatible solvents.*

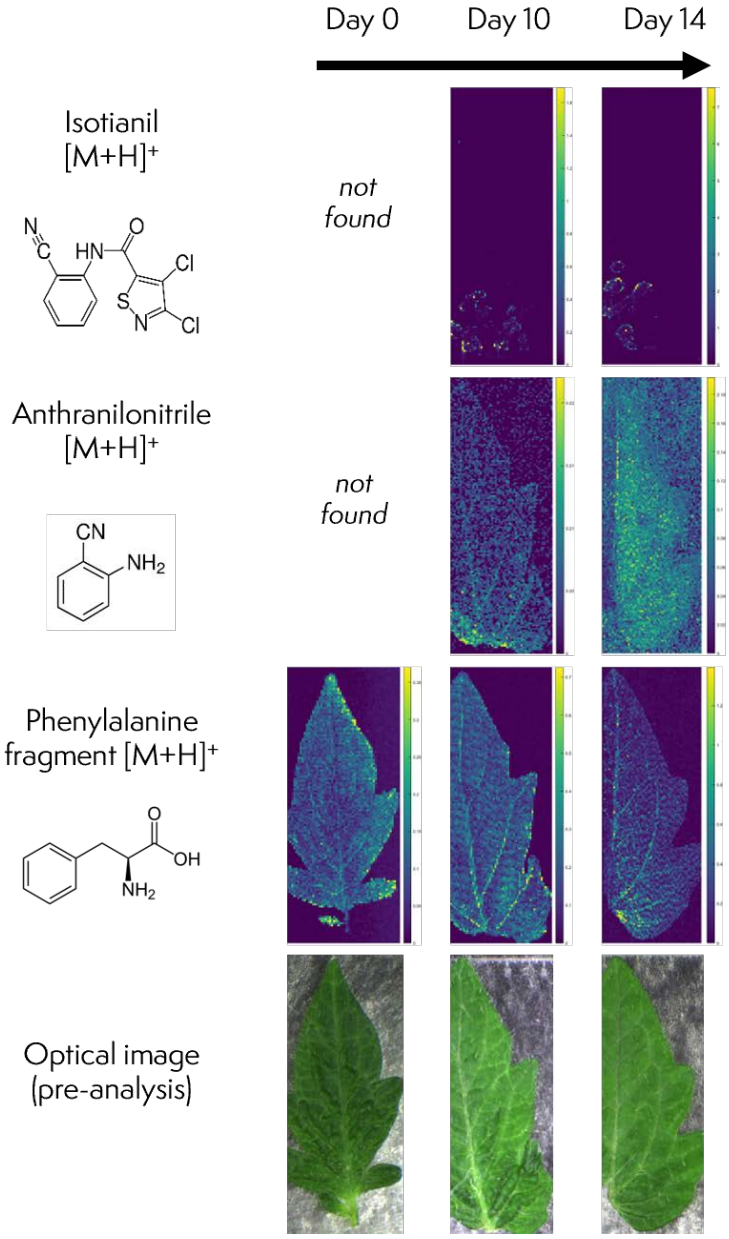

Figure S3.3: *MS images of isotianil, its metabolite anthranilonitrile and endogenous compound phenylalanine recorded in a secondary set of experiments. These datasets are recorded on a Q-Exactive HF mass spectrometer. The leaves were harvested at day 10, day 14 or directly after (day 0) application of 5 times 10 µl of 250 ppm isotianil formulation near the base of the leaf. The leaves were washed in 80% ACN prior to analysis to remove an excess isotianil formulation from the surface of the leaves. In the isotianil images the dried-droplet pattern of the formulation spots can be observed, even after 14 days. Its metabolite anthranilonitrile however is seen to be preferentially distributed near the base and inside the veins of the leaf after 10 days, and quite homogeneously distributed after 14 days. Phenylalanine is always similarly distributed, being visible throughout the tomato leaf, but most prominent in the veins.*

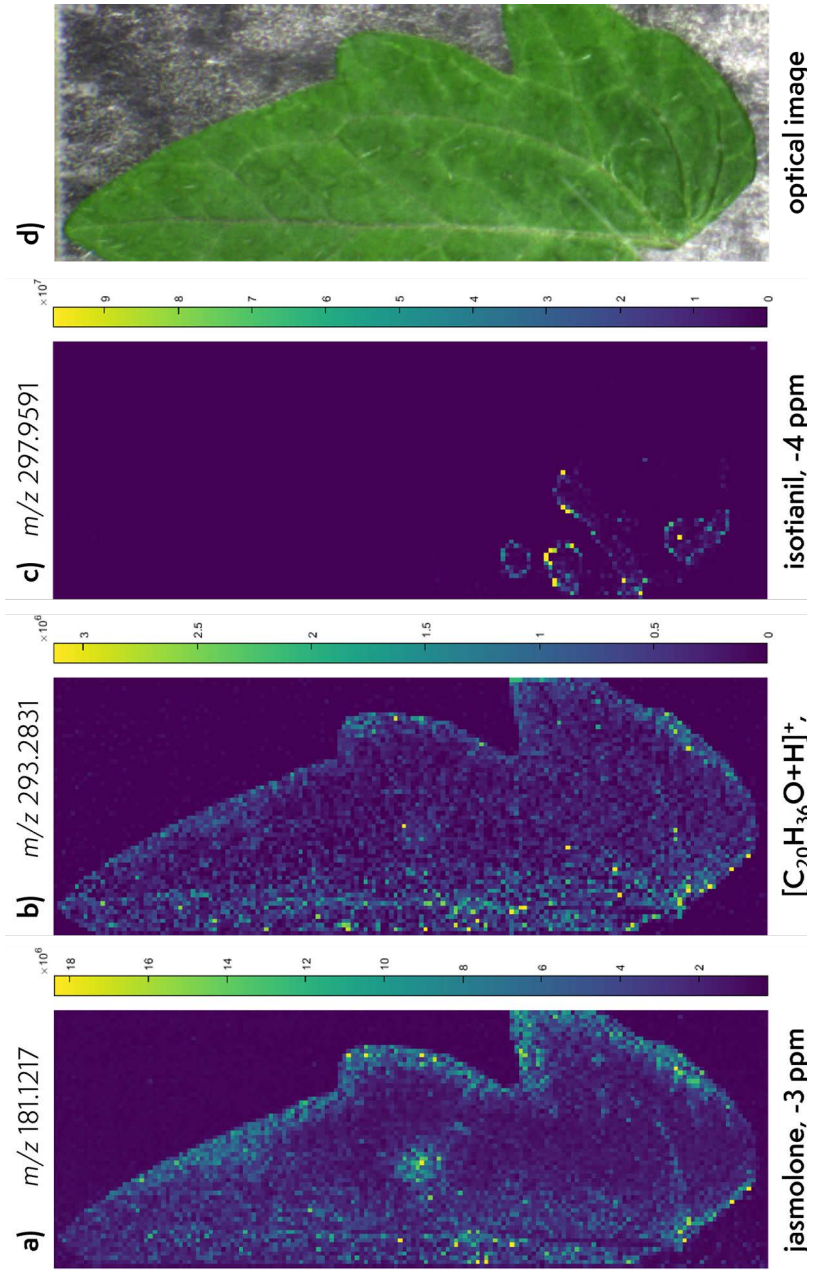

Figure S3.4: *mass spectral images of two tentatively identified endogenous compounds and isotianil recorded on a Thermo Orbitrap Elite mass spectrometer with LA-APCI. The set mass resolution was 30.000 and the injection time 300 ms. The tomato leaf was treated with five droplets of 10 µl isotianil formulation and harvested after 14 days. a) Jasmolone was tentatively identified and shows a distinct distribution pattern around the edges of the leaf and on a single site within the leaf surface. Multiple metabolites in the tomato leaves analysed show a similar (or contrasting) zone of high concentration in this area. b) distribution of an unknown compound with molecular formula $C_{20}H_{36}O$. c) the distribution of isotianil after 14 days, still immobilized in dried droplet patterns. d) the optical image added for reference.*

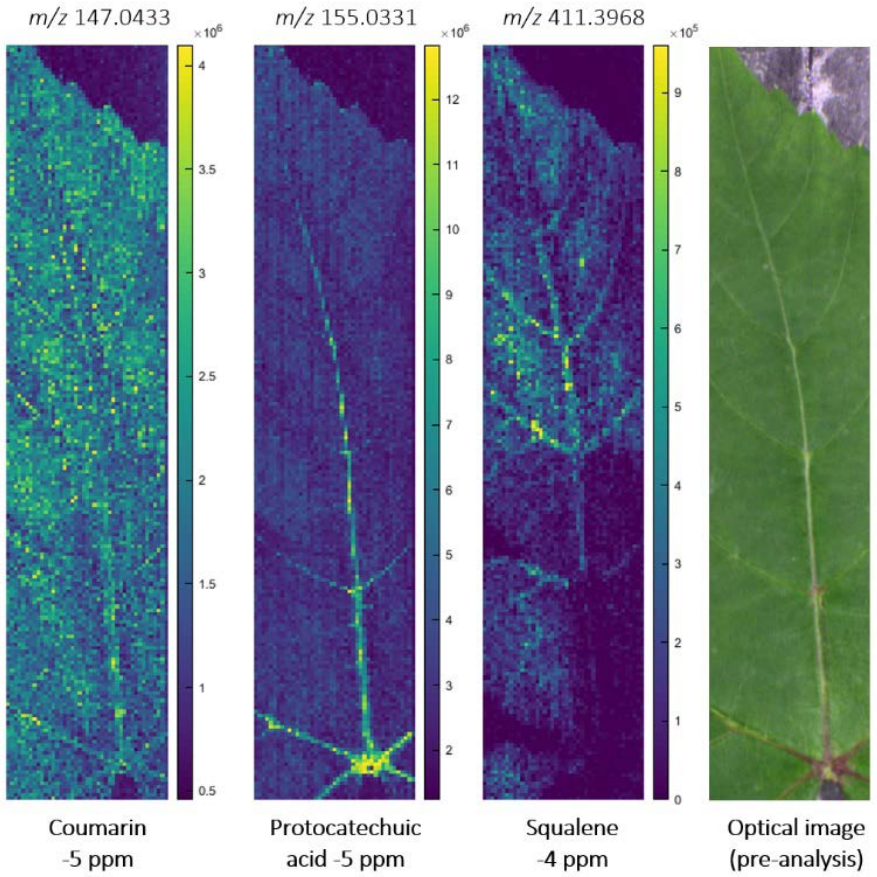

Figure S3.5: *tentative identification of compounds detected in a grapevine leaf by LA-APCI mass spectrometry imaging on a Thermo Orbitrap Elite mass spectrometer with a set mass resolution of 30.000 and 300 ms injection time. The image acquisition time was approximately 12 hours. Left to right: coumarin is found at m/z 147.0433 and seems rather homogeneously distributed throughout the leaf. Protocatechuic acid is found (m/z 155.0331) to be mostly present at the base and in the veins of the leaf. Squalene (m/z 411.3968) shows a very specific localization on some parts of the leaf. The optical image is added for reference. All images are plotted on a linear scale without normalization.*

Protocol S3.1: Reproduced with permission from Christopher R. Anderton & Akos Vertes (Feb/Mar 2016)

Benchmarking LAESI-MS platforms:

The motivation behind this document is to have a standard set of experiments to compare LAESI-MS platforms worldwide. This will provide the user with some indication of how their platform is performing in relation to other systems used elsewhere. Furthermore, it will aid in development of new source configurations in effort to continually push the technology forward.

Positive and negative ion mode limit of detection studies:

The mid-IR laser emitting 5 ns pulses at 2940 nm is operated at 10 Hz repetition rate. The laser fluence is selected in the range of 0.1 and 1.0 J/cm^2 to achieve stable signal. Using the 96-well plate-like dish provided by Protea® or a similar sample holder that can confine microliter volumes, place 20 µL of the standard solution, measured in mol/L, into each well.

For positive ion mode: use Verapamil (CAS Number: 152-11-4, from Sigma: V4629) in 50% MeOH. Please see Reference 239 for further information.

For negative ion mode: use taurocholate (CAS number: 345909-26-4, from Sigma: 86339) in 2:1 MeOH:$CHCl_3$.

Depth profiling measurement:

The ability to depth profile is a unique aspect of LAESI-MS in regards to other ambient mass spectrometry methods. The ideal standard is something that acts as a tissue surrogate. Agar is one such candidate, as the water content can be changed to modulate the tensile strength of the sample, it is commonly used substrate in microbiology, and the addition of positive and negative ion mode standards is easy (like those noted above). If a standard is added, the 1 mM to 100 µM range is sufficient.

Following a common microbiologist 'blank' protocol[242]: add 5 g of granulated agar (Difco, BD catalog number: 214530) in 500 mL MilliQ water (ultrapure water), stir to break up any large particles, then autoclave the solution. While the solution is still warm, pour into standard petri dishes, cover and seal, and let cool overnight. Store at 4 °C for up to one month.

The protocol above provides an agar content with 99% water (w/w%), increasing or reducing the granulated agar content by up to 500 mg will proportionally change the tensile strength of the plated agar. Too much granulated agar, and the plated agar becomes too stiff; too little, and it becomes too runny.

Beam size measurement:

ZAP-IT thermal paper (from Kentek, P/N: ZAP-IT). The paper should be placed in the focal spot of the focusing device (CaF_2 or ZnSe lens, reflective objective, or sharpened optical fiber) and exposed to a single laser shot. The spot characteristics (shape and diameter) are measured under a microscope.

Pulse energy measurement:

The laser pulse energy is measured before the focusing device and corrected by its transmission.

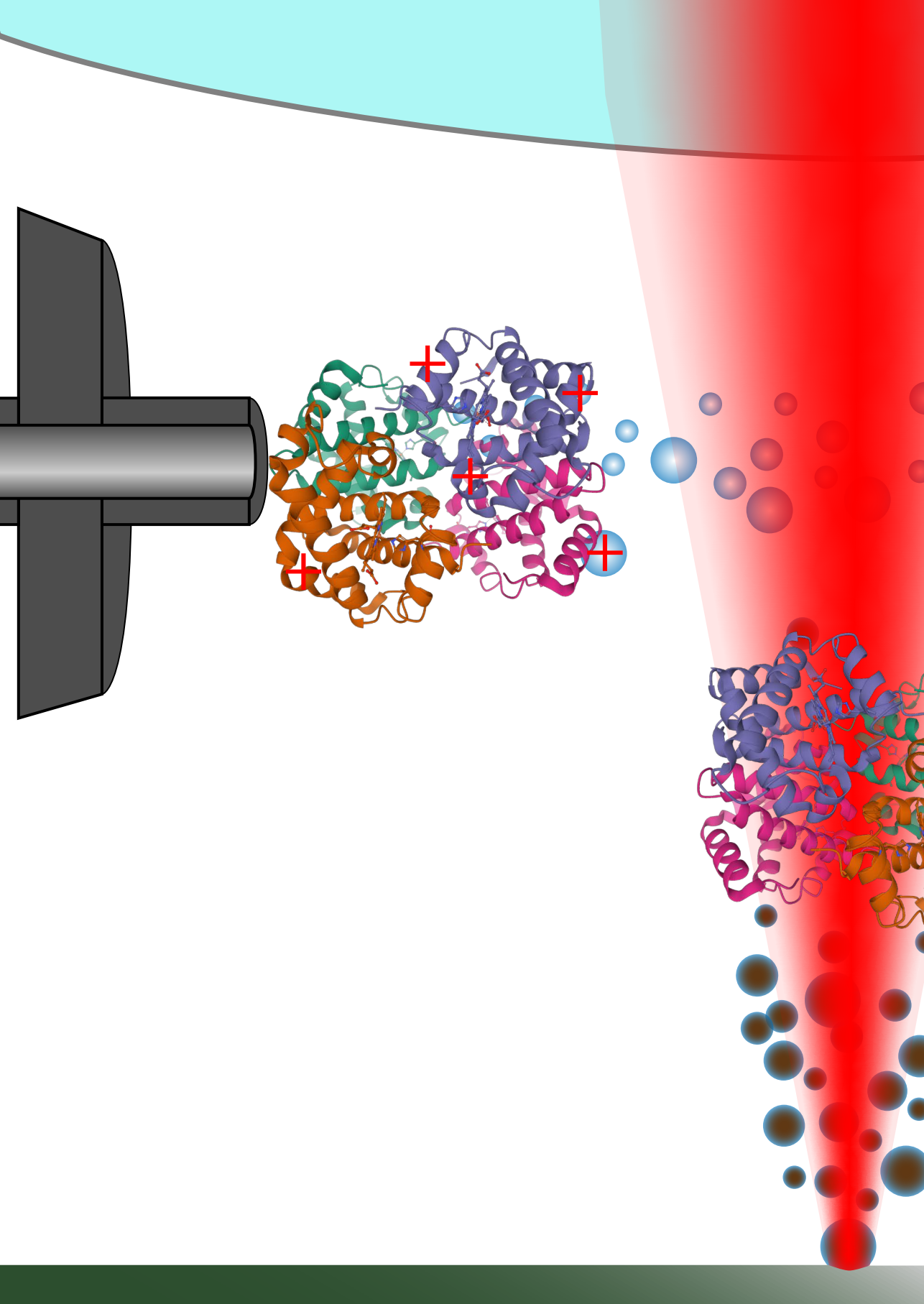

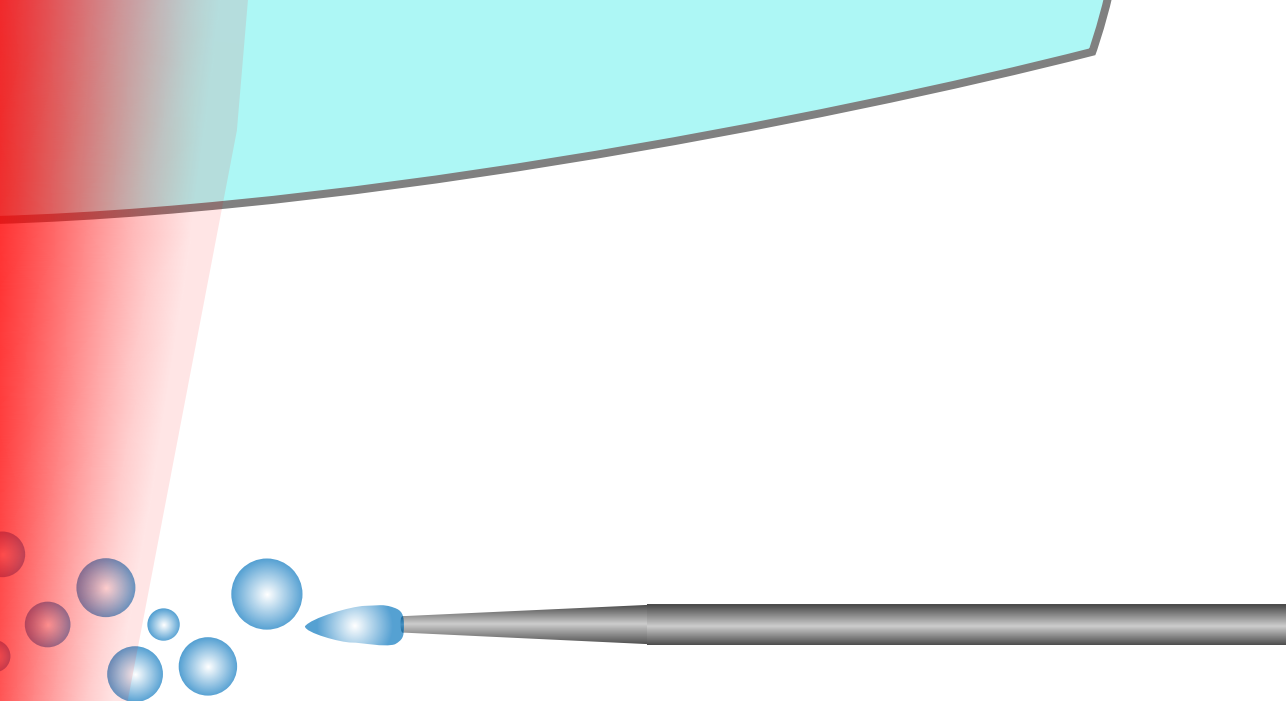

CHAPTER 4

AMBIENT COLLECTION AND IONIZATION OF INTACT PROTEIN COMPLEXES WITH LAESI

Based on

Infrared laser desorption and electrospray ionization of non-covalent protein complexes: generation of intact, multiply charged species

Pieter C. Kooijman, Anjusha Mathew, Shane R. Ellis and Ron M.A. Heeren

Analysis & Sensing 1 (2021): 44-7

ABSTRACT

We present a novel method enabling the infrared laser desorption and electrospray ionization (ESI) of protein complexes in their native state. Using this method, we demonstrate the surprising generation of intact, multiply charged ions of myoglobin, non-covalent haemoglobin complex and intact immunoglobulin G antibody in their native state. The observation of a surviving population of intact non-covalent complexes is characteristic of the low internal energy build up experienced during both laser desorption from solution and subsequent ionization. Compared to conventional nano-ESI our approach yielded slightly lower average charge states suggesting additional maintenance of tertiary structure during desorption and ionization, while also appearing more tolerant to salts enabling simpler sample purification procedures. This approach may enable the development of high-throughput native-MS methods capable of analysing the composition and sequence of multiple macromolecular samples per minute.

4.1. INTRODUCTION

The study of intact protein complexes by mass spectrometry has been gaining increasing interest over the past few decades.[243,244] Such methods are now extending MS to the field of structural biology, for example the coupling of MS and cryo-EM or X-ray crystallography data.[245-248] Native MS utilises nano-electrospray ionization (nano-ESI) of complexes from aqueous solution containing physiological buffer. Under such conditions quaternary structure is preserved and non-covalent complexes in the MDa range can be ionised and detected in their native confirmation.[249] Typically native MS is performed by manually loading a glass nanospray capillary with desalted and fractionated sample – an approach not well suited to high throughput analysis, e.g. drug-interaction screening. The ability to generate native MS spectra direct from a sample surface would provide a major step towards the localized and higher throughput analysis of macromolecular assemblies.[250]

Laser-based mass spectrometric (MS) strategies - which are extensively used for high throughput sampling approaches[251] – are rarely used under native conditions. For instance, matrix assisted laser desorption/ionization (MALDI) is frequently employed to analyse intact proteins[141] and peptides[252] from surfaces, but requires organic solvents and acidic matrices. These conditions, combined with the energetics of the desorption/ionization process, provide a denaturing environment that promotes dissociation and loss of quaternary structure.[253-256] Additionally, MALDI generates low charge state species (mostly singly and doubly charged) that are not well-suited for structural analysis by tandem mass spectrometry (MS/MS) and result in high mass-to-charge (*m/z*) values that may not be efficiently analysed.

Several studies have developed strategies that utilize laser desorption and/or electrospray to enable top-down analysis of intact proteins.[219,257] The group of Morgner has developed laser induced liquid bead ion desorption (LILBID), whereby charged and intact protein complexes are liberated from microdroplets in vacuum following IR laser desorption. LILBID shows good sensitivity and high salt tolerances. However, LILBID is still an infusion-based technique and - similar to MALDI - produces mostly singly and doubly charged ions.[258] Desorption electrospray ionization (DESI) has been successfully applied to non-covalent protein complexes by the group of Robinson, demonstrating desorption of spray-deposited protein complexes from a surface.[259] Additionally, liquid extraction surface analysis (LESA), a nano-ESI based surface sampling method has also been shown to be compatible with native-MS.[260]

Shiea et al.[261] and others[262,263] demonstrated laser ablation electrospray ionization (LAESI)-based analysis of various small proteins, such as myoglobin, cytochrome C and hemoglobin sub-units. These results were obtained with traditional electrospray solvents and additives, containing a high organic modifier percentage and high acidity. To the best of our knowledge none have demonstrated analysis of native non-covalent complexes.

Here, we demonstrate that LAESI-MS can in fact generate multiply charged non-covalent protein complexes in their native state. LAESI uses an infrared (IR) 2.94 µm laser to softly desorb analytes from aqueous solution at atmospheric pressure. Desorption is initiated via the coupling of laser energy into OH bonds of the solvent (e.g. water). The plume of desorbed material is intersected at some distance from the surface by an orthogonal electrospray (ESI) plume, where ionization occurs analogous to conventional ESI. Charged analyte molecules then enter the mass spectrometer through the inlet due to the electric field and gas flow gradients.

4.2. RESULTS

In this work all experiments were performed using a LAESI ion source coupled to a Orbitrap UHMR mass spectrometer optimised for native-MS and high mass transmission.[264] First, we developed a method to analyse small proteins with LAESI-MS in their native state. We chose myoglobin as a target molecule because it has a clear transition from a native to a denatured state characterised by loss of the heme group and the creation of ions with higher charge states. The key optimization parameters were the LAESI electrospray solvent composition and the analyte solution composition. The optimal solvent composition that we found - and that was used for all native LAESI experiments presented here - was 100 mM of ammonium acetate in water, with 10% of methanol as organic modifier. We formulated a sample matrix of 200 mM of ammonium acetate in water with 10% ethylene glycol, which we will refer to as "native matrix" for the remainder of this text. Addition of an ammonium acetate buffer ensures a constant pH in solution, a requirement to retain native protein confirmation. Ethylene glycol was found to improve desorption repeatability without inducing heme-myoglobin dissociation when added to the sample matrix. The full experimental description is provided in Supporting Information S1.

Figure 4.1 shows the mass spectrum of a myoglobin standard under optimized native LAESI conditions (Figure 4.1a) and that produced by conventional, denaturing LAESI conditions (Figure 4.1b). In both experiments the sample was 10 µl of 180 µM myoglobin solution in native matrix, which was spotted on a vendor-supplied plastic well plate. The native electrospray solvent composition dramatically lowers the amount of charges that attach to myoglobin, and dissociation of heme is largely avoided, both hallmark spectral features of native myoglobin. For comparison spectra generated with native-ESI and conventional microflow ESI are provided in Figure 4.1c, d.

The insets in Figure 4.1a and c show that fewer sodium and potassium adducts are observed in native LAESI compared to in native nano-ESI of myoglobin, even though the nano-ESI sample was dialysed prior to analysis and the LAESI sample was not. Adduct formation is identified as a key limitation in native mass analysis of large proteins.[265] The spray needle tip has been identified as the location where adduct

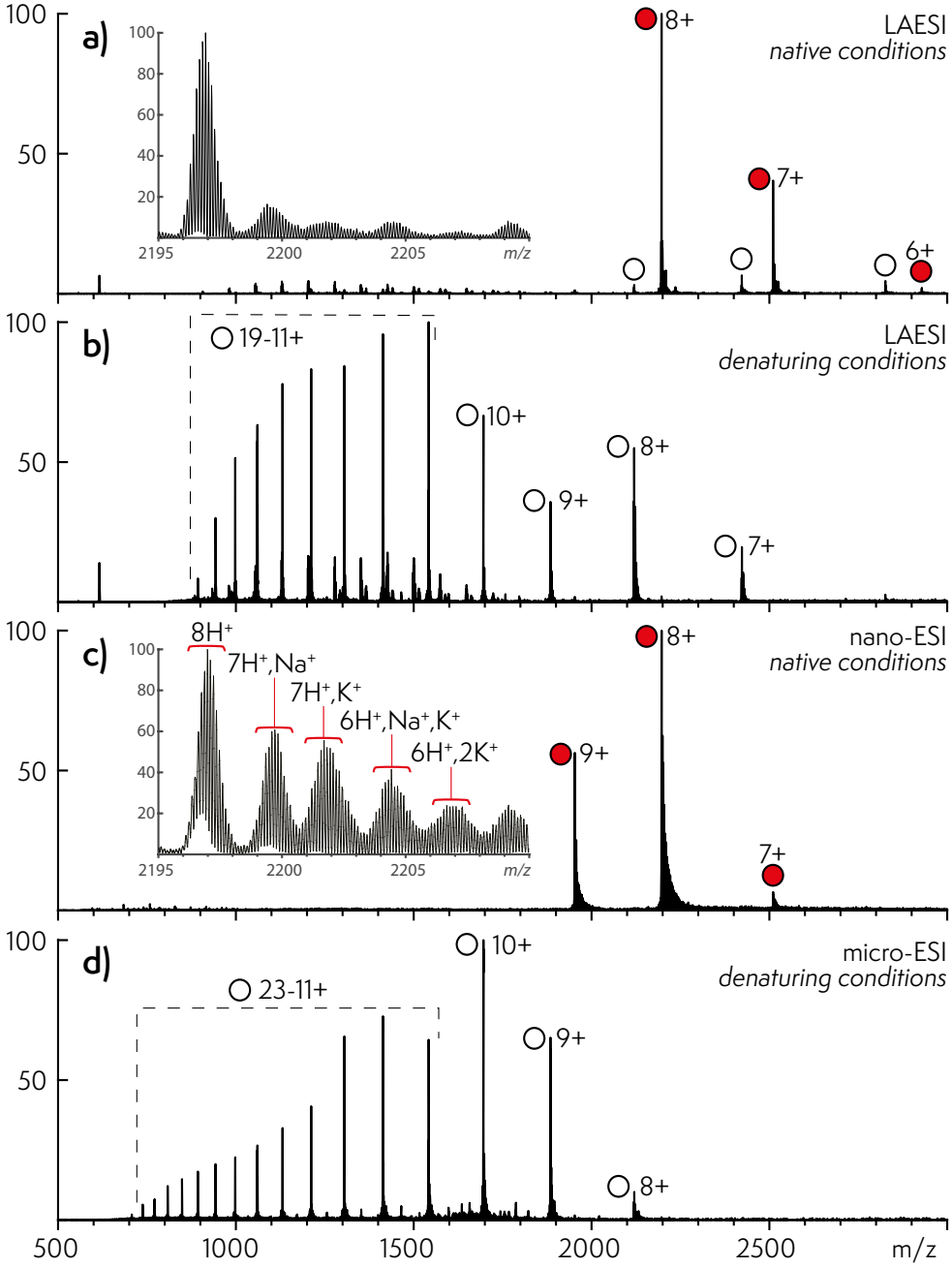

Figure 4.1: *Mass spectra recorded from solutions of myoglobin standard in native matrix with (A) LAESI under native spray conditions (10% MeOH, 100 mM NH4OAc), (B) LAESI under denaturing spray conditions (50% MeOH, 1% FA), (C) nano-ESI using native conditions (100 mM NH4OAc) and (D) micro-ESI using denaturing conditions (50% MeOH, 1% FA). Multiple charge states of myoglobin are observed, either as native - with the heme group still attached (red-filled circle) or as dissociated (empty circle).*

formation in ESI can occur, which explains the observed differences.[266] Alternatively, the glass nano-ESI capillary, as common in native MS, could be a source of sodium. The LAESI sample solution did not come into contact with glass.

Next, we analysed a non-covalently bound protein complex. We chose hemoglobin, one of the most common and essential protein complexes in human biology.[267] This tetrameric complex consists of two α and two β subunits, each containing a heme group, that are non-covalently bound. Figure 4.2a shows the spectra obtained from native LAESI-MS on 10 µl of 200 mM hemoglobin in native matrix. Monomeric units with and without heme are detected, as well as heme-containing dimeric and tetrameric ions. Tetrameric hemoglobin A species were found between *m/z* 3600 and 4315 (*z* = 17 to 14), with sufficient mass resolving power and sensitivity to deconvolute them to an intact mass of 64,660 Da (Supplemental Figure S4.1).

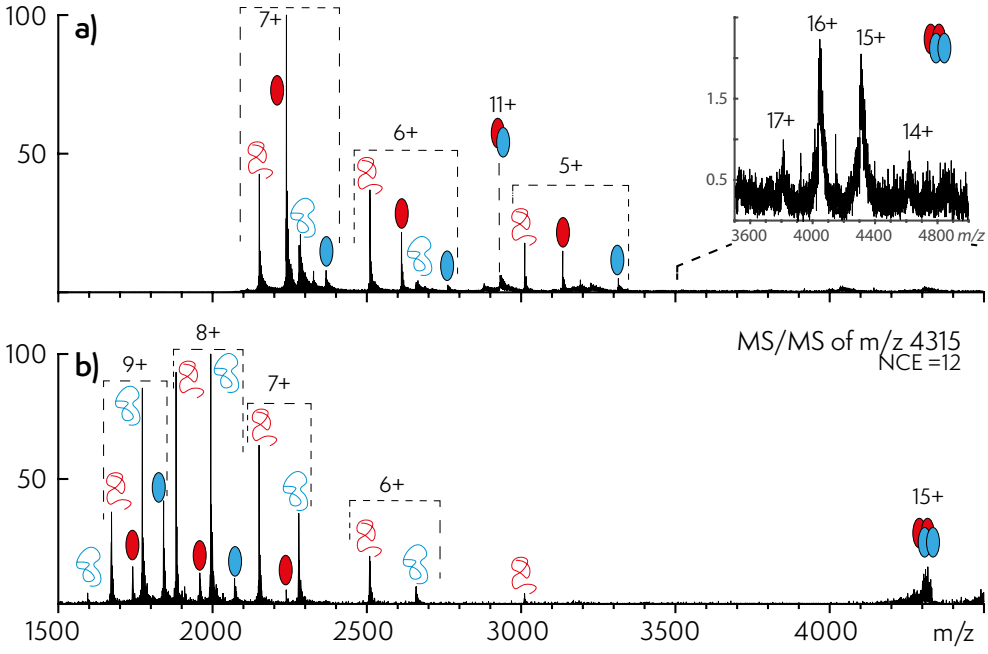

Figure 4.2: *(A) LAESI-MS spectra of 180 µM hemoglobin standard in native matrix, with heme bound α-monomers (red oval), heme bound β-monomers (blue oval), denatured monomer (string), dimer (blue and red oval) and native tetrameric hemoglobin (two blue and two red ovals). (A) full LAESI spectrum, whereas (B) HCD-MS/MS spectrum (NCE = 12) of the native hemoglobin species around m/z 4315 (z = 15), with a 30 Th wide isolation window. The spectra represent 100 shots, averaged from 40 scans over a period of 20 seconds. NCE = normalise collision energy. Peak were assigned within a mass error tolerance of 5 ppm.*

To unequivocally demonstrate the generation of a population of tetrameric hemoglobin we dissociated the +12-charge state using HCD-MS/MS. Figure 4.2b shows the HCD-MS/MS spectrum (NCE = 12) of the *m/z* 4315 (*z* = 15) tetrameric

precursor. Both α- and β-monomers were detected with and without a heme group. This confirms the identity of tetrameric hemoglobin A. The bulk of the detected monomers after HCD fragmentation have a charge state between 6+ and 9+, arising from well-known asymmetric charge partitioning between the ejected monomer and remaining trimer[268]. Supporting Figures S4.2 and S4.3 show the LAESI MS/MS fragmentation spectra of hemoglobin subunit α (HBA) and subunit β (HBB), respectively, to confirm their identity.

Next, we investigated the detection of Immunoglobulin G (IgG) antibodies using native-LAESI. Figure 4.3a shows a native LAESI-MS spectrum from 200 µM IgG solution. This sample was prepared simply by dissolving the commercially bought IgG in matrix solution. The corresponding native spectrum produced from SEC fractionated IgG using nano-ESI is shown for comparison in Figure 4.3b. Similar to the results above native-LAESI gives comparable, although slightly lower, charge state distribution as nano-ESI, supporting the hypothesis that that the tertiary structure of IgG is preserved during IR-laser desorption. The average IgG species that was detected for both LAESI and nano-ESI has a mass of approximately 148 kDa, as is expected for a glycosylated IgG sample. The broad peaks are indicative

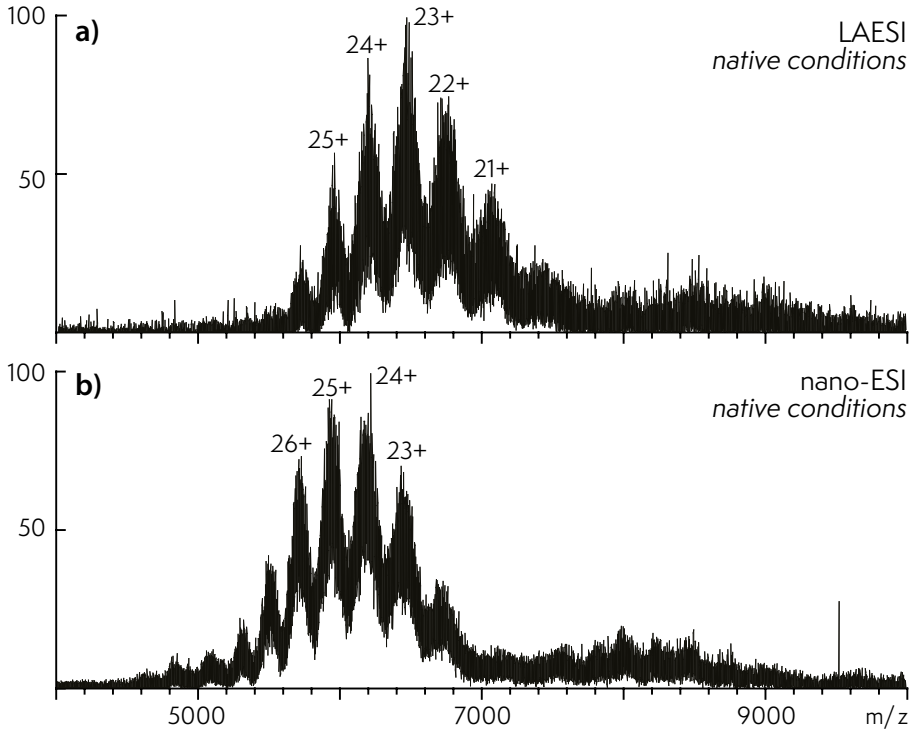

Figure 4.3: *Mass spectra of human IgG measured with (A) LAESI-MS from 10% ethylene glycol and 200 mM NH4OAc solution at 200 µM, and (B) ESI-MS from 100 mM NH4OAc solution in a SEC-fractionated sample at 1.5 µM. Both spectra are 38 scans averages (20 seconds / 10 LAESI laser shots).*

of the different glycosylation states of IgG. Figure 4.3b shows the native nano-ESI spectrum which was obtained from the same - but purified through SEC-fractionation - human IgG standard (see Supporting Information for details). For LAESI, the sample preparation was limited to dissolving an unfractionated sample in our native matrix solution.

All LAESI spectra shown here are very similar to their ESI counterpart (Figure 4.1 and Figure 4.3), except for the lower average charge state observed for LAESI spectra. As low average protein charge states can be attributed to more compact, folded structures, the degree of unfolding observed in ESI-analysis of proteins can be been correlated with higher internal energy values resulting in more extensive denaturing[269]. We surmise that a population of LAESI-generated ions exists that have experienced a lower increase in internal energy than produced under nano-ESI conditions. This is supported by the observation that also under denaturing conditions the LAESI generated charge state distribution is lower than the ESI generated distribution. Two other effects are could also contribute to this charge state reduction. First, proteins experience a shorter interaction time between the charge containing electrospray solution and the analyte molecules in LAESI, compared to nano-ESI. Second, the high electric field experienced by the proteins at the nano-ESI tip could contribute to the higher average charge state distribution of the ESI results.

4.3. DISCUSSION

This work demonstrates for the first time the intact laser desorption and ionization of non-covalent protein complexes using LAESI. Native-LAESI generated ions exhibit slightly reduced charge states compared to those generated from conventional nano-ESI performed under native conditions. These results suggest that neither the IR-desorption nor ESI post-ionization impart sufficient energy for complete loss of tertiary structure (although we note some populations of ions are the result of dissociate processes, e.g. Figure 4.2a). Results are consistent with observations made using: (i) LILBID-MS and (ii) the survival yield method demonstrating that LAESI using conventional denaturing solvents results in ions with comparable internal energies as those formed from ESI[270]. The former work demonstrates that in solution very little energy is transferred to solvated analytes. LILBID is also known to form lower charge states than nano-ESI suggesting that the lower charge states seen in our native-LAESI spectra may, in part, arise from a similar ejection of ionised proteins directly from the sample solution rather than purely an ESI-type ionization process. Given the ease in which multiple samples can be interrogated using LAESI, and the high tolerance to salt contaminants, our results suggest LAESI-based approaches are well suited for rapid analysis (multiple samples per minute) of protein complexes and other macromolecules.

4.4. MATERIALS AND METHODS

Chemicals

Myoglobin (equine heart), hemoglobin (bovine blood), immunoglobulin G (IgG, from human serum), ethylene glycol, formic acid and ammonium acetate were purchased from Sigma-Aldrich (Zwijndrecht, The Netherlands). Isopropyl alcohol, methanol and LC-MS grade water were purchased from Biosolve (Valkenswaard, The Netherlands).

Sample preparation

For LAESI, solutions were made of myoglobin (360 μM), hemoglobin (200 μM) and IgG (200 μM) in a "native matrix". The native matrix consisted of 200mM ammonium acetate and 10% ethylene glycol in water. For each analysis, a plastic 96-well plate (Protea Biosciences, USA) was spotted with 20 μl of analyte solution and placed into the analysis chamber.

For ESI, all lyophilized protein assemblies were dissolved to stock concentration of 100 μM in LC-MS grade water. For nanoESI, myoglobin was desalted and buffer exchanged with 100 mM ammonium acetate (6.8) using 3.5 kDa molecular weight cut-off (MWCO) dialysis membrane overnight followed by another 1-hour buffer exchange with a fresh ammonium acetate solution at 4 °C. Purification and buffer exchange of hemoglobin and IgG were performed using size exclusion chromatography (SEC) on a Superdex 200 Increase 3.2/300 column (GE Healthcare Biosciences AB , Sweden) with 100 mM ammonium acetate at pH 6.8. All samples were diluted to a final monomer concentration of 1.5 μM prior to nanoESI-MS experiments. 1 μM myoglobin diluted in 1:1 (v/v) methanol:water with 1% (v/v) formic acid was used for microESI experiments.

Mass spectrometry

MS and tandem MS data were collected on an ultra-high mass range (UHMR) Q-Exactive Orbitrap mass spectrometer (Thermo Fisher Scientific, Germany) in positive ion mode. Mass spectral resolution was set to 140,000 (at m/z=200) and the m/z range was adjusted for each analyte. Automatic gain control was turned off and a single microscan was recorded per scan. Detector m/z optimization for higher masses was used only for IgG measurements. The inlet capillary temperature was kept at 320 °C. S-Lens RF levels were kept at 200 V.

For LAESI: Injection times were kept at 500 ms, except for myoglobin recorded under denaturing conditions (Figure 1b) which was recorded with 250 ms injection time. S-Lens DC potential was kept at 0 V. Fragmentation was performed by high energy collision induced dissociation (HCD) at 12 or 24% normalized collision energy (NCE) using an isolation window of m/z 30 or 5 for hemoglobin tetramer and hemoglobin monomers, respectively.

For ESI: Injection times were set at 100 ms except for IgG, which was recorded with 250 ms. The S-Lens DC potential was kept at 21 V. All other parameters are kept similar to that of LAESI.

Ionization source parameters

LAESI

All LAESI experiments were performed on a standard DP-1000 LAESI unit (Protea Biosciences, USA) with 100 µm i.d. metal TaperTip emitter and extended inlet capillary heater. The extended inlet heater was maintained at 66 °C. The sample bay temperature was controlled at -10 °C, which did not freeze the sample solution. The 2.94 µm OPO laser was operated in bursts of 10 shots, at a frequency of 5 Hz with a laser fluence of 500 µJ (10 kJ/m2). All spectra shown are averages over a single burst (20 seconds). A low flow of bath gas was used to control the humidity in the analysis chamber.

The default LAESI electrospray solution was chosen as: 1:1 (v/v) methanol:water with 1% (v/v) formic acid at a flow rate of 0.8 µl/min. The spray potential was kept at +4000 V. No sheath gas was used.

The native LAESI electrospray solution was: 100 mM ammonium acetate with 10% (v/v) methanol in water. The electrospray flow rate was chosen between 0.6 to 1.2 ul/min, depending on the spray conditions. The spray potential was kept at +4000 V. No sheath gas was used.

ESI

All nano-ESI experiments were performed using in-house pulled gold coated borosilicate capillaries via a static nanoESI source. The ESI capillary voltage was set between 800 to 1200 V. All microspray ESI experiments were performed using the standard Ion max HESI ion source. A flow rate of 0.8 µl/min is used and the capillary voltage was kept at +4000 V.

Data analysis

All published mass spectra were analysed with and extracted from the Thermo Scientific Xcalibur software package. All spectral deconvolutions were performed with the software UniDec.[271]

4.5. SUPPORTING FIGURES

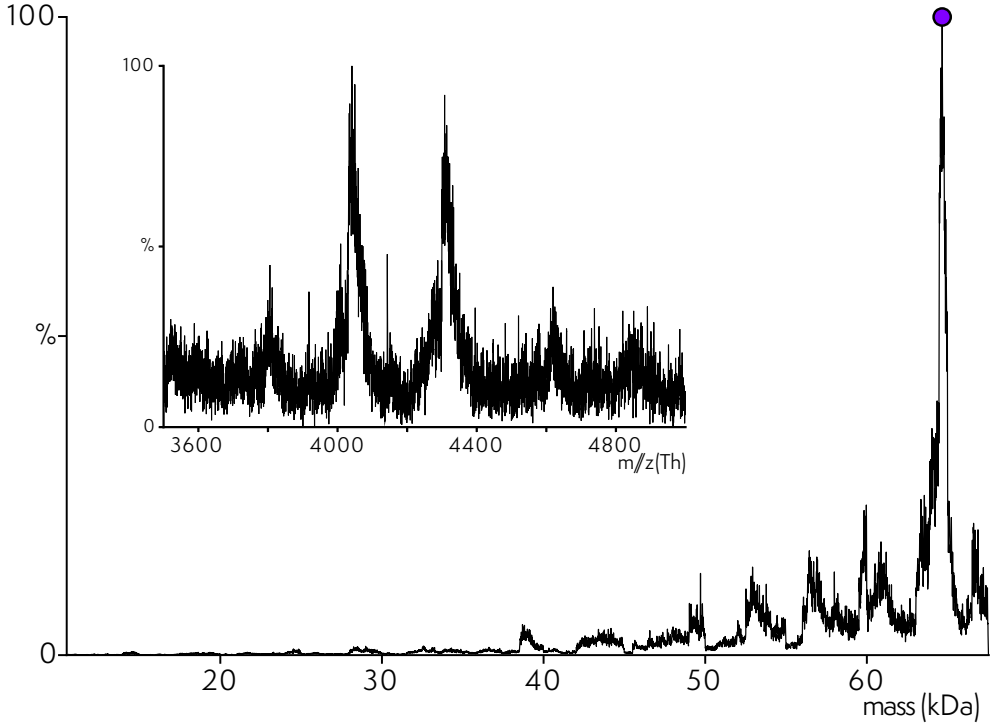

Figure S4.1: *Deconvoluted spectrum of tetrameric hemoglobin species from native LAESI-MS spectrum Figure 3a. (purple dot) Deconvoluted tetramer of hemoglobin, peak-picked at 64,660 Da. (inset) The mass range m/z 3500 – 5000 used for deconvolution, contains 17+ through 13+ charged species of tetrameric hemoglobin. The deconvolution was performed with UniDec software.*[31]

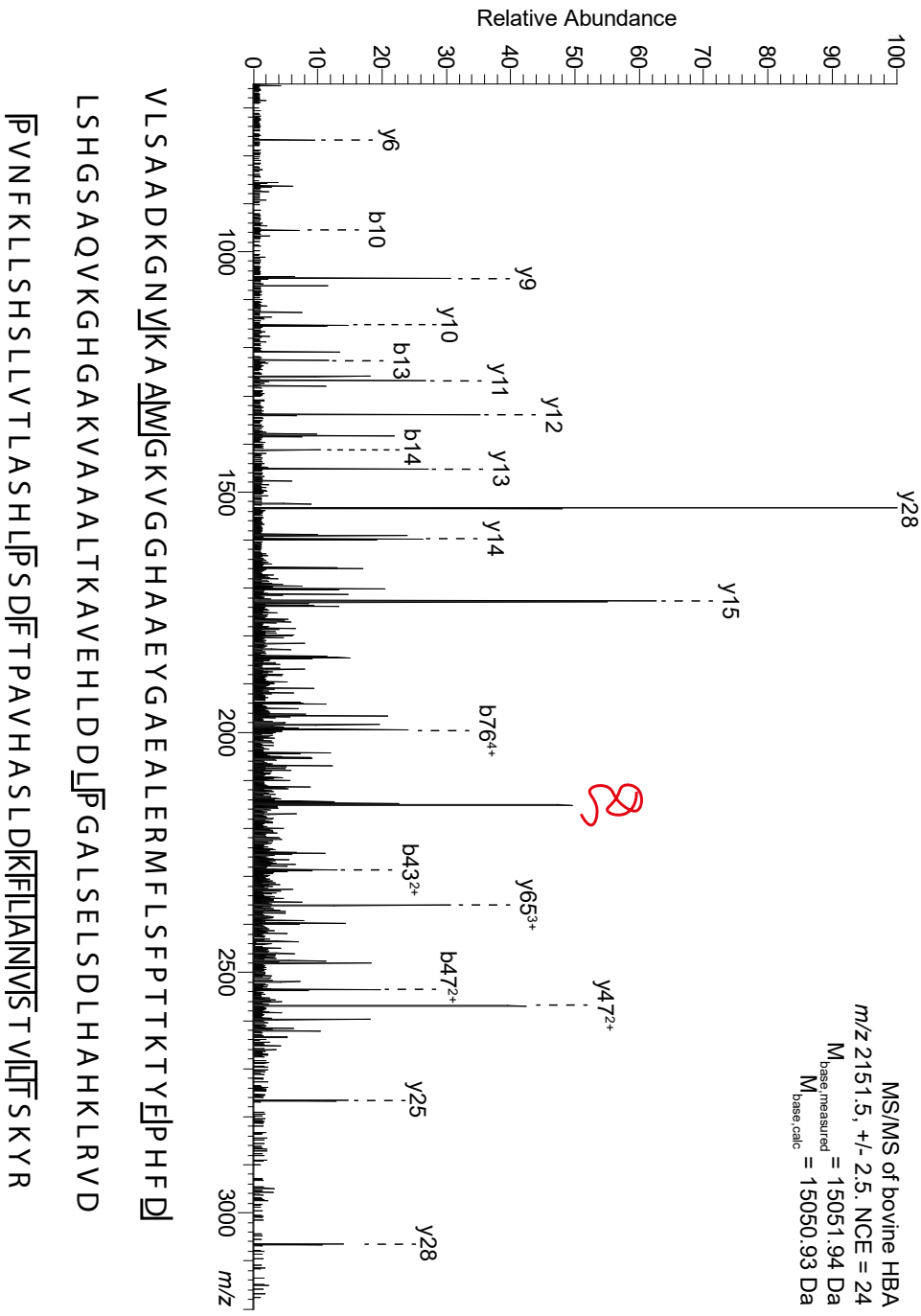

Figure S4.2: *HCD spectrum of bovine hemoglobin subunit α (HBA) with z = 7, isolated from the native hemoglobin LAESI experiment shown in Figure 2a of the main text.*

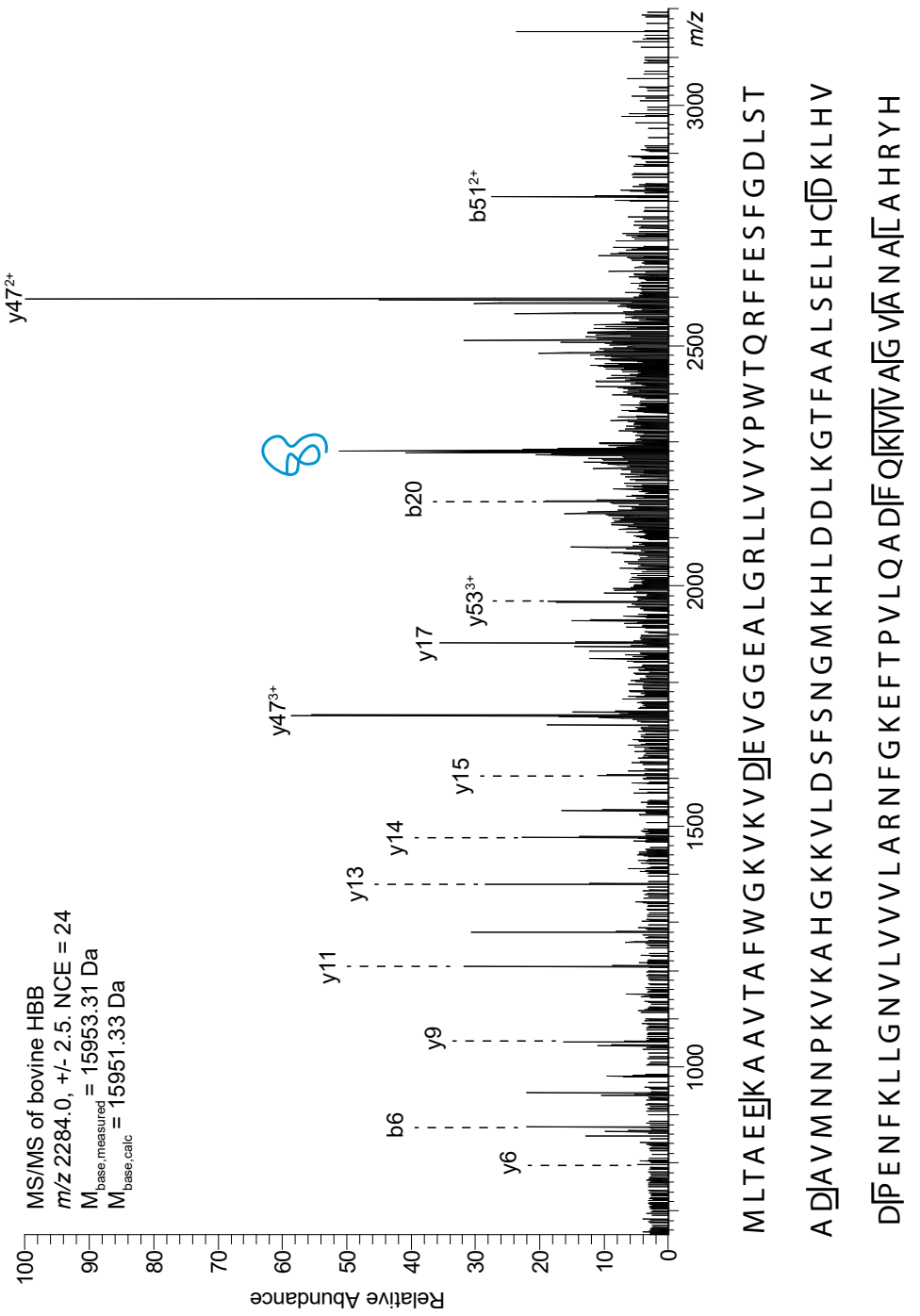

Figure S4.3: *HCD fragmentation spectrum of bovine hemoglobin subunit β (HBB) with z = 7, isolated from the native hemoglobin LAESI experiment shown in Figure 2a of the main text.*

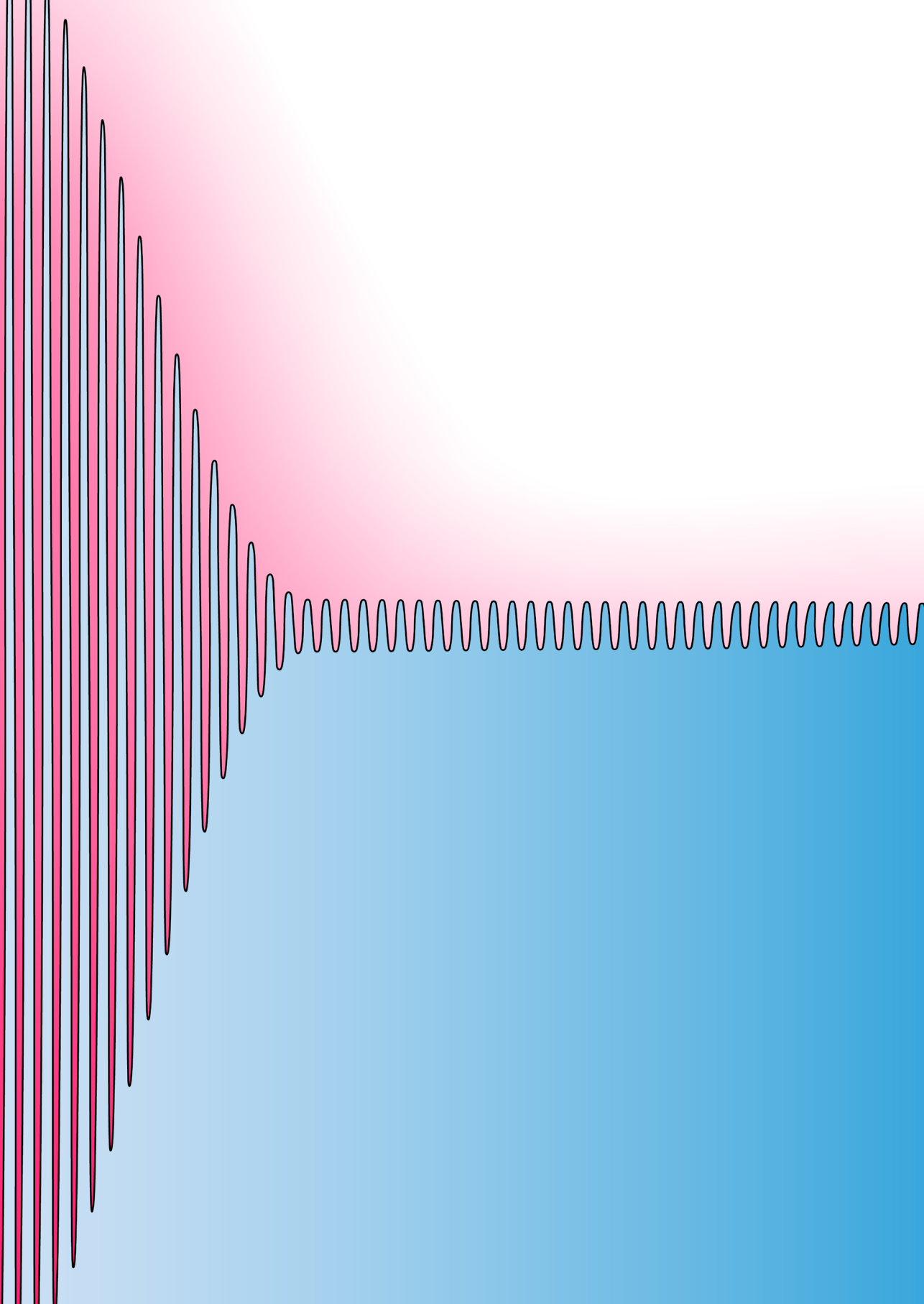

CHAPTER 5

EXTENDING THE DETECTION LIMITS IN AMBIENT MASS SPECTROMETRY IMAGING

Based on

Increased throughput and ultra-high mass resolution in DESI FT-ICR MS imaging through new-generation external data acquisition system and advanced data processing approaches

Pieter C. Kooijman, Konstantin O. Nagornov, Anton N. Kozhinov, David P.A. Kilgour, Yury O. Tsybin, Ron M.A. Heeren and Shane R. Ellis

Scientific reports 9.1 (2019): 1-11

ABSTRACT

Desorption electrospray ionization-mass spectrometry imaging (DESI-MSI) is a powerful imaging technique for the analysis of complex surfaces. However, the often highly complex nature of biological samples is particularly challenging for MSI approaches, as options to appropriately address mass spectral complexity are limited. Fourier transform ion cyclotron resonance mass spectrometry (FT-ICR MS) offers superior mass accuracy and mass resolving power, but its moderate throughput inhibits broader application. Here we demonstrate the dramatic gains in mass resolution and/or throughput of DESI-MSI on an FT-ICR MS by developing and implementing a sophisticated data acquisition and data processing pipeline. The presented pipeline integrates, for the first time, parallel ion accumulation and detection, post-processing absorption mode Fourier transform and pixel-by-pixel internal re-calibration. To achieve that, first, we developed and coupled an external high-performance data acquisition system to an FT-ICR MS instrument to record the time-domain signals (transients) in parallel with the instrument's built-in electronics. The recorded transients were then processed by the in-house developed computationally-efficient data processing and data analysis software. Importantly, the described pipeline is shown to be applicable even to extremely large, up to 1 TB, imaging datasets. Overall, this approach provides improved analytical figures of merits such as: (i) enhanced mass resolution at no cost in experimental time; and (ii) up to 4-fold higher throughput while maintaining a constant mass resolution. Using this approach, we not only demonstrate the record 1 million mass resolution for lipid imaging from brain tissue, but explicitly demonstrate such mass resolution is required to resolve the complexity of the lipidome.

5.6. INTRODUCTION

The field of direct surface analysis mass spectrometry has seen a tremendous growth in the last decade, particularly in methods that enable analysis to be performed in the open environment at atmospheric pressure.[162,167,272] These methods require minimal-to-no sample preparation but can still provide detailed chemical information in short time. Applications in forensics, security, food industry and medical diagnostics have already been demonstrated.[273-278]

However, the amount of spectral information provided by these methods can also pose a challenge, particularly in the analysis of complex biological samples. The sheer number of chemical components can quickly overwhelm the resolving power of the mass spectrometer. This becomes a major consideration when ambient mass spectrometry is used in imaging approaches, referred to as mass spectrometry imaging (MSI), for instance to study the spatial distributions of isobaric molecules in complex samples such as biological tissues that can have distinct biochemical functionalities.[163] Selective approaches, such as derivatization or multiple reaction monitoring, are undesirable for discovery studies that is currently the main strength of MSI. Furthermore, spectral simplification, by reducing the number of ion adduct species (e.g., protonated or sodiated) through washing steps,[279,280] can add to sample preparation time and introduces the risk of analyte delocalisation.

For this reason, the coupling of high mass resolving power analysers — namely ion cyclotron resonance (ICR) and Orbitrap Fourier transform (FT) instruments — to imaging interfaces has received particular attention. For example, Dilillo *et al.* have recently applied FT-ICR MSI with matrix-assisted laser desorption/ionization (MALDI) to study both intact proteins and metabolites in glioblastomas. This approach enabled them to separate both isobaric protein and metabolite signals[281], while Cornett *et al.* demonstrated the power of MALDI FT-ICR MSI to unambiguously image drugs in tissues[282]. Various studies have also coupled ambient imaging methods such as desorption electrospray ionization (DESI)[283-285] — the most widely used ambient MSI technique[286] — and laser ablation electrospray ionization (LAESI),[219,287,288] with Orbitrap and ICR-based FTMS instrumentation. FTMS resolution and mass accuracy can enable assignment of elemental or sum-composition formula to detected ions (including those with isotopic tags), thus providing detailed information regarding the local chemical composition of the sample.[289]

Routine ICR and Orbitrap FTMS instrumental methods can, nevertheless, often be insufficient to distinguish certain isobaric ion pairings. A powerful example of this occurs in lipidomics where, for example, one requires a mass resolution of >150,000 to fully resolve lipid signals containing 2 atoms of ^{13}C from the monoisotopic ion of analogous lipids with one fewer site of unsaturation (Δm = 8.9 mDa).[290] Even higher mass resolution is required to resolve sodiated lipid ions from the corresponding protonated lipid containing two more carbons and three more double bonds in the

acyl chains (e.g., $[PC(34:1)+Na]^+$ vs $[PC(36:4)+H]^+$, Δm = 2.4 mDa). Shevchenko *et al.* have recently shown that ultra-high resolution performance capable of baseline-resolving peaks of ^{13}C isotopes of unlabelled and monoisotopic peaks of ^{15}N labelled lipids (Δm = 6.3 mDa) opens new avenues for quantitative shotgun lipidomics.[291] FTMS based instruments are able to tackle these challenges by simply increasing the time-domain signal (transient) recording time, which has an (approximately) linear correlation to mass resolution. For example, extending the ion detection time from one to five seconds will result in a theoretical five-fold improvement in mass resolution. However, given that a typical MS image can consist of tens of thousands of pixels, acquisition time may become a constraining factor. Therefore, mass resolution is often sacrificed in favour of speed.[292]

In this paper we present an approach to significantly improve the experimental mass resolution and accuracy per time unit in FT-ICR based MS imaging, enabling MS imaging with unparalleled mass resolving power. To achieve this result, we developed a novel architecture of a data acquisition system for time-domain signals (transients) recording from FTMS instruments and an advanced data processing pipeline to maximize the extraction of accurate mass spectral information from these transients. The developed data acquisition and processing pipeline targets the following procedures and capabilities: (i) parallel ion accumulation and detection for transients of any length; (ii) absorption mode FT post-processing adapted for big data processing; and (iii) efficient internal re-calibration. The current state-of-the-art in these three domains is briefly summarized below.

Parallel ion accumulation and detection

Parallel ion accumulation and detection refers to an ability of FTMS instruments to record a transient in an FTMS cell for a given scan during ion accumulation in another ion trap for the following scan. In case when ion accumulation and ion detection times are comparable, for example both of them are about 0.1-1 s, this capability can significantly increase the throughput of FTMS measurements. Historically, perhaps the first implementation of parallel ion detection and accumulation was realized when two ICR cells were placed in a high magnetic field and operated independently.[293] The dual cell configuration allowed to accumulate ions in one cell while ion detection was taking place in the second cell. More recently, Bruce and co-workers developed this original idea into a more sophisticated configuration that included an array of ICR cells.[294] Up to date, none of these configurations has been realized in a commercial instrument and has not been employed for MSI experiments. The second type of parallel ion accumulation and detection capability is based on the use of ion accumulation in ion traps external to the magnetic field with a parallel ion detection taking place in the ICR cell for a pre-defined ion detection time. The up-to-date implementation of this approach relied on the data acquisition systems

that allowed recording of transients for a certain pre-defined duration, e.g., 128 ms, 256 ms, 512 ms, *etc*. The increment of the length of these transients followed the 2-fold rule which follows from the architecture of the data acquisition systems. Therefore, in cases where the ion accumulation time exceeds a pre-defined transient length for a certain scan, there will be no ion detection taking place during the excess time. The first mentioning of an experimental implementation of this approach to maximize the measurement duty cycle appeared around the same time as the dual-trap concept as a result of developments by Senko and co-workers.[295] A decade later, the same laboratory reported on the implementation of a higher performance data acquisition system that facilitated the overall experiment control and expanded the range of capabilities.[296] Interestingly, being implemented in FT-ICR MS for the past 20 years according to the published reports,[295,297] it is not explicitly mentioned as an employed method in the peer-reviewed papers. Furthermore, the only use of this capability in a commercial FT-ICR MS instrument, where it is known to be realized as an "accumulation during detect", or ADD function (FT-ICR MS from Bruker Daltonics), has been mentioned in a conjunction with a related technology of ion mobility.[298] It should be noted, that the modern generations of Orbitrap FTMS instruments are capable of routinely performing parallel ion accumulation and detection in the way described above (pre-defined transient duration, 2-fold duration increment).

Implementation of parallel ion accumulation and detection in the present work principally differs from the prior art by using the high-performance data acquisition system. The "high-performance" terminology is usually employed to signify the use of the new-generation electronics components with embedded advanced capabilities for in-line digital signal processing.[299] As it will be shown below, the high-performance data acquisition systems allow transient detection for any duration and for all the time ions are trapped inside of the ICR cell. That means a fully parallel ion detection to external ion accumulation, fragmentation and eventual overheads. With respect to a DESI MSI application it means that any ion accumulation period can be matched with the ion detection period, without a need to adjust ion accumulation to a pre-defined transient length.

In case ultra-high resolution is required from an FTMS instrument, transient length can be increased up to 2-10 seconds and more, thus significantly shifting the scan rate principal contribution from ion accumulation to ion detection. Long transients and thus low scan rates are particularly detrimental to MSI due to a large number of pixels to constitute an image. Therefore, further measures to reduce the transient length without the loss of a resolution can be considered. In modern FTMS these methods include increasing the magnetic fields strength, up to 21 T presently,[300] and performing frequency multiples measurements, with the experimentally implemented quadruple frequency multiple FT-ICR MS operation as the highest one.[301,302]

Absorption mode Fourier transform MSI

Efficient processing of transients in modern FTMS implies spectral representation in absorption mode FT (aFT), which can be compared with the magnitude mode FT (mFT) spectra representation.[303-306] This switch provides a theoretical improvement in mass resolution of up to 2-fold, and an improvement in both signal-to-noise ratio and the mass accuracy for the same transient length.[307] So far, Smith *et al.* have provided the only report on the use of absorption mode FT-ICR for MSI. The data presented a mass resolving power of approx. 300,000 at *m/z* 700 in a MALDI approach with a scan time per pixel of 1.8 s, which is one of the highest resolutions reported for any MSI approach.[308] Some spectral features were still unresolved, which confirms the need for further improvements in MSI mass resolution. Absorption mode processing has not been regularly applied to MSI datasets because the procedure can be rather complex and time consuming. With newly developed data processing software we demonstrate the first implementation of absorption mode FT for FT-ICR MS imaging in combination with ambient ionization technologies (DESI), including processing of very large, up to 1 TB, datasets.

Pixel-based internal recalibration

Conversion of frequency spectra represented in the aFT mode into accurately calibrated mass spectra is another challenge in FT-based MSI. Due to substantial scan-to-scan (or pixel-to-pixel) possible variation of a number of ions (charges) in the ICR cell, peak shifts may be prominent (space charge influence). Therefore, internal re-calibration is typically required for MSI datasets acquired with any FTMS instrument as calibration parameters vary from pixel to pixel. Performing a single point (lock mass) re-calibration is the simplest method employed. More sophisticated methods include several known peaks, as for example implemented for MALDI FT-ICR MSI by Smith and co-workers.[309] Another approach employed a number of ions present in the ambient laboratory environment, namely polydimethylcyclosiloxanes, as suggested by Barry and co-workers.[310] A number of mass spectra re-calibration procedures are known in general for FTMS non-imaging applications, as published and reviewed elsewhere.[311,312] In this work, we adapted one of the recent algorithms for re-calibration of FTMS mass spectra that is based on an iterative use of binomial averaging for calculating a non-linear re-calibration function.[313]

By applying all of the above to lipid imaging of both brain and kidney tissue on a hybrid 7 Tesla LTQ FT-ICR MS instrument we demonstrate the power of ultra-high mass resolution MSI for biological tissue imaging.

5.7. RESULTS

Influence of ion accumulation time on mass accuracy and signal-to-noise ratio

An ICR cell requires a pre-set number of charges (typically 10^5-10^6) to be acquired for each scan (pixel) to achieve maximum analytical performance, both in mass accuracy and sensitivity.[314] To a point, larger ion populations in the ICR cell lead to higher sensitivity. Routine mass calibration is therefore performed using continuous electrospray infusion with automatic gain control (AGC) set to accumulate a fixed number of charges in the ICR cell (5×10^5 in our case). In contrast, DESI MSI experiments are typically performed in the absence of AGC to ensure equidistant pixel distribution in an image. Additionally, an accurate estimation of a number of charges for application of the AGC function is jeopardized because heterogeneous tissues inevitably produce fluctuating ion yields, which results in over- or under-filling of the ICR cell throughout an MSI experiment. This leads to characteristic *m/z* shifts, due to space charge effects.[315] If the average pixel-to-pixel *m/z* shift is greater than the *m/z* difference between isobaric compounds of interest, it is not possible to generate clear mass spectral images of these compounds. It is therefore of importance to ensure that, for most pixels, the ICR cell is filled within the optimal range of charge numbers.

Therefore, we first investigated the influence of ion accumulation time on both signal-to-noise ratio (SNR) and on ppm mass error relative to the default calibration optimised for 5×10^5 charges target on a hybrid 7 Tesla LTQ FT-ICR MS instrument (Figure 5.1). Averaged DESI mass spectra were recorded from consecutive rows on a (relatively) homogenous area of a rat brain section. The length of each row and the number of scans was kept the same (8.6 mm, 65 scans), while the stage speed was adjusted inversely with the ion accumulation time to ensure the pixel size was the same for each row. The base peak SNR and the mass error for four abundant lipid species (Supplementary Table S5.1) were calculated using the full averaged mass spectrum of each experiment.

As can be seen in Figure 5.1a, larger ion numbers result in a mass shift towards higher *m/z* values for a constant calibration function, whereas negative mass errors are observed at low accumulation times. The smallest mass error was found at an ion accumulation time of 3000 ms. Based on this data and the fact that the instrument is calibrated for 5e5 charges we can estimate an ion generation rate of approx. $1.6\text{x}10^5$ ions/second in our experiment, assuming a constant generation rate and singly charged ions. It was observed that the SNR increases with injection time (Figure 5.1b), flattening off towards longer accumulation times. This was expected, as DESI is able to generate stable signal from a single tissue location for at least several seconds. Most importantly, the optimal ion accumulation time range for maximum sensitivity under these experimental conditions turned out to be from 1000 till 4000

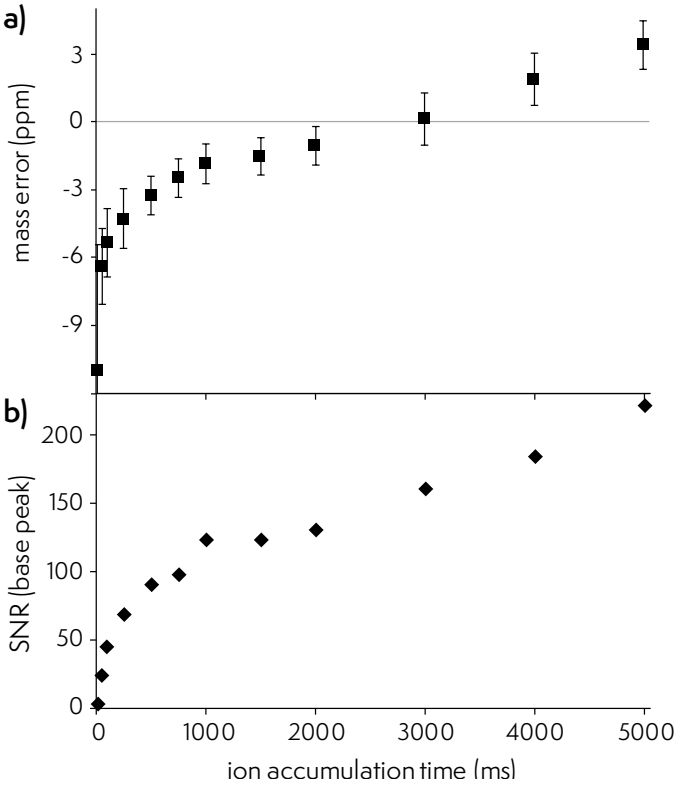

Figure 5.1: *Method development on a DESI 7 T LTQ FT mass spectrometer. (a) Plot showing the measured 4-peak average mass error and (b) the base peak signal-to-noise ratio (SNR) with varying ion accumulation time. Data collected via subsequent line scans across a rat brain tissue section with varying ion accumulation times. Values shown are calculated from the averaged mass spectrum via Thermo Xcalibur Qual Browser with SNR calculated on the base peak and mass error calculated as the average error for four highly abundant lipid species (details in Supplementary Table S5.1).*

ms, much longer than typically used. Of course, larger ion populations increase the chance of peak coalescence between isobaric species with minimal mass difference. To separate minimal mass differences sensitivity might need to be sacrificed, as will be demonstrated below.

Increased duty cycle and mass resolution per unit time via modified acquisition sequence

The commercial LTQ-FT system does not support accumulation of ions in the external ion trap during acquisition of the transient signal in the ICR cell, as discussed above. In regular electrospray experiments, with ion accumulation times of <100 ms and typical transients in the order of hundreds of milliseconds, this does not significantly prolong analysis time. However, in ambient FT-ICR imaging such as DESI-MSI, both the optimal ion accumulation times and the acquisition times can be in the order of

seconds, as shown above. In this case, parallel ion accumulation and signal acquisition provides immediate gains in throughput or both in sensitivity and mass resolution.

Figure 5.2, Scheme 1 shows a single acquisition cycle of the original LTQ-FT mass spectrometer. Typically, after the ICR cell quench, followed by a next ion population trapping and excitation events, the transient is recorded for a set period (correlated to the desired resolution). Once the ion detection is over, and after some overhead time required for electronic and on-the-fly data processing, the accumulation of ions for the next pixel is started and the sequence is repeated. In our approach, recording of the transient is performed in parallel with the standard LTQ-FT data acquisition by using an external high-performance data acquisition (DAQ) unit (Figure 5.2, Schemes 2a-c). By doing so, the external transient acquisition continues whilst ions are accumulated for the next pixel; the transient recording continues up until the ICR cell is quenched to prepare for the next analysis cycle. This results in a longer transient (and thus a higher mass resolution) for the same overall scan time. Due to the advanced electronics architecture in the external DAQ system, the length of the transient can match any actual total ion detection time. That favourably compares to the previous generation DAQ systems, as discussed in Introduction.

Figure 5.2, Scheme 1 displays a conventional DESI-LTQ-FT analysis workflow (750 ms ion accumulation time, 100k mass res. in 1.6 second scan time per pixel). With these settings, adding an external DAQ approach provides an estimated 2-fold gain in mass resolution with improved sensitivity at identical throughput by doubling the transient length (Figure 5.2, Scheme 2a). However, the external DAQ unit can be used much more efficiently: the ion accumulation time can be lengthened to approximately 90% of the total scan time without adding to the total scan time by reducing the instrument resolution setting to 12.5k, as shown in Figure 5.2, Scheme 2b. Extending the ion accumulation time in this way improves the sensitivity by about 25% (Figure 5.1) without compromising in mass resolution or throughput. Alternatively, the parallel operation can be used to increase the analysis throughput without sacrificing sensitivity or mass resolution, as shown in Figure 5.2, Scheme 2c. In this way, the resulting sensitivity is identical to that obtained via Scheme 1, while the theoretical mass resolution is more than doubled (approx. 230k at *m/z* 400) even though the analysis time is halved.

High-throughput, high-mass resolution imaging

The analytical benefit of our approach is demonstrated in Figure 5.3 showing spectra generated from rat kidney tissue using three different acquisition sequences. Figure 5.3a corresponds to the conventional workflow as shown in Figure 5.2, Scheme 1. The conventional LTQ-FT was optimized for a "fast" imaging experiment at 1 scan per second. As expected, the measured mass resolution was approx. 25k at *m/z* 800, in accordance with the 50k at *m/z* 400 specifications. Simultaneously,

the dataset displayed in Figure 5.3b was acquired on the external DAQ unit and FT processed in magnitude mode (mFT). The resulting 71k (at *m/z* 800) mass resolution shows a significant (2.9-fold) improvement over the spectrum recorded using the conventional system for an identical scan time. The increase in resolving power reveals some additional mass spectral features. When this experiment is repeated on an adjacent tissue section, but now with sensitivity and resolution optimized similar to Figure 5.2, Scheme 2b, and absorption mode FT processing (aFT) is used instead of mFT processing, all features are baseline separated with a mass resolution of 160k (Figure 5.3c). A 6-fold overall improvement in mass resolving power compared to the conventional approach is the result without sacrificing throughput.

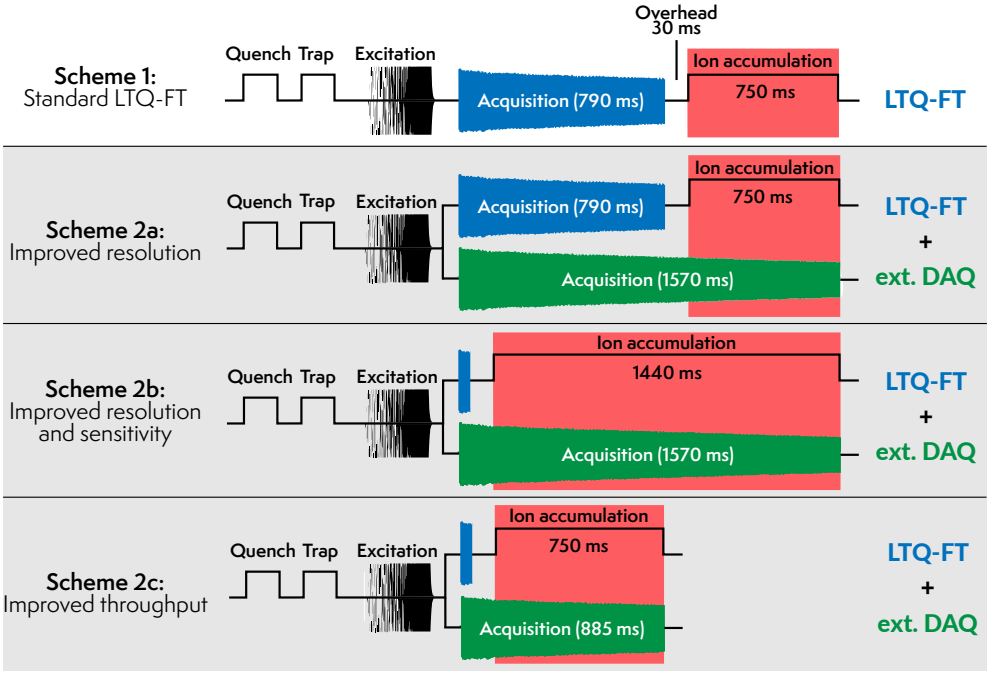

Figure 5.2: *Accumulation and transient acquisition scheme options. (1) conventional acquisition at a set mass resolution of 100k at m/z 400; (2a) parallel acquisition via the conventional scheme and external data acquisition (DAQ) unit FTMS Booster X1, the latter providing an estimated 220k resolution in magnitude mode and 430k in absorption mode at m/z 400; (2b) parallel acquisition via the external DAQ unit, optimized for both mass resolution and sensitivity; (2c) parallel acquisition via the external DAQ unit, optimized for throughput without sacrificing sensitivity or mass resolution compared to Scheme 1. *The timespans indicated for acquisition and accumulation are typical examples at 100k mass resolution instrument setting (at m/z 400).*

To demonstrate the value of our approach for MSI, we show examples of ion distribution images from the first (Figure 5.3a) and third (Figure 5.3c) dataset in Figure 5.4. The single peak detected at *m/z* 828.55 in the conventional LTQ-FT setup (Figure 5.4b, blue) revealed six isobaric species in the external DAQ approach, with aFT processing (Figure 5.4b, red). Of these six species three could be tentatively

identified as monoisotopic lipid species and two as isotope peaks (^{41}K and 2x^{13}C) of phosphocholine 36:1 (PC(36:1)). Species *m/z* 828.5364 (Figure 5.4f) was not fully resolved from *m/z* 828.5315 (Figure 5.4e) but each reveals a clearly distinct spatial distribution. Both datasets were uploaded to METASPACE[316] and processed against the HMDB-v4 database with a maximum FDR of 10%, a minimum metabolite-signal match (MSM) score of 0.5 and a mass error ≤3 ppm.[317,318] The conventional LTQ-FT dataset resulted in 34 annotations in the 700-900 *m/z* range versus 66 annotations for the external DAQ aFT dataset.

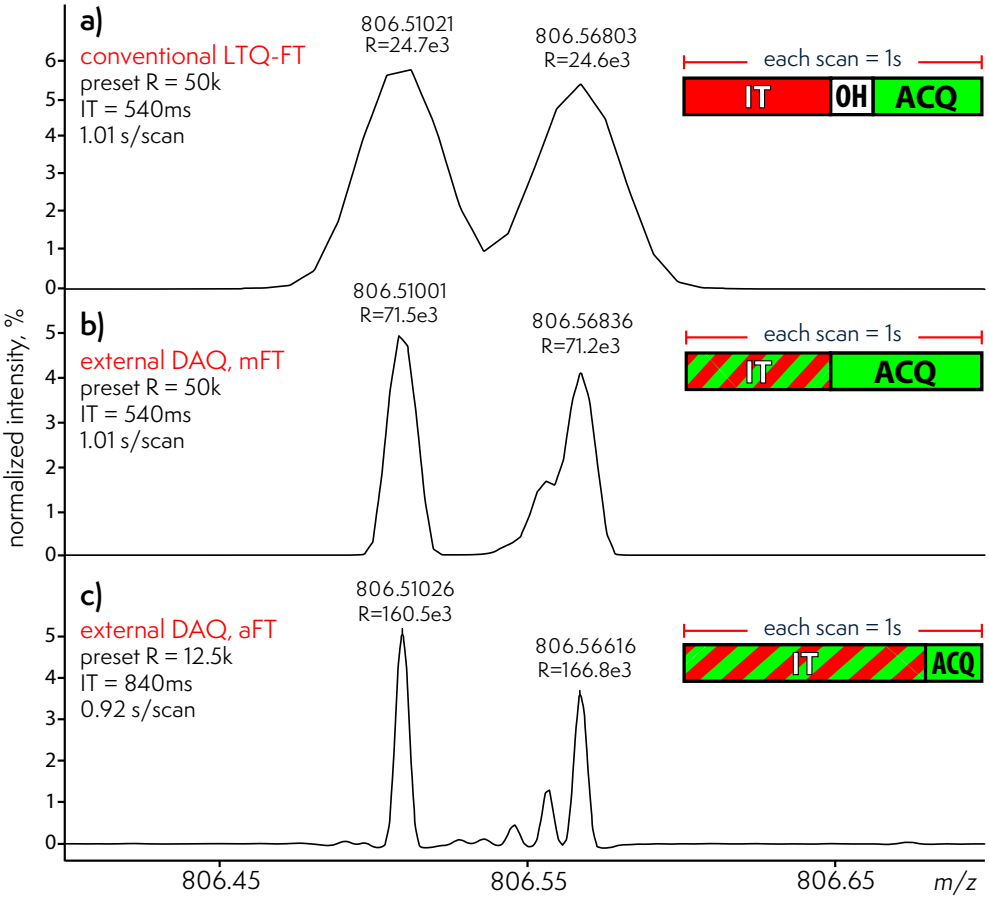

Figure 5.3: *Mass spectral quality comparison between recording and processing modes for 1 pixel per second analyses of a rat kidney section. Zoom-ins of full image average reduced profile spectra of: (a) typical LTQ-FT performance at 50k (at m/z 400) resolution setting; (b) in parallel acquired spectrum on the external data acquisition (DAQ) unit and obtained with mFT processing; (c) resolution and sensitivity optimized experiment for the external DAQ unit, with aFT processing. *IT = accumulation time; OH = overhead time; ACQ = acquisition time. Spectra are normalized to the spectrum base peak. The full profile aFT version of (c) is provided as Supplementary Fig. S1.*

Exploring limits of high mass resolution DESI imaging

As can be seen in Figure 5.4, the use of high mass resolution in DESI imaging unravels a range of nearly isobaric (cat)ionization variants and overlapping isotope species. Minute mass differences, such as the difference between ^{13}C and CH (4.5 mDa) or SH_4 and C_3 (3.4 mDa), can be resolved by taking advantage of the high mass resolving power offered by FT-ICR MS. The combined resolving power and mass accuracy supports confident assignment of elemental compositions of biological species. And by resolving more spectral features, the spatial distribution of an increasing variety of distinct chemical species can be revealed, as demonstrated in Figure 5.4.

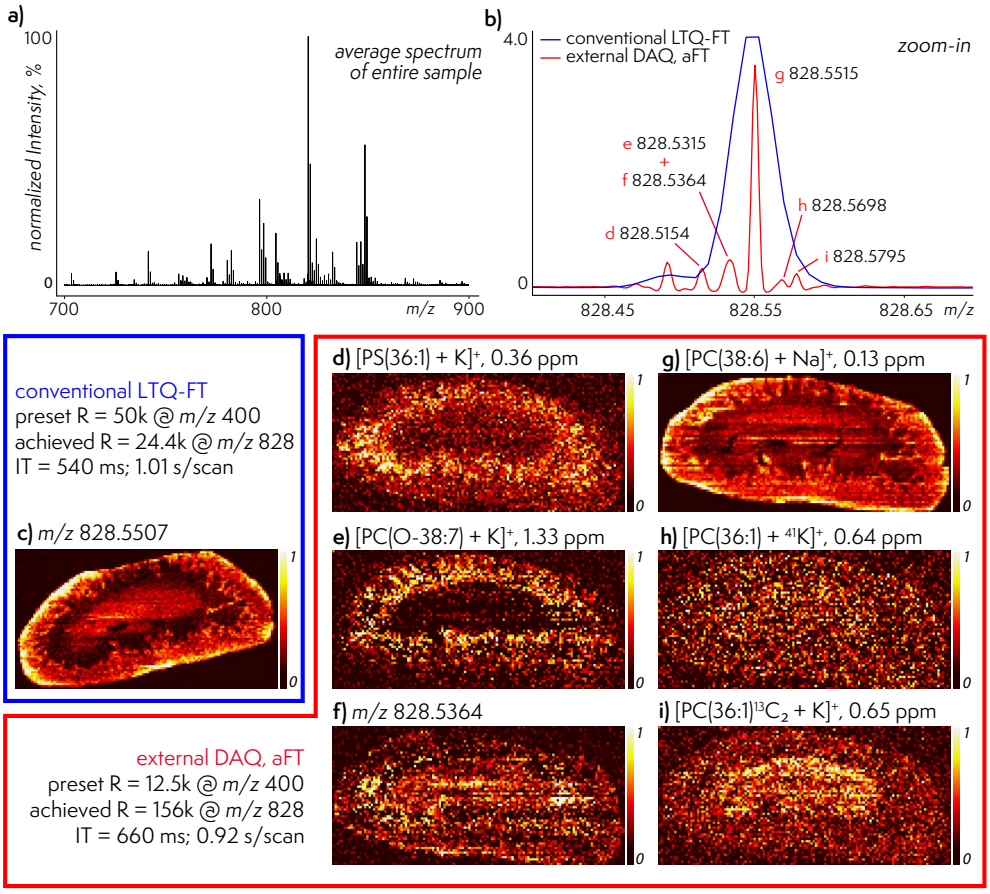

Figure 5.4: *Mass spectral images of lipid species detected around m/z 828.55 in approx. 1 scan per second experiments on adjacent rat kidney sections. Top-right shows the spectrum around m/z 828.55, for the conventional LTQ-FT setup (blue) and the external DAQ (red). The achieved mass resolution on the most abundant m/z 828.55 peak was 24.4k and 156k, respectively (average spectrum of entire sample area). Image recording took 2 hours for each image at 150 µm by 150 µm pixel size, with both datasets containing approximately 8000 pixels. All images are TIC normalized and plotted on a linear intensity scale. Given the very low abundance of some species, a 5% image intensity threshold was applied to each image to reduce noise. The full profile aFT version of (b) is provided as Supplementary Fig. S2.*

One of the challenges left to resolve is the distribution of different cationized lipid adduct species. For example, changes in ratios of adduct species (e.g., sodiated and potassiated adducts of PC lipids) can infer insight into altered biochemical processes in tissues. As an example, a reduction in PC $[M+K]^+$ ions was correlated with an increase in $[M+Na]^+$ at the site of traumatic brain injury in mice and attributed to loss of Na^+/K^+-ATPase activity.[319] Unambiguous detection of individual adduct species can be challenging as the accumulated mass defects are usually compounded by the presence of different monoisotopic or isotope peaks. For this reason, we have explored the current limits in high mass resolution DESI imaging by resolving the *m/z* difference between the sodiated species of phosphocholine (34:1) $[PC(34:1)+Na]^+$ and the protonated species of phosphocholine (36:4) $[PC(36:4+H]^+$. Here, both species are separated only by 2.4 mDa, or 3.1 ppm. To properly resolve this difference a mass resolving power of approx. 900k at *m/z* 782 is theoretically required, assuming equal peak height, as shown in Supplementary Fig. S5.3, generated using a method described earlier[320]. Here, properly resolved is defined as achieving the deepest possible valley between the two peaks (see Supplementary Video S1).

We acquired an image dataset of a rat brain section with an acquisition time per pixel of approx. 6.3 seconds. Baseline separation of $[PC(34:1)+Na]^+$ and $[PC(36:4+H]^+$ in a single spectrum could have been achieved with a considerably shorter transient. Figure 5.5 shows the baseline separation of $[PC(34:1)+Na]^+$ and $[PC(36:4+H]^+$ species with a mass resolution of approx. 1M in the full image average spectrum (Supplementary Fig. S5.4). The insets of Figure 5.5 show the spatial distribution of PC(34:1) and PC(36:4) across the rat brain section. PC(34:1) is quite homogenously distributed, whereas PC(36:4) shows higher abundance near the cortex but is nearly absent in the cerebellum. To generate clear MS images of these two species, care had to be taken to avoid any space-charge and peak coalescence effects. Therefore, the ion population in the ICR cell was intentionally kept low by restricting the ion accumulation time to 3000 ms, restricting the mass range to *m/z* 765-832 and reducing the solvent flow rate to 3 µl/min (in contrast to 5 µL/min used for datasets shown above). Naturally, reducing the ion populations in the cell lowered the dynamic range of the experiment to about two orders of magnitude, as shown by Figure 5.5. Total acquisition time for this dataset was 31 hours, a comparison of data file sizes is included as Supplementary Table S5.3. Measured mass accuracy (after internal recalibration) of these two ions throughout the experiment is shown in Supplementary Fig. S5.5. Analogous separation and distinct ion distribution imaging of sodiated phosphocholine (36:1) and protonated phosphocholine (38:4) are provided in Supplementary Fig. S5.6. The corresponding mass errors are provided in in Supplementary Fig. S5.7. The distributions of some common lipid species are added in Supplementary Fig. S5.8.

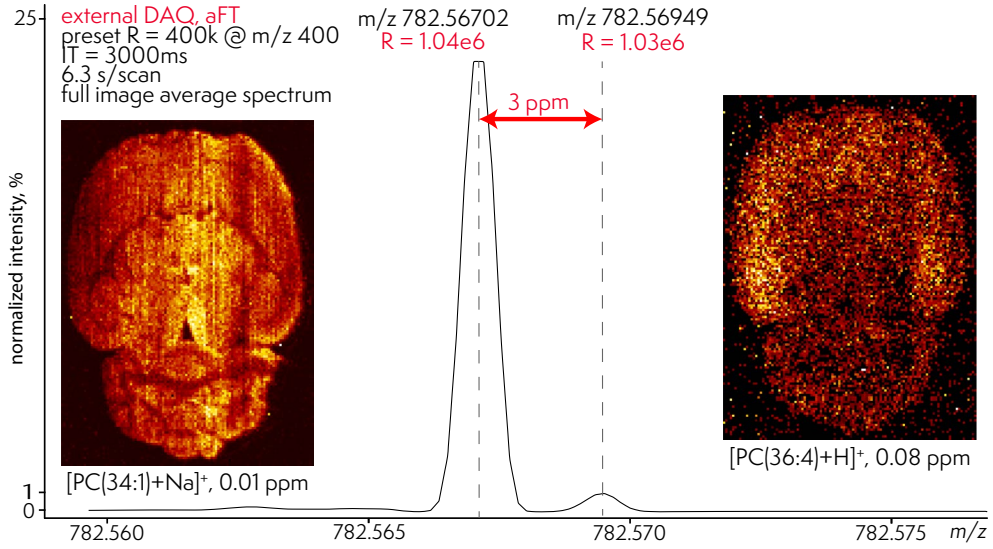

Figure 5.5: *Full image average mass spectrum showing the separation of [PC(36:4+H]⁺ and [PC(34:1)+Na]⁺. The data was acquired on the external DAQ unit and processed with aFT. Acquisition time of 16761 spectra at a pixel size of 150 µm was approximately 31 hours. Insets: the spatial distributions of [PC(34:1)+Na]⁺ and [PC(36:4+H]⁺, noted with the annotation mass error. The images are TIC normalized and spectral abundance is indicated as relative to the base peak (m/z 798.5) in the full mass range (m/z 700-900). Note the achieved mass resolution (1 million @ m/z 782).*

5.8. DISCUSSION

We have demonstrated an approach to drastically improve the sensitivity, mass resolution and/or throughput of DESI-FT-ICR MS imaging experiments on a 7 Tesla LTQ-FT instrument. For the first time, absorption mode FT processing has been applied in an ambient imaging setting and its benefits (about 2-fold resolution increase over magnitude mode) have been shown. We have shown that our parallel data acquisition approach makes it possible to achieve 6-times higher mass resolution in the same experimental time period, which is crucial for imaging approaches. In 1 scan/second experiments isotopic lipid patterns could be revealed (Figure 5.4), demonstrating that in positive mode DESI-imaging at conventional mass resolution the spatial distributions of multiple isobaric lipid species merge, which will almost inevitably lead to incorrect interpretation. Enabling ion accumulation for extended periods of time benefits specifically continuous ionization methods, such as DESI MSI applications, to provide enhanced sensitivity. For MALDI-MSI ionization events are usually 10-100-fold shorter (10-100s of milliseconds), which reduces the benefit of performing parallel ion accumulation and detection. Nevertheless, the possibility to extend the ion accumulation period can also be beneficial for MALDI and other pulsed ionization methods when increased sensitivity is required, such as MS/MS applications where precursor ions from multiple adjacent sampling regions may collected for enhanced

sensitivity. Furthermore, the approach presented here also enables ion detection in parallel to other processes external to the ICR cell, not only to ion accumulation. That includes, among others, overhead time that is required for on-the-fly data processing, which may take >100 ms per pixel in a conventional MALDI FT-ICR MSI experiment.

MSI with one million mass resolution was demonstrated for a variety of lipid species, which resolved some of the smallest mass differences encountered in lipid imaging of biological tissues. To the best of our knowledge, this is the highest mass resolution imaging dataset reported to-date. We have shown that ultra-high mass resolution can increase the information content of imaging experiments and can add confidence to the validity of experimental results. It must be noted that all annotations provided in this manuscript are limited to lipid class, total chain length and double bond count (i.e., sum-composition level), which is the limit of high mass resolution and accuracy in the absence of MS/MS data.[321] However, by using ultra-high resolution imaging confidence in mass spectral annotation is greatly increased and many more "pure" sum-composition level images are obtained, as demonstrated by the METASPACE annotation queries. Moreover, with the recent demonstration of intact protein imaging with DESI[322] our approach could readily be applied to MSI spectral performance for protein imaging, where increased sensitivity and identification of charge states of large, highly charged protein ions are key steps towards improved protein identification.

To enable high mass resolution ambient imaging the accumulation of ions, acquisition of FT-ICR MS transients, and allied data processing approaches need to be optimal. Our approach extracts exceptional performance from a standard 7 Tesla LTQ-FT instrument equipped (without hardware and data acquisition software modifications) with an external DAQ system, delivering unprecedented sensitivity, mass resolution and speed. This approach is applicable to other types of FTMS instruments, including other designs of FT-ICR MS and Orbitrap FTMS instruments, where it may provide comparable advantages for all or for certain parts of the imaging workflow presented here. The authors feel that the ability to record and store the transient in high quality and full length is crucial, as it will enable even higher performance as data processing methods become more sophisticated. Currently, endeavours to push (ultra-)high mass resolution imaging are still scarce, for mostly practical reasons. Until now, there were no commercial or open-source solutions available capable of working with MSI data of this quality. Specifically, the developed imaging software allowed processing image datasets of any size, with an example of an up to 1 TB image processed in the current work, without image splitting into a number of smaller chunks or using a mass resolution reducing "binning" method. We feel confident this work will help to make ultra-high mass resolution imaging more accessible to the field.

5.9. METHODS

Materials

Sections of 12 µm thickness were cut from fresh frozen healthy rat brain (transverse) and kidney (coronal) using a cryo-microtome (HM525; MICROM Walldorf, Germany) at -19 °C and -21 °C, respectively. These sections were thaw-mounted onto plain glass slides and stored at -80 °C until further processing. The mounted sections were placed in a desiccator for 20 minutes to remove excess water prior to analysis. HPLC-grade methanol and formic acid 99% (Biosolve B.V., Valkenswaard, The Netherlands) were used for the DESI spray solvent.

Desorption electrospray ionization (DESI) MS

All MSI experiments were performed using a 2D-DESI source (Prosolia Inc., Indianapolis, IN, USA) coupled to a 7 Tesla LTQ-FT Classic mass spectrometer (Thermo Fisher Scientific, Bremen, Germany). That implies an original, prior to Ultra ICR cell design, ICR cell configuration was employed. All images were recorded with a 150 µm pixel size. To ensure square pixels were acquired, the continuous stage motion speed was set to cover 150 µm during each single scan. The ion accumulation time — automatic gain control (AGC) was disabled — was optimized prior to analysis, depending on the experimental requirements.

All data were recorded in positive ion mode with mass spectrometer settings as follows: tube lens voltage of +100 V, capillary voltage of +44 V, and a capillary temperature of 320 °C. DESI was performed with an electrospray voltage of +5 kV and 7.0 bar nitrogen nebulizing gas pressure. The spray solvent consisted of methanol with 0.7% formic acid and was delivered via syringe pump at a flow rate of 5 µl/min (with the exception of 3 µL/min to generate the data shown in Figure 5.5 and Supplementary Fig. S5.4-5.8).

Parallel data acquisition

The instrument was coupled to an external high-performance data acquisition (DAQ) system (FTMS Booster X1, Spectroswiss, Lausanne, Switzerland) to record the transients in parallel with the LTQ-FT signal processing unit.[299] The employed DAQ system was developed on the platforms of high-performance field-programmable gate array (FPGA) and PXI-Express technologies. The system combines, on a high data transfer speed chassis, a high sampling frequency digitizer with an FPGA chip onboard for high-throughput in-line digital signal processing (DSP) algorithms, a dedicated computer for data co-processing, and an amplifier for signal conditioning. The DSP algorithms on the FPGA chip include a low-jitter digital decoder that detects start and stop triggers from the host instruments, enabling full transient acquisition. The DSP algorithms were developed and deployed to the FPGA using Xilinx compilation tools and LabVIEW (National Instruments, Ennetbaden, Switzerland). The

DAQ system is interfaced to an FTMS instrument of interest via standard FTMS digital and analog output connectors. Recorded data files are integrated with metadata from the host FTMS through software interfaces to vendors' file formats, e.g., .RAW. The external DAQ unit records transient in parallel to the built-in electronics, which enables evaluation and comparison between datasets. Recording transients at higher quality allows for more sophisticated processing, resulting in higher quality mass spectra compared to the original system. The source, instrument and external DAQ unit were synchronized and controlled via Omnispray 2.0.1 (Prosolia Inc.), Xcalibur 2.1 (Thermo Fisher Scientific) and FTMS Booster Ctrl (Spectroswiss), respectively.

Data processing

Mass spectra and images were generated from the recorded transients using Peak-by-Peak software for data processing and conversion. AutoVectis software was used for absorption mode Fourier transform (aFT) signal processing. A newly developed feature in the AutoVectis software enabled efficient (aFT) processing on whole imaging datasets acquired with LTQ-FT coupled with the FTMS Booster data acquisition systems for the first time.[323] Full apodization was used to generate absorption mode spectra with no long-range baseline deviation. The F-value for the absorption mode processing was equal to 0.5, with 3 zero pads (fills). Note that the conventional LTQ-FT data acquisition and analysis approach exclusively uses magnitude mode Fourier transform (mFT) processing, whereas the external DAQ unit and associated processing/analysis software enables the use of aFT processing for imaging. The conventional LTQ-FT data is acquired following the standard procedures and stored as reduced profile mass spectra in Thermo RAW format. Both datasets are then converted into H5 file format for further processing using Peak-by-Peak. Following additional developments performed for the current manuscript, both imaging data processing and analysis software packages, Peak-by-Peak and AutoVectis, are now available commercially (Spectroswiss).

Noise thresholding, internal recalibration, peak picking and image generation was performed using the newly developed Peak-by-Peak imaging software. Noise thresholding level was determined as standard deviation of noise multiplied by a user-defined factor. The standard deviation was calculated by using a data-dependent noise thresholding algorithm.[324]

Each pixel of a whole dataset was internally re-calibrated using a reference mass list (Supplementary Fig. S5.9). The selected reference masses are well known, highly abundant lipid species spread over the lipid mass range of interest (Supplementary Table S5.2). The non-linear mass re-calibration method is described in Kozhinov *et al.*[313]. Search of an experimental mass in a single mass spectrum was performed within a mass tolerance window with its centre at the corresponding reference mass. To exclude the picking of parasitic sidebands and side-lobes instead

of analyte peaks, which can potentially disturb mass-recalibration, the highest peak in the mass tolerance window was selected. Single or several re-calibration iterations with different mass tolerance windows (± 2 – 30 ppm) were performed depending on the quality of initial (external) mass calibration and influence of space charge effects on frequency deviation.

Image generation

Image generation was performed by selecting the highest peak within a preselected mass tolerance window around the requested image mass value for each pixel. The mass tolerance window was adjusted to match the accuracy of the dataset. Parallel (multi-core) calculations, including 3-point interpolation peak picking of a reduced profile mass spectrum and a finding of peaks corresponding to the requested mass values in each pixel, were performed for the generation of images each time. This method allowed processing image datasets of any size, without loading all the data into the RAM memory, and was found to be more suitable for analysis of ultra-high mass resolution datasets than the prevalent "binning" method of MSI processing. Additionally, the distribution of mass errors between the requested and experimental mass values calculated in each pixel was plotted for an image, which helps to control image quality. The requested image mass value was adjusted in case the mean of mass error distribution was larger than 0.1 ppm. The resulting average image mass is shown in the spectra; its deviation from the annotated exact mass is the reported mass error value. All images shown are plotted on a linear intensity scale. All annotations given are tentative, based on measured *m/z* only, and are thus only reported to the sum-composition level.

5.10. DATA AVAILABILITY

Two annotated datasets are made publicly available via METASPACE.[317,318] All datasets generated during and/or analysed during the current study are available from the corresponding author on request.

5.11. SUPPLEMENTARY INFORMATION

Table S5.1: *Lipid species used for determination of mass error in main text Figure 5.1a*

ID	species	mol. formula	theoretical *m/z*
PC(32:0)	$[M+K]^+$	C40H80NO8P	772.5253
PC(34:1)	$[M+Na]^+$	C42H82NO8P	782.5670
PC(34:1)	$[M+K]^+$	C42H82NO8P	798.5410
PC(36:1)	$[M+K]^+$	C44H86NO8P	826.5723

Table S5.2: *Exact mass values used for pixel-by-pixel internal calibration*

ID	species	mol. formula	*m/z*
PC(34:1)	$[M+H]^+$	C42H82NO8P	760.585082
PC(36:0)	$[M+K]^+$	C40H80NO8P	772.525313
PC(34:1)	$[M+K]^+$	C42H82NO8P	798.540964
PC(36:4)	$[M+K]^+$	C44H80NO8P	820.525313
PC(36:1)	$[M+K]^+$	C44H86NO8P	826.572263
PC(38:6)	$[M+K]^+$	C46H80NO8P	844.525313
PC(38:4)	$[M+K]^+$	C46H84NO8P	848.556613
PC(40:6)	$[M+K]^+$	C48H84NO8P	872.556613

Table S5.3: *File size comparison between vendor original reduced profile data and external DAQ data*

Data type	File size (MB)
LTQ-FT reduced profile (.raw)	275
ext. DAQ aFT reduced profile (.h5)	3838
ext. DAQ transients (.h5)	763904

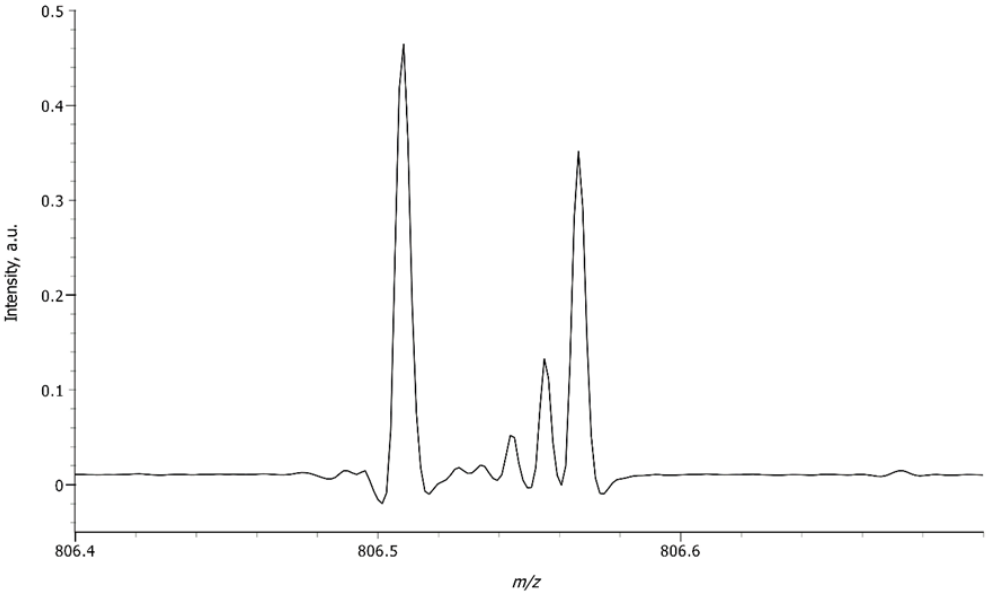

Figure S5.1: *Full image average full profile aFT spectrum of Figure 5.3c in the main text*

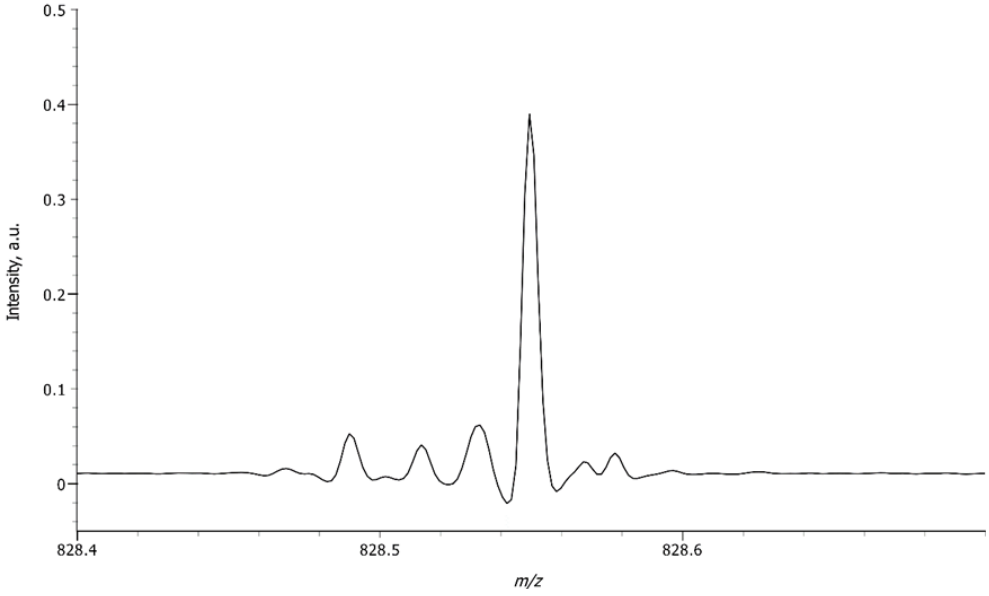

Figure S5.2: *Full image average full profile aFT spectrum of Figure 5.4b in the main text*

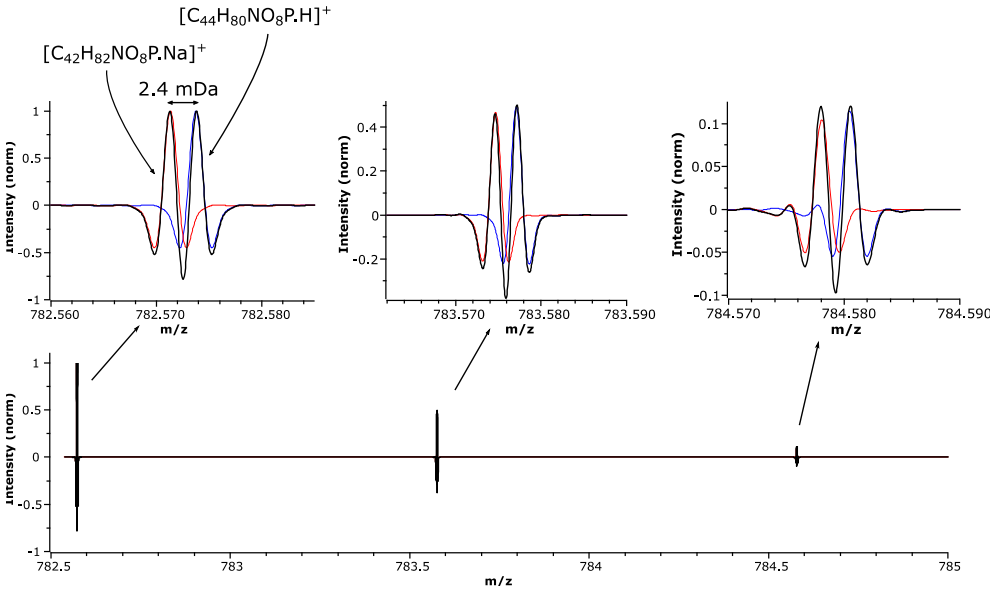

Figure S5.3: *Simulated mass spectra of the sodiated species of phosphocholine (34:1) [PC(34:1)+Na]+ and the protonated species of phosphocholine (36:4) [PC(36:4+H]+ at a mass resolving power of 900k, assuming equal peak height*

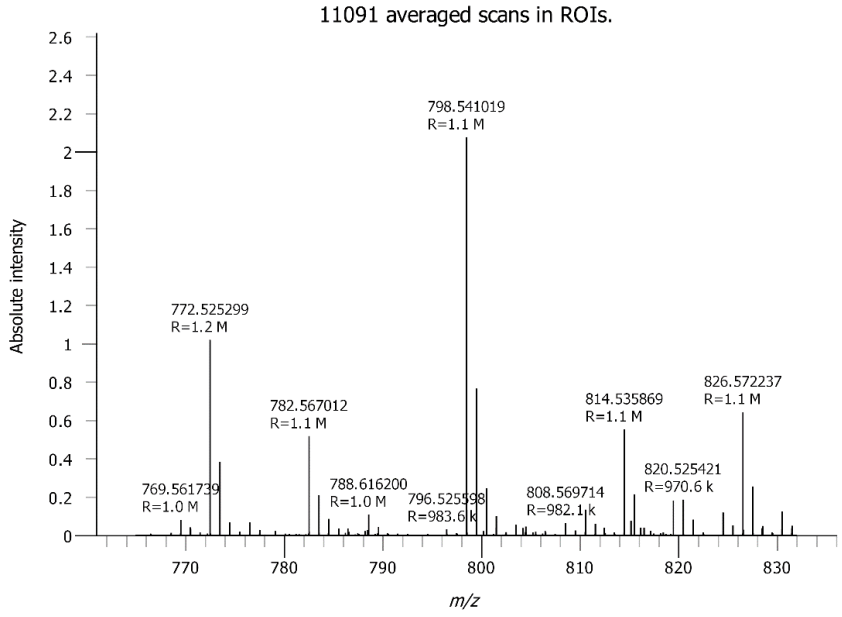

Figure S5.4: *Full average mass spectrum of the rat brain imaging dataset presented in Figure 5.5. Mass range limited to m/z 765-832*

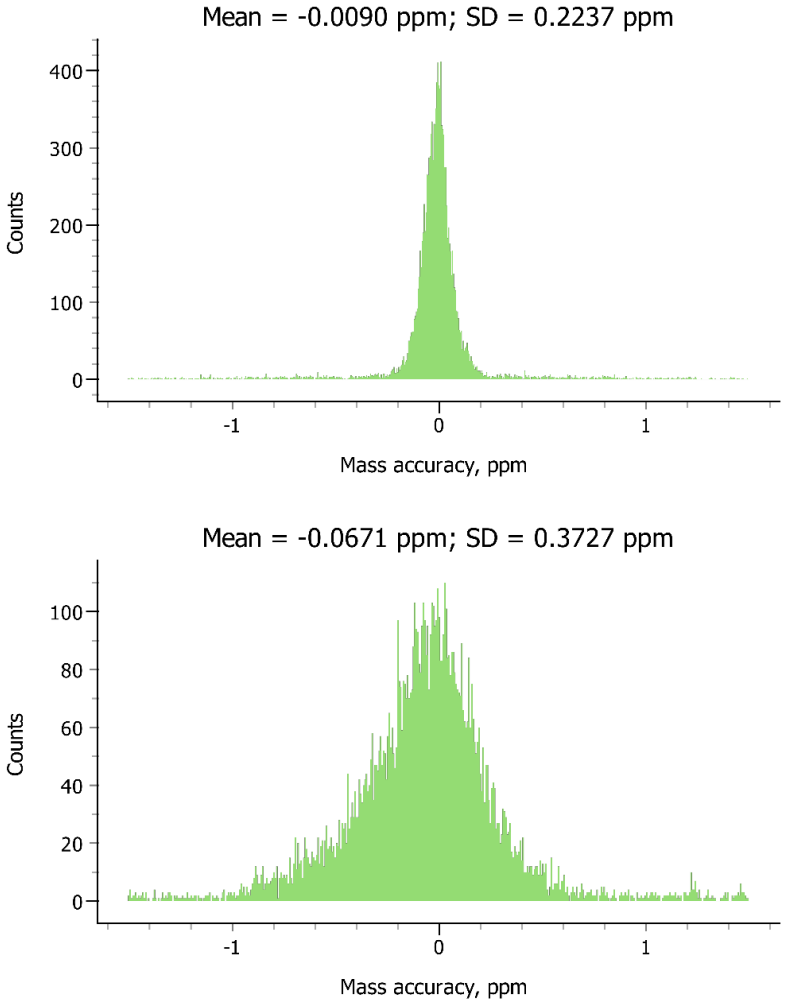

Figure S5.5: *Mass error distributions for the image of (top) [PC(34:1)+Na]+ and (bottom) [PC(36:4+H]+ . The corresponding images are shown on Figure 5.5 in the main text*

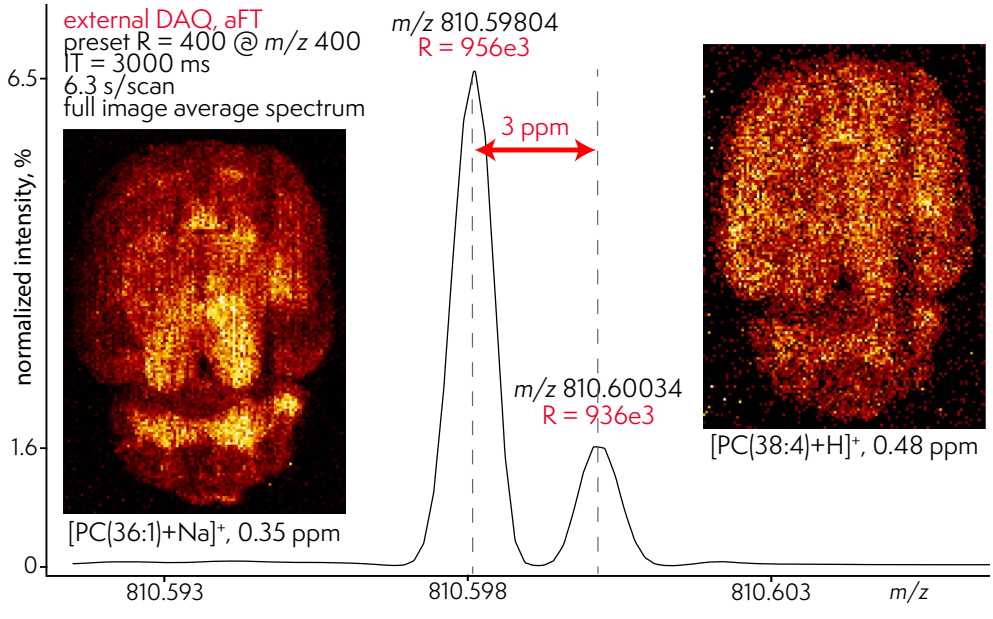

Figure S5.6: *MSI separation of sodiated phosphocholine (36:1) from protonated phosphocholine (38:4). A narrow mass window of the full image average spectrum is shown*

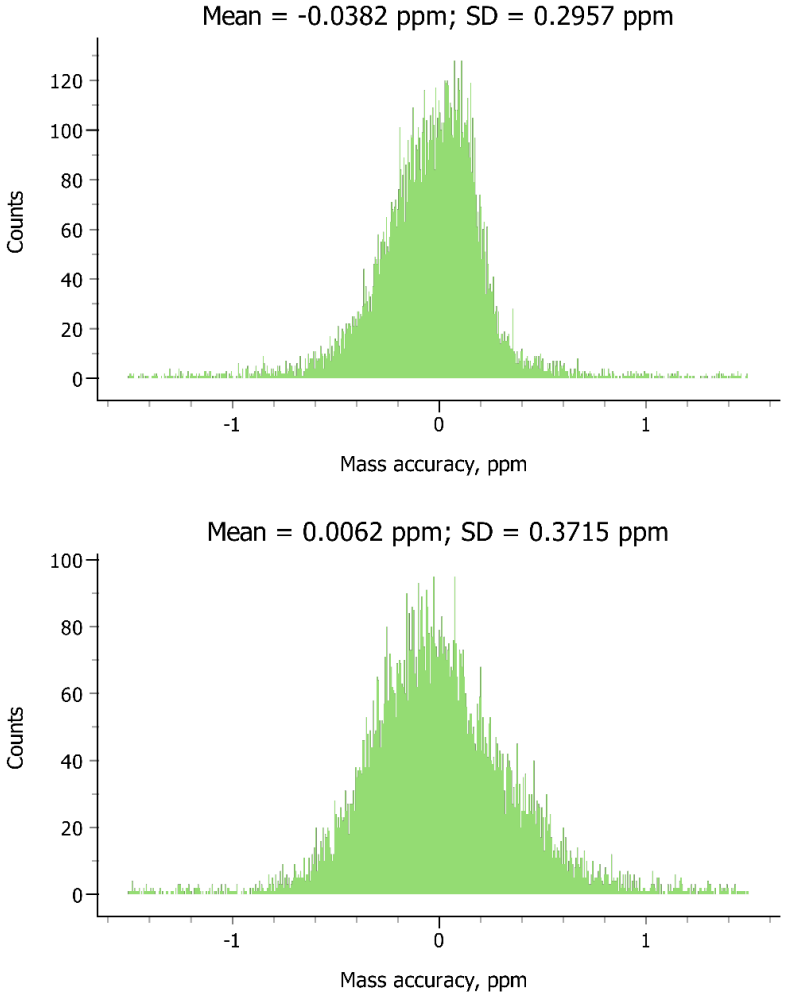

Figure S5.7: *Mass error distributions for the image of (top) [PC(36:1)+Na]+ and (bottom) [PC(38:4+H]+. The corresponding images are shown on Supplementary Figure S5.4 above.*

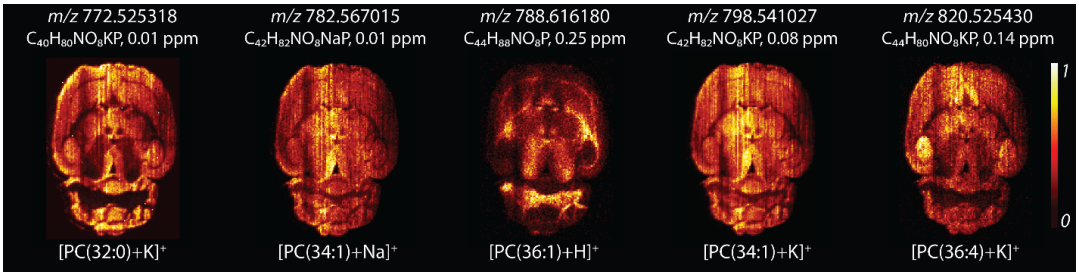

Figure S5.8: *Relative distributions of five commonly observed lipid species obtained by DESI-FT-ICR MSI on a rat brain section. All images are plotted without TIC normalization.*

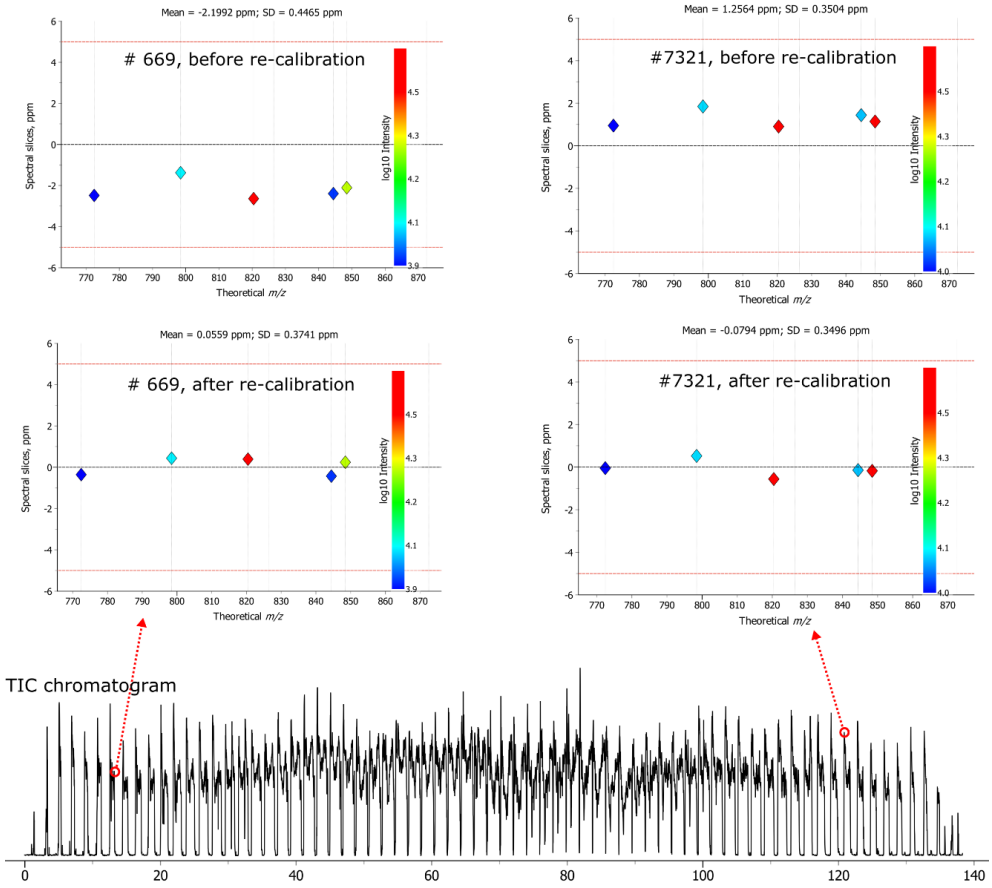

Figure S5.9: *Pixel-by-pixel internal mass re-calibration of DESI imaging experiment of kidney tissue using the reference mass list in Table S5.2. (Bottom panel) total ion current (TIC) chromatogram of the experiment. Mass error distribution of found experimental masses corresponding to the reference ones in certain scan numbers (top panel) before and (middle panel) after mass re-calibration procedure.*

Supplemental Video S5.1

https://www.nature.com/articles/s41598-018-36957-1

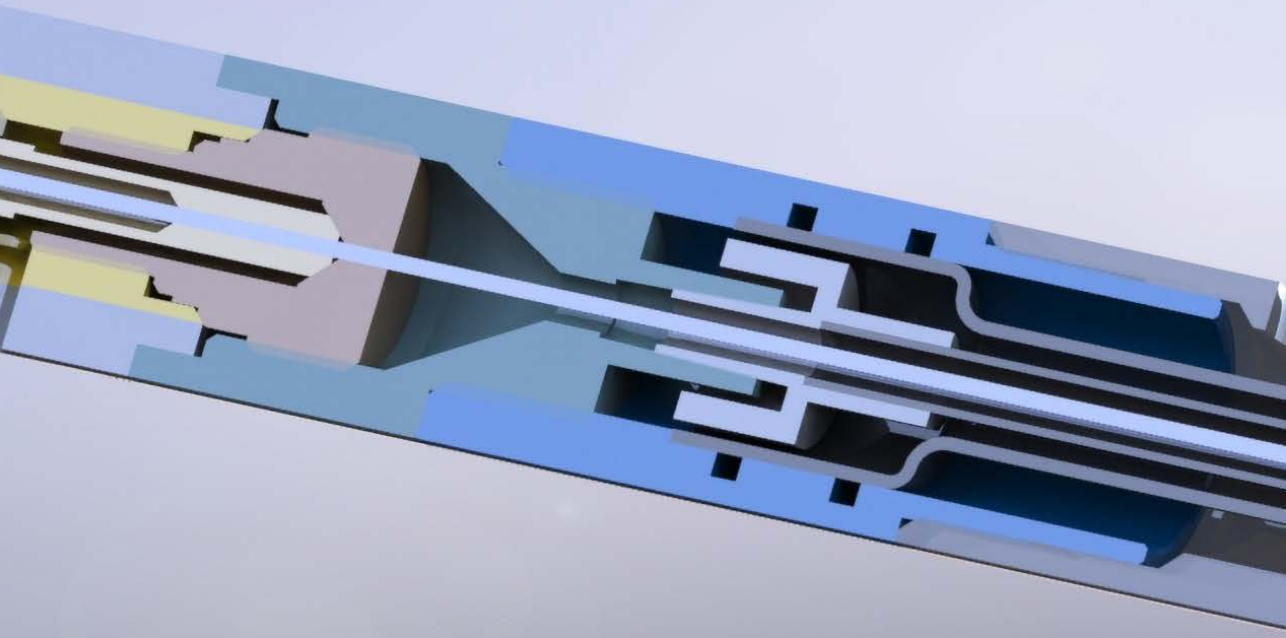

CHAPTER 6

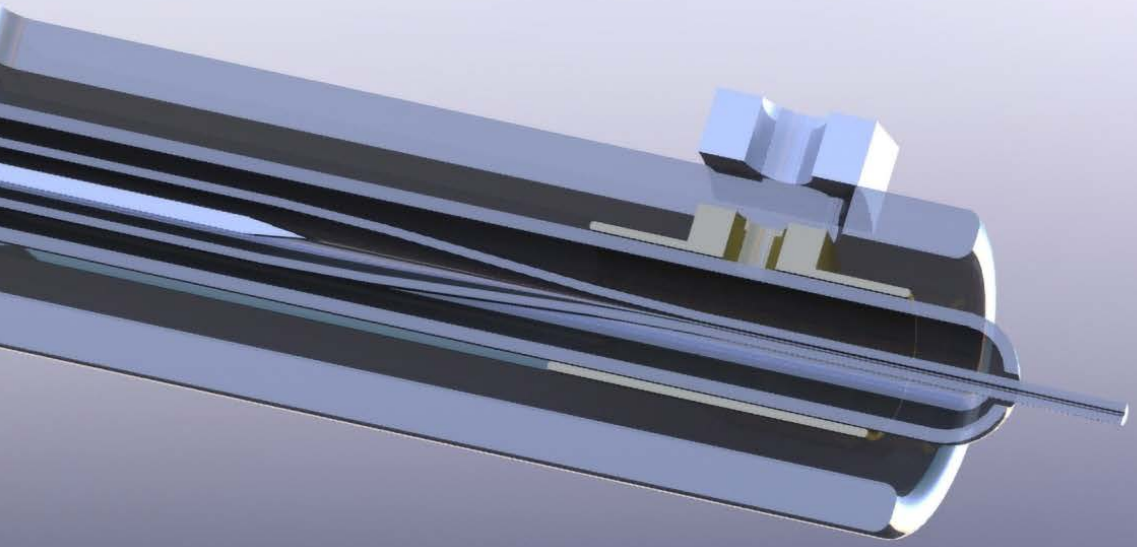

IMPACT

6.1. OBJECTIVE

The objective of this thesis research was to advance mass spectrometry imaging techniques for challenging real-world samples and analytes. The motivation stems from the belief that better tools enable better research, consequently an increased understanding of the world around us. We have focussed on ambient mass spectrometry because, in comparison to vacuum-based MSI, it is more flexible in terms of sample size, sample material and analyte properties. Infrared laser-based techniques are especially suitable for the analysis of water-containing samples such as biological tissues, foodstuffs, and novel synthetic materials such as hydrogels.

6.2. MASS SPECTROMETRY IMAGING OF BIOMATERIALS

In **Chapter 2** we present the current possibilities in molecular imaging of biomaterials, to lay the foundation upon which the research in this thesis builds. This published review forms a solid knowledge base for anyone who wants to familiarize themselves with the topic. At the same time, the writing and data gathering process has increased the depth knowledge of the authors in this topic, which enabled them to direct their research efforts more effectively.

6.3. AMBIENT PLASMA IONIZATION: NOVEL PROBE DESIGN AND APPLICATIONS

Chapter 3 shows for the first time that atmospheric pressure chemical ionization (i.e. "plasma") can successfully be incorporated in an MSI setup, and demonstrates clear benefits over the - more common - electrospray ionization alternative. In this project we collaborated with Bayer Crop Science, who are very keen to investigate new analysis techniques to gain more knowledge about their products. In this chapter we investigated how one of their antifungal agents spreads and converts inside a plant. Such information is highly valuable for the creation of more effective antifungal products.

The new combined LAESI/LA-APCI platform has high potential for the analysis of natural materials, such as organic versus non-organic agriculture. Comparisons of agricultural products on a localized, molecular level can produce new insights on their nutritional value and the underlying biological processes. This, in turn, has the potential to influence the public debate on this matter. To spread the knowledge about this novel instrumentation as broadly as possible we published the scientific results from **Chapter 3** in an open access journal and presented it at multiple academic meetings. We designed the two latest prototypes (one at Maastricht University and one at Wageningen University) to a high standard for reliability and safety. Therefore, we feel this design is ready to be commercialised, for which we are seeking an industry partner. The design will be very difficult to copy without direct

access to our prototypes and the raw data, which should protect it from being copied by competitors.

6.4. AMBIENT COLLECTION AND IONIZATION OF INTACT PROTEIN COMPLEXES WITH LAESI

Native MS could be used in high-throughput diagnostic screening approaches by use of infrared laser ablation, as described in **Chapter 4**. Native MS holds great promise for the analysis of dysfunctional enzymes, which are the root cause of many illnesses. Native MS is not quite ready for such approaches, yet. With this, the social impact of our research is still very much undecided. However, our method has only recently been published in an open-access journal, and we expect swift adoption by the scientific community once diagnostic native MS applications have been developed. The impact on the diagnosis and treatment of metabolic diseases with such a screening methodology cannot be overstated.

Interestingly, a few months after the publication of our results the group of Bunch published results of non-covalent protein complex analysis by DESI-MS.[325]

6.5. EXTENDING THE DETECTION LIMITS IN AMBIENT MASS SPECTROMETRY IMAGING

The methods and approaches presented and described in **Chapter 5** are expected to be incorporated in new (commercial) analytical equipment and software, for enhanced performance without time or hardware requirements. In fact, our high mass resolution MSI platform was developed in collaboration with Spectroswiss, an industry partner which specialises in advanced add-on data acquisition systems and data processing tools. The platform is commercially available and has already been implemented in other investigations.[326-328] The data processing and analysis software was recently launched by Spectroswiss as software product "Mozaic", which is used at the M4i institute in novel academic research. Currently, there are ongoing

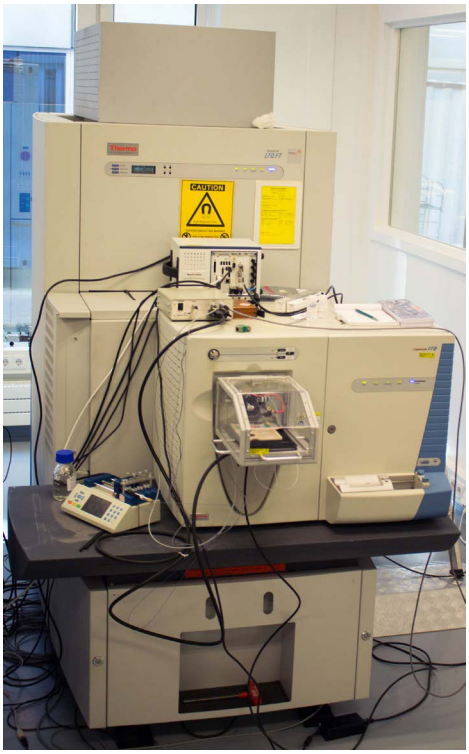

Figure 6.1: *The ultra-high mass resolving power MSI platform as present at Maastricht University*

collaborations with Spectroswiss for further improvements in high resolution and high throughput MSI at the M4i institute. This research project is a good example of a complete technological development cycle: academic research leads to a product, which in turn leads to improved academic research.

In addition, the published results should help to raise awareness on the potential interferences observed with (low-resolution) mass spectrometry. Any researcher should be vigilant that their results might be compounded by other ion species, potentially affecting their interpretation. We ensured quick dissemination of our results by publishing in an open-access journal (Scientific Reports) and making the experimental data available in a public database (Metaspace). The effective dissemination of this publication is confirmed by a citation rate of 28, at the time of writing.

6.6. ADDITIONAL IMPACT

In addition to the published works upon which this thesis is based, the research project at Maastricht University yielded other significant results. Two examples are the multi-purpose ambient imaging setup, and the low-temperature plasma (LTP) probe which were developed in collaboration with IDEE from Maastricht University (see Figure 6.2). The multi-purpose imaging setup has been developed and used to optimize novel ambient ionization probes accurately and fast.

The LTP probe has been developed to provide accurate (approx. 100 µm) spatial resolution plasma desorption and ionization. Though the spatial resolution and ionization were achieved, the desorption capabilities of the low-temperature plasma probe are too weak for practical applications. Only volatile compounds (e.g. capsaicin from peppers) could be successfully imaged, which we judged to be insufficiently novel for publication. However, the knowledge obtained in this project did lay the foundation for the combined LAESI/LA-APCI probe from **Chapter 3**. The LTP probe itself can be used in future LA-APCI imaging instruments. The dense and narrow plasma stream would be ideal for a miniaturized LA-APCI imaging source, which could surpass the sensitivity and spatial resolution of the current LAESI/LA-APCI MSI instrument. In this role the LTP probe can be of great value for an industry partner during commercialisation of LA-APCI.

Throughout this PhD research we have been keen to apply our technological advances to (commercial) challenges. Academic collaborators, as well as industry partners such as DSM and Bayer Crop Science provided samples for which they sought suitable analytical techniques. Examples include fungal colonies on agar, plant seeds and roots, cheese, contact lenses, human hair and lung mucus of a patient. The experiments allowed our project partners to make informed decisions on which technologies are able to answer their research questions.

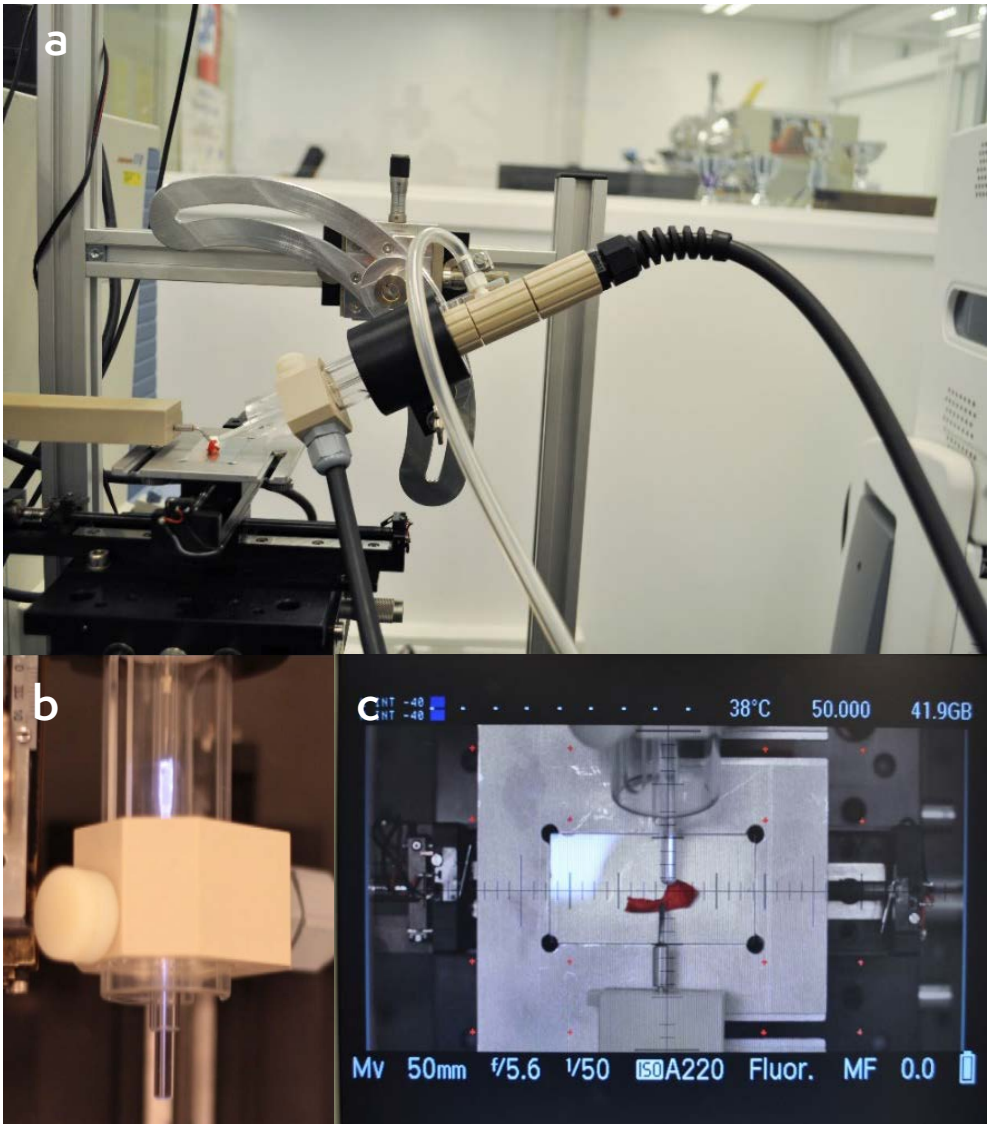

Figure 6.2: *The Maastricht University low-temperature plasma (LTP) probe in the multi-purpose ambient imaging setup (a). The probe produces a tight (approx. 100 µm) stream of charged gas (b), to be directed onto a surface. The ambient imaging setup (c) can be accurately tuned to the optimal geometry of any probe.*


6

CHAPTER 7

SUMMARY
NEDERLANDSE SAMENVATTING

7.1. SUMMARY

Ambient mass spectrometry imaging is – even more so than MSI in general – an emerging, developing, and fragmented field, as we argue in **Chapter 2**. For some analytical challenges commercial MSI techniques are now available (such as DESI), while other challenges can only be addressed through academic prototypes or not at all. As an example, DESI has proven very useful for the analysis of highly soluble analytes present in the top sample layer. Biological tissues are therefore thinly sectioned prior to analysis and washed to remove undesired molecular classes. This somewhat moves away from the ambient ideal (minimal sample preparation) but can help to answer the research question. Laser and thermal desorption are less analyte specific and can penetrate deeper into the sample. This makes them less reliant on sample preparation but adds complexity and cost to the source design. Considerations will always need to be made to select an analysis technique suitable to answer the active research question, though progress will undoubtedly lead to more universal ambient mass spectrometry imaging methods in the future. In this thesis we described several technological and methodological advancements made towards this goal. We will now discuss and summarize these advancements in the grander scheme, working in order from desorption to detection.

Desorption / ionization

All desorption and ionization techniques in ambient mass spectrometry have their benefits and limitations. Laser based desorption is relatively a-selective and therefore useful for wider screening approaches. Solvent-based desorption can lead to high sensitivity because it can be naturally coupled to a highly efficient ionization technique (e.g. DESI or LESA). **Chapter 3** demonstrates the power and versatility of a platform that separates the desorption and ionization steps via the combination of ESI and APCI in a single infrared laser-ablation based MSI source.

LA-APCI works very well for a significant range of analytes, partly overlapping with LAESI but superior for less polar analytes. We have demonstrated the advantages of APCI for use in an MSI instrument over ESI, most notably the improvements in repeatability and reproducibility. As stated in **Chapter 3**, we feel this approach has great potential for agrochemical investigations, but also for non-biological imaging experiments where non-polar compounds are investigated such as synthetic polymer characterisation.

We have demonstrated that infrared laser desorption can be used to desorb non-covalent protein complexes from solutions in their native state. The analysis of intact non-covalent protein complexes has now, 25 years since its inception[329], reached the level of sensitivity and robustness that this "native-MS" can be used for analytical applications. **Chapter 4** extends this ground-breaking research by demonstrating that this can be coupled to laser sampling technologies. In fact, our

results suggest a significant part of the LAESI-generated ions might reach the mass spectrometer in a more native state than with the current state-of-the-art, nano-ESI. In addition, the method has proven robust and highly tolerant to salt contaminants – which is a significant limitation of nano-ESI. As the native-MS field advances we expect applications to move towards more routine, high-throughput screening of clinical samples for diagnosis - for which LAESI could be well suited.

Infrared lasers are a powerful tool for desorption of biological sample material. A separate desorption and ionization step is crucial for robust, broadly applicable ambient mass spectrometry imaging. Completely decoupling the ESI spray generation and the interaction with ablated sample material (i.e. adding a second ambient stage) in LAESI-MSI could add much in terms of repeatability and image quality.

Ion capture / transfer

The transfer of analyte ions from the ambient environment to the mass spectrometer vacuum is an important aspect in ambient mass spectrometry. In contrast to vacuum-based mass spectrometry, the ions need to be captured and separated from the excess of neutral molecules around them without losing ions. A very high ionization efficiency, as described in the previous paragraph, is only valuable if those ions manage to reach the detector. This principle holds for any ambient ionization technique, not just imaging techniques. ESI sources are optimized in distance, temperature, enclosures, angles and potentials for the best capture of ions possible. However, imaging sources must compromise in these respects due to the requirements of the sample (stage) and desorption setup. Ambient imaging sources are therefore less efficient in capturing ions than ambient non-imaging sources.

This is only true for the first stage of ion transfer, from ambient pressure to the first vacuum stage. The successive ion transfer stages are not impacted by the type of ion source, and they are commonly not considered as limiting factors in academic mass spectrometry imaging research. For **Chapter 4** however, these transfer stages were crucial to be able to measure the large protein complexes. Very heavy ions require quite different instrumental parameters in terms of quadrupole frequencies and timings, for instance. Typical instruments are designed for a much lower mass range and are therefore not sensitive enough for protein complexes. For this reason, we employed an ultra-high mass range (UHMR) Q-Exactive Orbitrap mass spectrometer in **Chapter 4**.

In this thesis we do not present instrumental developments on the ion capture or transfer. We have put significant efforts in the development of an interface for controlled ion capture in LAESI. An active aerodynamic and electrostatic ion funnel was built and tested for controlled, more gradual, and more efficient analyte particle-electrospray droplet interaction and capture in the mass spectrometer. Unfortunately, our ion funnel design did not improve the sensitivity of our LAESI setup and has

therefore not been published. The biggest challenge was to visualize the effect of many - often dependent - variables. Computational modelling of gas fluidics is a very powerful tool, and often used in the design of ion transfer systems. However, it is highly dependent on the accuracy of the input design. Small variations in clearances, fluid characteristics or air humidity (to name a few) can have a profound effect on the efficiency of the system. Which is something inherent to ambient MSI ion sources, unfortunately. The approach chosen has a lot of potential but requires more development efforts to mature. It is still a topic of interest and development.

Separation / detection

The analysis of complex samples with ionization across a broad range of analytes (i.e. the objective of this thesis research) automatically leads to highly complex mass spectra. This issue is further aggravated by the unavoidable background contamination experienced in any ambient ionization technique. In **Chapter 5** we describe the development of an electronic signal processing platform and software package for high mass resolution MSI to combat this issue. Using new advanced signal recording, processing, and post-processing techniques we are able to separate ion species closer in mass than ever before in an imaging experiment (see a picture of the physical setup in Figure 6.1). These results highlight the problem of isobaric ion species facing all one-dimensional separation techniques, such as MSI. Researchers can be more certain of the validity of their data during interpretation, if they would apply the method presented here. It comes with drawbacks, of course. Ultra-high resolution mass spectrometry imaging as shown in **Chapter 5** is too slow (and therefore costly) in terms of measurement and data processing time to become standard practise. However, the techniques we published are applicable to all Fourier transform mass spectrometry imaging experiments and will find their way into next generation equipment and software packages, as we discuss in **Chapter 6**.

High mass resolution alone will never be able to fully resolve the molecular complexity of biological samples. In imaging experiments orthogonal separation dimensions are difficult to implement, so MSI spectra are typically highly complex. Notable attempts to add separation dimensions are made with ion mobility spectrometry (IMS) and LESA, but thus far they fall short of the challenge in combination with MSI. Aside from isobaric compounds causing a complex spectrum, isomer analysis is a field that is largely untapped in MSI. A lot of biological information is hidden from sight by overlap with more abundant ion species. In the best case, this information remains hidden, in worst case it interferes with the interpretation of the more abundant ion species distribution. There is a clear need for an orthogonal separation dimension at the timescale of imaging experiments. IMS and infrared ion spectroscopy (IRIS) are exciting candidates for this position.

The constraints and outlook of ambient MSI

Ambient MSI is a fascinating, creative, and highly developing field of analytical chemistry. Where vacuum-based MSI has outgrown the academic "proof-of-principle stage" and its range of applications is growing, ambient MSI is not there yet. Ambient mass spectrometry imaging is mainly held back by the lacking repeatability and sensitivity of measurements. Real-world applications rarely concern the incidental detection of highly abundant analytes, and for those purposes usually a host of techniques can be used. To have an impact on the general society, ambient MSI techniques need to produce reliable results every time, which is in direct opposition to their ambient, minimal sample preparation, versatile nature. The sensitivity of ambient MSI methods is generally much lower for those same reasons. Both the sensitivity and the robustness of ambient MSI are primarily constrained by the efficiency of analyte capture towards the MS vacuum. Depending on the technique, this is more of an ionization or ion transfer challenge. A radical new design is needed for an interface that collects and guides neutral analytes towards the mass spectrometer, while promoting charge transfer regardless of the ionization principle. Control over the air flow between the sample and MS will be crucial in such a design.

Despite the hurdles left to take, ambient MSI is moving forward and has the potential to unlock molecular information in real-world situations that no other technique can. When combined with the advances made in the field of miniaturized mass spectrometers (outside of the scope of this thesis) the path forward seems bright. Star Trek tricorder-like devices - able to analyse any sample in real time by point-and-click – might still be the stuff of dreams for now, but who knows for how much longer? With the strides taken in recent decades - to which this thesis is proud to add - it is a matter of time before mass spectrometry leaves the analytical lab and moves into the hands of the general public.

7.2. NEDERLANDSE SAMENVATTING

Ambient massa spectrometry imaging (MSI) is – nog meer dan MSI in het algemeen – een opkomend, ontwikkelend en gefragmenteerd veld, zoals bediscussieerd in **Hoofdstuk 2**. Voor sommige analytische MSI uitdagingen zijn tegenwoordig commerciele instrumenten beschikbaar (zoals DESI), terwijl andere uitdagingen enkel geaddresseerd kunnen worden met academische prototypes, als die al bestaan. DESI heeft zich bijvoorbeeld bijzonder nuttig getoond voor de analyse van zeer goed oplosbare analyten uit enkel de bovenste lagen van een monster. Biologische weefsels worden hiervoor in dunne coupes gesneden en gewassen om ongewenste moleculaire klasses te verwijderen ter voorbereiding op analyse. Dit doet iets af aan de "minimale monstervoorbewerking"-ideaal van ambient massa spectrometrie, maar kan helpen om de onderzoeksvraag te beantwoorden. Laser en thermale desorptie zijn minder analiet-afhankelijk en kunnen het monster dieper penetreren dan DESI. Dit maakt deze technieken minder afhankelijk van monster voorbereiding, maar voegt wel complexiteit en kosten toe aan het technische ontwerp van de MS bron.

Men zal altijd moeten afwegen welke analyse techniek het meest geschikt is om de onderzoeksvraag te beantwoorden, ook al zal technische vooruitgang ongetwijfeld tot meer universele ambient massa spectrometrie technieken leiden. In dit proefschrift hebben wij verschillende technologische en methodologische verbeteringen beschreven die ons dichter bij dit doel brengen. We zullen deze verbeteringen hier samenvatten en bediscussieren, in volgorde van desorptie naar detectie.

Desorptie / ionisatie

Alle desorptie en ionisatie technieken in ambient massa spectrometrie hebben hun voor- en nadelen. Laser-gebaseerde desorptie is relatief a-specifiek en daarom bruikbaar voor bredere screening toepassingen. Vloeistof-extractie gebaseerde desorptie kan leiden tot een hoge gevoeligheid door de (relatief) gemakkelijke koppeling met een efficiente ionisatie techniek (zoals DESI of LESA). In **Hoofdstuk 3** lieten wij de kracht en veelzijdigheid zien van een platform dat de desorptie en ionisatie stappen scheidt (door ESI en APCI te combineren met infrarood laser ablatie in één MSI bron).

De LA-APCI modus van deze bron is geschikt voor een groot bereik aan analiet eigenschappen. Het bereik overlapt deels met de LAESI modus, maar is superieur voor weinig polaire analieten. Wij tonen aan wat de voordelen van LA-APCI zijn voor ambient MSI applicaties ten opzichte van LAESI, zoals hogere herhaalbaarheid en reproduceerbaarheid. In **Hoofdstuk 3** beargumenteren wij waarom deze aanpak veel potentie heeft voor agrochemische onderzoeken, maar ook voor niet-biologische imaging experimenten waar niet-polaire stoffen worden onderzocht, zoals synthetische polymeren.

We tonen aan dat infrarood laser desorptie kan worden gebruikt om niet-covalent gebonden eiwit complexen uit oplossing te halen – zonder de oorspronkelijke quartenaire structuur te verstoren. De analyse van intacte niet-covalent gebonden eiwit complexen heeft inmiddels, 25 jaar na de eerste experimenten[329], het niveau van gevoeligheid en robuustheid bereikt dat deze zogenaamde "natieve-MS" kan worden gebruikt voor analytische applicaties. **Hoofdstuk 4** borduurt voort op dit revolutionaire onderzoek door aan te tonen dat natieve-MS gekoppeld kan worden aan laser-gebaseerde bemonstering methoden. Onze resultaten suggereren zelfs dat een significant deel van de LAESI-gegenereerde ionen de massa spectrometer kan bereiken in een meer natieve staat dan met nano-ESI, wat de huidige toonaangevende techniek voor natieve MS ionisatie is. Tevens is onze methode robuust en heeft veel minder last van zouten in de monsteroplossing dan nano-ESI. Wij verwachten dat de applicaties van natieve MS richting meer routinematige, grote studies zal bewegen naarmate het natieve MS veld verder ontwikkelt. Hierin zou LAESI een rol kunnen spelen.

Infrarood lasers, zoals gebruikt in ons instrument, zijn een krachtig instrument voor de bemonstering van biologische materialen. Het hebben van afzonderlijke desorptie en ionisatie stappen is cruciaal voor robuuste, breed toepasbare ambient massa spectrometrie imaging. Het compleet loskoppelen van de "electrospray mist creatie" van de interactie met het gedesorbeerde monster materiaal (door het fysiek splitsen van het atmosferische druk brongedeelte) zou LAESI-MS veel op kunnen leveren, in termen van herhaalbaarheid en MSI beeld kwaliteit.

Ionenvangst / transport

De begeleiding van analiet ionen van atmosferische omstandigheden naar het massa spectrometer vacuum is een belangrijk aspect in ambient massa spectrometrie. In tegenstelling tot vacuum-gebaseerde massa spectrometrie moeten de ionen zonder verlies gevangen en gescheiden worden van de omringende neutrale moleculen. Een zeer hoge ionisatie efficientie, zoals beschreven in de vorige paragraaf, is alleen waardevol als die ionen ook de detector weten te bereiken. Dit principe geldt voor elke ambient massa spectrometrie techniek, dus ook de niet-imaging technieken. ESI bronnen zijn geoptimaliseerd in termen van geometrie, temperatuur, afscherming en voltages voor de meest efficiente ionen vangst. Imaging bronnen zijn gelimiteerd in deze opzichten door de vereisten van het monster (plateau) en de desorptie installatie. Door deze combinatie zijn ambient imaging bronnen altijd minder efficient in het vangen van ionen dan (ambient) niet-imaging bronnen.

Gelukkig is dit enkel waar voor het eerste stadium van het ionen transport, van atmosferische druk naar het eerste vacuum gedeelte. De overige ionen transport gedeeltes worden niet beinvloed door het type ionenbron. Deze gedeeltes worden gebruikelijk niet gezien als limiterende factoren in academisch onderzoek naar

massa spectrometrie imaging. Toch waren juist deze transport gedeeltes cruciaal in **Hoofdstuk 4** om grote eiwit complexen te kunnen meten. Zeer zware ionen vereisen significant andere instrumentele parameters, zoals bijvoorbeeld de quadrupole frequenties en timings. Doorgaans worden instrumenten ontworpen voor ionen in een veel lager massa bereik, waardoor het ionen transport niet efficient genoeg is voor eiwit complexen. In **Hoofdstuk 4** hebben wij daarom een ultra-hoge massa bereik (UHMR) Q-Exactive Orbitrap mass spectrometer gebruikt.

In dit proefschrift presenteren wij geen instrumentele ontwikkelingen op het gebied van ionen vangst of transport. Wel hebben wij flinke inspanningen gedaan om een LAESI bron te ontwikkelen met meer gecontroleerde ionenvangst. We hebben een actieve aerodynamische electrostatische ionentrechter ontworpen en gebouwd, met als doel de interactie tussen analiet en electrospray druppel te verhogen en de ionen begeleiding naar het eerste vacuumdeel te faciliteren. Helaas heeft ons ontwerp de gevoeligheid van onze LAESI setup niet kunnen verhogen, en is het daarom nooit gepubliceerd. De grootste uitdaging lag in het visualiseren van het effect van de vele (veelal afhankelijke) variabelen. Het computationeel modelleren van gas fluidica is een zeer krachtig, vaak gebruikt gereedschap in het ontwerp van ionen transport systemen. Helaas is het ook zeer afhankelijk van de nauwkeurigheid van de ingevoerde parameters. Kleine veranderingen in toleranties, vloeistof karateristieken of luchtvochtigheid kunnen een groot effect hebben op de efficientie van het systeem. Helaas zijn zulke variaties inherent aan ambient MSI ionenbronnen. We zijn ervan overtuigd dat de gekozen aanpak zeker potentie heeft, maar dat nog meer inspanningen vereist zijn om een succesvol prototype te ontwikkelen.

Scheiding / detectie

De analyse van complexe monsters met behulp van een breed ionisatie bereik (oftewel het doel van het onderzoek in dit proefschrift) leidt onherroepelijk tot zeer complexe massa spectra. Dit probleem wordt verergerd door de onvermijdelijke achtergrond contaminatie die aanwezig is bij iedere ambient ionisatie techniek. In **Hoofdstuk 5** beschrijven we de ontwikkeling van een elektronisch signaal verwerkings- en softwareplatform die deze uitdaging aangaat met behulp van hoge massa resolutie MSI data. Met nieuwe, geavanceerde signaal opname, verwerking en nabewerking technieken laten wij zien ionen populaties te onderscheiden die extreem dicht bij elkaar liggen qua massa ("isobaar"), dichter dan ooit eerder gerapporteerd in een imaging experiment. Deze resultaten onderstrepen ook de uitdaging waar alle één-dimensionale scheidingstechnieken (zoals MSI) mee te maken hebben: de zekerheid waarmee uitspraken gedaan kunnen worden over zuiverheid en identiteit van gedetecteerde moleculen is direct gerelateerd aan de behaalde scheidingsresolutie. De methode zoals gepresenteerd in **Hoofdstuk 5** representeert in die zin de hoogste zekerheid die in een één-dimensionaal MSI experiment behaalt

kan worden. Dit gaat wel ten koste van snelheid (en daarmee geassocieerde kosten), waardoor routinematige implementatie onrealistisch is. Gelukkig zijn de technieken die wij hebben gerapporteerd algemeen toepasbaar in Fourier transformatie massa spectrometrie experimenten, inclusief experimenten met een hogere doorvoerssnelheid. Deze technieken zullen worden geincorporeerd in de volgende generatie commerciele instrumenten en software pakketten, zoals beargumenteerd in **Hoofdstuk 6**.

De moleculaire complexiteit van biologische monsters zal nooit volledig kunnen worden gekarakteriseerd met hoge massa resolutie alleen. In imaging experimenten zijn orthogonale scheidings dimensies lastig toe te passen, waardoor MSI spectra gewoonlijk zeer complex zijn. Voorname pogingen om scheidings dimensies toe te voegen zijn ion mobiliteits spectrometrie (IMS) en vloeibare extractie oppervlakte analyse (LESA), maar deze zijn tot dusverre lastig te implementeren in MSI experimenten. Naast de complexiteit van isobare moleculen (**Hoofdstuk 5**) is ook isomeer scheiding een nog onvoldoende geaddresseerde uitdaging in MSI. Zo blijft er veel biologische complexiteit verborgen. In het beste geval wordt additionele informatie gemist, maar vaker verstoord het ook de interpretatie van de meest intens gedetecteerde ionen populatie. Er is dus een duidelijke vraag naar een orthogonale scheidings dimensie die compatibel is met de tijdsschaal van MSI experimenten. IMS en infrarood ionen spectroscopie (IRIS) zijn veelbelovende kandidaten om deze vraag te beantwoorden.

De beperkingen en toekomst van ambient MSI

Ambient MSI is een fascinerend, creatief en snel ontwikkelend veld binnen de analytische chemie. Waar vacuum-gebaseerde MSI het academische stadium al deels ontgroeit is, met een steeds groter wordend spectrum van applicaties, is ambient MSI nog niet zo ver. Ambient MSI wordt voornamelijk beperkt door de tekort schietende herhaalbaarheid en gevoeligheid. Maatschappelijke toepassingen vragen zelden om incidentele detectie van ruimschoots aanwezige analieten, en voor die toepassingen is meestal een breed scala aan technieken geschikt. Om van waarde te zijn voor de algemene maatschappij moeten ambient MSI technieken iedere keer betrouwbare resultaten kunnen produceren, wat in strijd lijkt met hun ambient, minimale monster voorbereiding, en veelzijdige natuur. De gevoeligheid van ambient MSI technieken is om vergelijkbare redenen doorgaans ook flink lager. Zowel de gevoeligheid en robuustheid van ambient MSI zijn voornamelijk gelimiteerd door de efficientie waarmee ionen van atmosferische druk naar het MS vacuum worden geleid. Afhankelijk van de techniek is dit meer een ionisatie of een transport uitdaging. Een radicaal nieuw ontwerp is nodig voor een instrument dat neutrale analiet moleculen verzamelt en richting de massa spectrometer leidt, terwijl gelijktijdig de lading

overdracht van ionenbron naar analiet molecuul wordt gestimuleerd. Controle over de luchtstromen tussen het monster oppervlak en de MS zal daarin cruciaal zijn.

Ondanks de obstakels die nog overkomen moeten worden beweegt ambient MSI snel vooruit. Daarbij heeft het de potentie om moleculaire informatie te ontsluiten in echte toepassingen, buiten het lab, waar geen andere technieken voor geschikt zijn. Wanneer ambient MSI gecombineerd wordt met mobiele massa spectrometers (geen onderdeel van dit proefschrift) tekent een duidelijk pad zich af. Over Star Trek tricorder-achtige apparaten - in staat ieder willekeurig object te moleculair te analyseren door simpelweg erop te mikken - kan nu alleen nog maar gedroomd worden, maar wie kan voorspellen hoe lang dat nog duurt? Met de stappen die de laatste decennia gezet zijn - waaraan dit proefschrift trots is toe te voegen - is het een kwestie van tijd voordat massa spectrometrie het analytisch lab verlaat en de algemene maatschappij gaat verrijken.

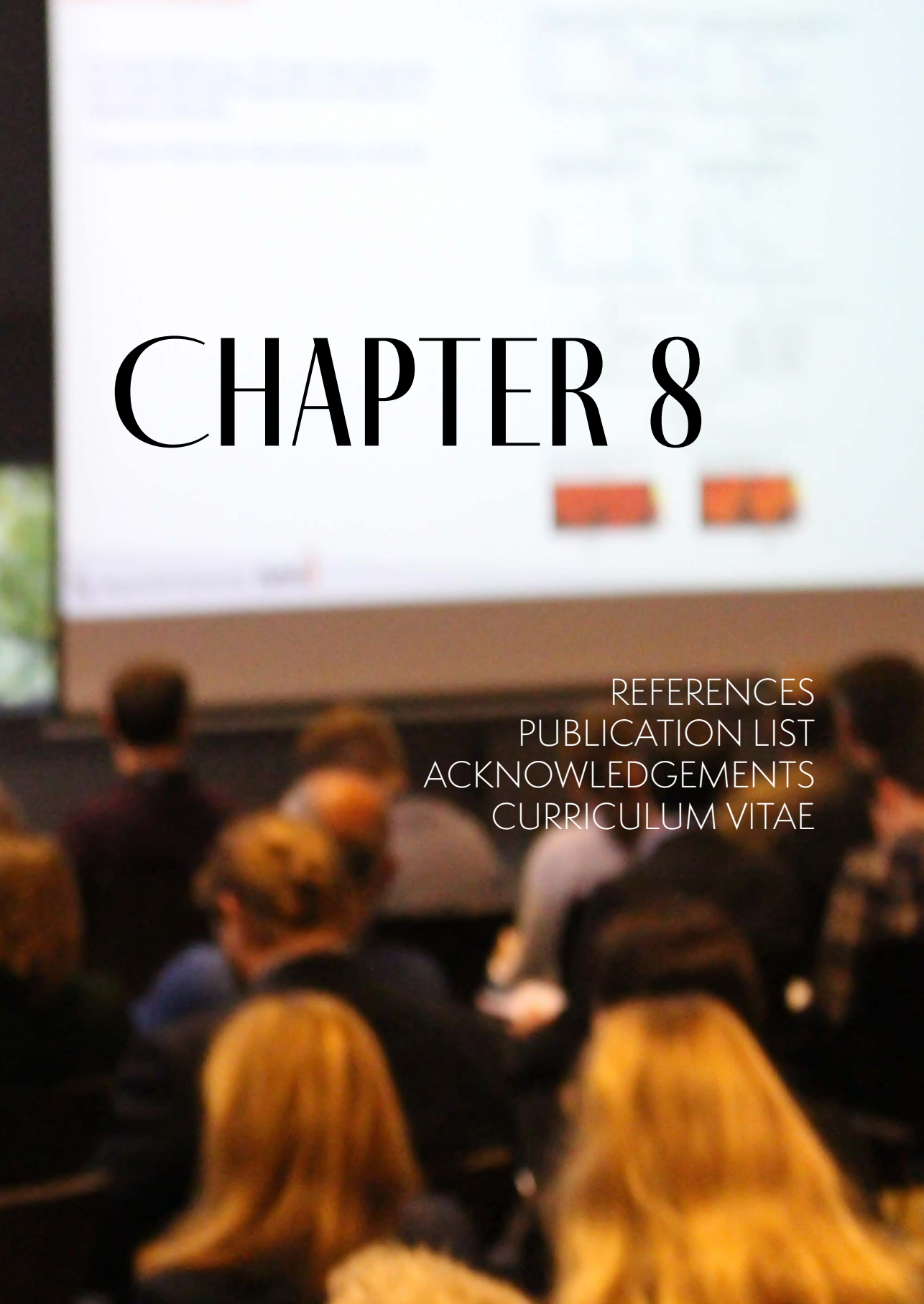

CHAPTER 8

REFERENCES
PUBLICATION LIST
ACKNOWLEDGEMENTS
CURRICULUM VITAE

8.1. REFERENCES

1 Hu, Q. *et al.* The Orbitrap: a new mass spectrometer. *J. Mass Spectrom.* **40**, 430-443, doi:10.1002/jms.856 (2005).

2 Makarov, A., Hardman, M. E., Schwartz, J. C. & Senko, M. W. (Google Patents, 2005).

3 Belu, A. M., Graham, D. J. & Castner, D. G. Time-of-flight secondary ion mass spectrometry: techniques and applications for the characterization of biomaterial surfaces. *Biomaterials* **24**, 3635-3653, doi:10.1016/s0142-9612(03)00159-5 (2003).

4 Ratner, B. D., Chilkoti, A. & Castner, D. G. in *Biol. Mod. Polym. Biomater. Surf.* Vol. 11 (ed E. Piskin) 25-36 (Springer, 1992).

5 López, M., Jiménez, J. & Gutiérrez, A. XPS characterization of surface modified titanium alloys for use as biomaterials. *Vacuum* **85**, 1076-1079, doi:10.1016/j.vacuum.2011.03.006 (2011).

6 Jandt, K. D. Atomic force microscopy of biomaterials surfaces and interfaces. *Surf. Sci.* **491**, 303-332, doi:10.1016/S0039-6028(01)01296-1 (2001).

7 Ong, J. L. & Lucas, L. C. Auger electron spectroscopy and its use for the characterization of titanium and hydroxyapatite surfaces. *Biomaterials* **19**, 455-464, doi:10.1016/S0142-9612(97)00224-X (1998).

8 Menzies, K. L. & Jones, L. The impact of contact angle on the biocompatibility of biomaterials. *Optom. Vis. Sci.* **87**, 387-399, doi:10.1097/OPX.0b013e3181da863e (2010).

9 Taddei, P., Tinti, A. & Fini, G. Vibrational spectroscopy of polymeric biomaterials. *J. Raman Spectrosc.* **32**, 619-629, doi:10.1002/jrs.723 (2001).

10 Leung, B. O., Brash, J. L. & Hitchcock, A. P. Characterization of biomaterials by soft X-ray spectromicroscopy. *Materials* **3**, 3911-3938, doi:10.3390/ma3073911 (2010).

11 Tsuji, K., Nakano, K., Takahashi, Y., Hayashi, K. & Ro, C.-U. X-ray Spectrometry. *Anal. Chem.* **84**, 636-668, doi:10.1021/ac202871b (2012).

12 Senoner, M. & Unger, W. E. S. SIMS imaging of the nanoworld: applications in science and technology. *J. Anal. At. Spectrom.* **27**, 1050-1068, doi:10.1039/c2ja30015j (2012).

13 Adriaens, A., Van Vaeck, L. & Adams, F. Static secondary ion mass spectrometry (S-SIMS) Part 2: Material science applications. *Mass Spectrom. Rev.* **18**, 48-81, doi:10.1002/(Sici)1098-2787(1999)18:1<48::Aid-Mas2>3.0.Co;2-I (1999).

14 Crecelius, A. C., Vitz, J. & Schubert, U. S. Mass spectrometric imaging of synthetic polymers. *Anal. Chim. Acta* **808**, 10-17, doi:10.1016/j.aca.2013.07.033 (2014).

15 Benninghoven, A. Chemical analysis of inorganic and organic surfaces and thin films by static time-of-flight secondary ion mass spectrometry (TOF-SIMS). *Angew. Chem., Int. Ed.* **33**, 1023-1043, doi:10.1002/anie.199410231 (1994).

16 Amstalden van Hove, E. R., Smith, D. F. & Heeren, R. M. A. A concise review of mass spectrometry imaging. *J. Chromatogr. A* **1217**, 3946-3954, doi:10.1016/j.chroma.2010.01.033 (2010).

17 Bodzon-Kulakowska, A. *et al.* Desorption electrospray ionization-based imaging of interaction between vascular graft and human body. *J. Biomed. Mater. Res., Part B* **104**, 192-196, doi:10.1002/jbm.b.33385 (2016).

18 Stoeckli, M., Chaurand, P., Hallahan, D. E. & Caprioli, R. M. Imaging mass spectrometry: a new technology for the analysis of protein expression in mammalian tissues. *Nat. Med. (N. Y., NY, U. S.)* **7**, 493-496, doi:10.1038/86573 (2001).

19 Winograd, N. Nanoscale chemical imaging of biomaterials with mass spectrometry. *J. Biomol. Techn.* **23**, S8-S9 (2012).

20 Cui, Y. *et al.* Molecular imaging and depth profiling of biomaterials interfaces by femtosecond laser desorption postionization mass spectrometry. *ACS Appl. Mater. Interfaces* **5**, 9269-9275, doi:10.1021/am4020633 (2013).

21 Herzog, R. F. K. & Viehböck, F. P. Ion source for mass spectrography. *Phys. Rev.* **76**, 855-856, doi:10.1103/PhysRev.76.855 (1949).

22 Heeren, R. M. A. Getting the picture: The coming of age of imaging MS. *Int. J. Mass Spectrom.* **377**, 672-680, doi:10.1016/j.ijms.2014.04.021 (2015).

23 Vickerman, J. C. Impact of mass spectrometry in surface analysis. *Analyst* **119**, 513-523, doi:10.1039/AN9941900513 (1994).

24 Pachuta, S. J. & Cooks, R. G. Mechanisms in molecular SIMS. *Chem. Rev.* **87**, 647-669, doi:10.1021/cr00079a009 (1987).

25 Lechene, C. *et al.* High-resolution quantitative imaging of mammalian and bacterial cells using stable isotope mass spectrometry. *J. Biol.* **5**, 20, doi:10.1186/jbiol42 (2006).

26 Slodzian, G., Daigne, B., Girard, F., Boust, F. & Hillion, F. Scanning secondary ion analytical microscopy with parallel detection. *Biol. Cell* **74**, 43-50, doi:10.1016/0248-4900(92)90007-n (1992).

27 Kraft, M. L. & Klitzing, H. A. Imaging lipids with secondary ion mass spectrometry. *Biochim. Biophys. Acta* **1841**, 1108-1119, doi:10.1016/j.bbalip.2014.03.003 (2014).

28 Guerquin-Kern, J. L., Wu, T. D., Quintana, C. & Croisy, A. Progress in analytical imaging of the cell by dynamic secondary ion mass spectrometry (SIMS microscopy). *Biochim. Biophys. Acta* **1724**, 228-238, doi:10.1016/j.bbagen.2005.05.013 (2005).

29 Lozic, I. *et al.* Enabling dual cellular destinations of polymeric nanoparticles for treatment following partial injury to the central nervous system. *Biomaterials* **74**, 200-216, doi:10.1016/j.biomaterials.2015.10.001 (2016).

30 Wilson, R. L. *et al.* Fluorinated colloidal gold immunolabels for imaging select proteins in parallel with lipids using high-resolution secondary ion mass spectrometry. *Bioconjugate Chem.* **23**, 450-460, doi:10.1021/bc200482z (2012).

31 Steinhauser, M. L. & Lechene, C. P. Quantitative imaging of subcellular metabolism with stable isotopes and multi-isotope imaging mass spectrometry. *Semin. Cell Dev. Biol.* **24**, 661-667, doi:10.1016/j.semcdb.2013.05.001 (2013).

32 Steinhauser, M. L. *et al.* Multi-isotope imaging mass spectrometry quantifies stem cell division and metabolism. *Nature* **481**, 516-519, doi:10.1038/nature10734 (2012).

33 Enikolopov, G. *et al.* Brain stem cell division and maintenance studied using multi-isotope imaging mass spectrometry (MIMS). *Surf. Interface Anal.* **46**, 140-143, doi:10.1002/sia.5675 (2014).

34 Senyo, S. E. *et al.* Mammalian heart renewal by pre-existing cardiomyocytes. *Nature* **493**, 433-436, doi:10.1038/nature11682 (2013).

35 Scharlach, C. *et al.* LA-ICP-MS allows quantitative microscopy of europium-doped iron oxide nanoparticles and is a possible alternative to ambiguous Prussian blue iron staining. *J. Biomed. Nanotechnol.* **12**, 1001-1010, doi:10.1166/jbn.2016.2230 (2016).

36 Elci, S. G. *et al.* Quantitative imaging of 2 nm monolayer-protected gold nanoparticle distributions in tissues using laser ablation inductively-coupled plasma mass spectrometry (LA-ICP-MS). *Analyst* **141**, 2418-2425, doi:10.1039/c6an00123h (2016).

37 Amerstorfer, F. *et al.* Long-term in vivo degradation behavior and near-implant distribution of resorbed elements for magnesium alloys WZ21 and ZX50. *Acta Biomater.* **42**, 440-450, doi:10.1016/j.actbio.2016.06.025 (2016).

38 Draxler, J. *et al.* The potential of isotopically enriched magnesium to study bone implant degradation in vivo. *Acta Biomater.* **51**, 526-536, doi:10.1016/j.actbio.2017.01.054 (2017).

39 Meischel, M. *et al.* Bone-implant degradation and mechanical response of bone surrounding Mg-alloy implants. *J. Mech. Behav. Biomed. Mater.* **71**, 307-313, doi:10.1016/j.jmbbm.2017.03.025 (2017).

40 Zoriy, M. V. & Becker, J. S. Imaging of elements in thin cross sections of human brain samples by LA-ICP-MS: A study on reproducibility. *Int. J. Mass Spectrom.* **264**, 175-180, doi:10.1016/j.ijms.2007.04.009 (2007).

41 Ellis, S. R., Bruinen, A. L. & Heeren, R. M. A. A critical evaluation of the current state-of-the-art in quantitative imaging mass spectrometry. *Anal. Bioanal. Chem.* **406**, 1275-1289, doi:10.1007/s00216-013-7478-9 (2014).

42 Pozebon, D., Scheffler, G. L. & Dressler, V. L. Recent applications of laser ablation inductively coupled plasma mass spectrometry (LA-ICP-MS) for biological sample analysis: a follow-up review. *J. Anal. At. Spectrom.* **32**, 890-919, doi:10.1039/c7ja00026j (2017).

43 Winograd, N. The magic of cluster SIMS. *Anal. Chem.* **77**, 142 A-149 A, doi:10.1021/ac053355f (2005).

44 Passarelli, M. K. & Winograd, N. Lipid imaging with time-of-flight secondary ion mass spectrometry (TOF-SIMS). *Biochim. Biophys. Acta* **1811**, 976-990, doi:10.1016/j.bbalip.2011.05.007 (2011).

45 Winograd, N. Imaging mass spectrometry on the nanoscale with cluster ion beams. *Anal. Chem.* **87**, 328-333, doi:10.1021/ac503650p (2015).

46 Weibel, D., Lockyer, N. & Vickerman, J. C60 cluster ion bombardment of organic surfaces. *Appl. Surf. Sci.* **231**, 146-152, doi:10.1016/j.apsusc.2004.03.098 (2004).

47 Weibel, D. *et al.* A C_{60} primary ion beam system for time of flight secondary ion mass spectrometry: its development and secondary ion yield characteristics. *Anal. Chem.* **75**, 1754-1764, doi:10.1021/ac026338o (2003).

48 Cheng, J., Kozole, J., Hengstebeck, R. & Winograd, N. Direct comparison of Au_3^+ and C_{60}^+ cluster projectiles in SIMS molecular depth profiling. *J. Am. Soc. Mass Spectrom.* **18**, 406-412, doi:10.1016/j.jasms.2006.10.017 (2007).

49 Jones, E. A., Lockyer, N. P. & Vickerman, J. C. Mass spectral analysis and imaging of tissue by ToF-SIMS—The role of buckminsterfullerene, C_{60}^+, primary ions. *Int. J. Mass Spectrom.* **260**, 146-157, doi:10.1016/j.ijms.2006.09.015 (2007).

50 Gillen, G., Walker, M., Thompson, P. & Bennett, J. Use of an SF 5+ polyatomic primary ion beam for ultrashallow depth profiling on an ion microscope secondary ion mass spectroscopy instrument. *J. Vac. Sci. Technol., B: Microelectron. Nanometer Struct.--Process., Meas., Phenom.* **18**, 503-508, doi:10.1116/1.591221 (2000).

51 Fuoco, E. R., Gillen, G., Wijesundara, M. B. J., Wallace, W. E. & Hanley, L. Surface analysis studies of yield enhancements in secondary ion mass spectrometry by polyatomic projectiles. *J. Phys. Chem. B* **105**, 3950-3956, doi:10.1021/jp0033317 (2001).

52 Appelhans, A. D. & Delmore, J. E. Comparison of polyatomic and atomic primary beams for secondary ion mass spectrometry of organics. *Anal. Chem.* **61**, 1087-1093, doi:10.1021/ac00185a009 (1989).

53 Davies, N. *et al.* Development and experimental application of a gold liquid metal ion source. *Appl. Surf. Sci.* **203-204**, 223-227, doi:10.1016/S0169-4332(02)00631-1 (2003).

54 Touboul, D., Kollmer, F., Niehuis, E., Brunelle, A. & Laprévote, O. Improvement of biological time-of-flight-secondary ion mass spectrometry imaging with a bismuth cluster ion source. *J. Am. Soc. Mass Spectrom.* **16**, 1608-1618, doi:10.1016/j.jasms.2005.06.005 (2005).

55 Li, Z., Verkhoturov, S. V. & Schweikert, E. A. Nanovolume analysis with secondary ion mass spectrometry using massive projectiles. *Anal. Chem.* **78**, 7410-7416, doi:10.1021/ac0603779 (2006).

56 Rabbani, S., Barber, A. M., Fletcher, J. S., Lockyer, N. P. & Vickerman, J. C. TOF-SIMS with Argon gas cluster ion beams: a comparison with C60+. *Anal. Chem.* **83**, 3793-3800, doi:10.1021/ac200288v (2011).

57 Ninomiya, S. *et al.* A fragment-free ionization technique for organic mass spectrometry with large Ar cluster ions. *Appl. Surf. Sci.* **255**, 1588-1590, doi:10.1016/j.apsusc.2008.05.004 (2008).

58 Toyoda, N., Matsuo, J., Aoki, T., Yamada, I. & Fenner, D. B. Secondary ion mass spectrometry with gas cluster ion beams. *Appl. Surf. Sci.* **203**, 214-218, doi:10.1016/S0169-4332(02)00628-1 (2003).

59 Postawa, Z. *et al.* Enhancement of sputtering yields due to C_{60} versus Ga Bombardment of Ag{111} as explored by molecular dynamics simulations. *Anal. Chem.* **75**, 4402-4407, doi:10.1021/ac034387a (2003).

60 Tian, H., Sparvero, L., Amoscato, A.A., Kagan, V., Bayir, H., Winograd, N. in *Proceedings of the 65th ASMS Conference on Mass Spectrometry and Allied Topics.* (ASMS 2017 Indianapolis).

61 Tian, H., Six, D. A., Krucker, T., Leeds, J. A. & Winograd, N. Subcellular chemical imaging of antibiotics in single bacteria using C60-secondary ion mass spectrometry. *Anal. Chem.* **89**, 5050-5057, doi:10.1021/acs.analchem.7b00466 (2017).

62 Fletcher, J. S., Lockyer, N. P. & Vickerman, J. C. Developments in molecular SIMS depth profiling and 3D imaging of biological systems using polyatomic primary ions. *Mass Spectrom. Rev.* **30**, 142-174, doi:10.1002/mas.20275 (2011).

63 Wucher, A., Fisher, G. L. & Mahoney, C. M. in *Cluster Secondary Ion Mass Spectrometry* 207-246 (John Wiley & Sons, Inc., 2013).

64 Niehuis, E., Moellers, R., Rading, D. & Bruener, P. Dual beam depth profiling of organic materials: assessment of capabilities and limitations. *Surf. Interface Anal.* **46**, 70-73, doi:10.1002/sia.5631 (2014).

65 Wucher, A., Cheng, J., Zheng, L. & Winograd, N. Three-dimensional depth profiling of molecular structures. *Anal. Bioanal. Chem.* **393**, 1835-1842, doi:10.1007/s00216-008-2596-5 (2009).

66 Bich, C., Touboul, D. & Brunelle, A. Cluster TOF-SIMS imaging as a tool for micrometric histology of lipids in tissue. *Mass Spectrom. Rev.* **33**, 442-451, doi:10.1002/mas.21399 (2014).

67 Bich, C., Touboul, D. & Brunelle, A. Biomedical studies by TOF-SIMS imaging. *Biointerphases* **10**, 7, doi:10.1116/1.4901511 (2015).

68 Winograd, N. & Garrison, B. J. Biological cluster mass spectrometry. *Annu. Rev. Phys. Chem.* **61**, 305-322, doi:10.1146/annurev.physchem.040808.090249 (2010).

69 Fletcher, J. & Vickerman, J. A new SIMS paradigm for 2D and 3D molecular imaging of bio-systems. *Anal. Bioanal. Chem.* **396**, 85-104, doi:10.1007/s00216-009-2986-3 (2010).

70 Chughtai, K. & Heeren, R. M. A. Mass Spectrometric Imaging for biomedical tissue analysis. *Chem. Rev.* **110**, 3237-3277, doi:10.1021/cr100012c (2010).

71 Touboul, D., Laprevote, O. & Brunelle, A. Micrometric molecular histology of lipids by mass spectrometry imaging. *Curr. Opin. Chem. Biol.* **15**, 725-732, doi:10.1016/j.cbpa.2011.04.017 (2011).

72 Lanni, E. J., Rubakhin, S. S. & Sweedler, J. V. Mass spectrometry imaging and profiling of single cells. *J. Proteom.* **75**, 5036-5051, doi:10.1016/j.jprot.2012.03.017 (2012).

73 Lockyer, N. P. Secondary ion mass spectrometry imaging of biological cells and tissues. *Methods Mol. Biol.* **1117**, 707-732, doi:10.1007/978-1-62703-776-1_32 (2014).

74 Yang, J. & Gilmore, I. Application of secondary ion mass spectrometry to biomaterials, proteins and cells: a concise review. *Mater. Sci. Technol.* **31**, 131-136, doi:10.1179/1743284714y.0000000613 (2015).

75 Mahoney, C. M. Cluster secondary ion mass spectrometry of polymers and related materials. *Mass Spectrom. Rev.* **29**, 247-293, doi:10.1002/mas.20233 (2010).

76 Bailey, J. *et al.* 3D ToF-SIMS imaging of polymer multilayer films using Argon cluster sputter depth profiling. *ACS Appl. Mater. Interfaces* **7**, 2654-2659, doi:10.1021/am507663v (2015).

77 Mouhib, T., Delcorte, A., Poleunis, C. & Bertrand, P. C60 molecular depth profiling of bilayered polymer films using ToF-SIMS. *Surf. Interface Anal.* **43**, 175-178, doi:10.1002/sia.3539 (2011).

78 Ren, X., Weng, L.-T., Chan, C.-M. & Ng, K.-M. Hollow interior structure of spin-coated polymer thin films revealed by TOF-SIMS three-dimensional imaging. *Anal. Chem.* **84**, 8497-8504, doi:10.1021/ac3014466 (2012).

79 Patel, I. F., Kiryukhin, M. V., Yakovlev, N. L., Gupta, H. S. & Sukhorukov, G. B. Naturally inspired polyelectrolyte multilayer composite films synthesised through layer-by-layer assembly and chemically infiltrated with CaCO3. *J. Mater. Chem. B* **3**, 4821-4830, doi:10.1039/C5TB00055F (2015).

80 Jung, S., Foston, M., Kalluri, U. C., Tuskan, G. A. & Ragauskas, A. J. 3D chemical image using TOF-SIMS revealing the biopolymer component spatial and lateral distributions in biomass. *Angew. Chem., Int. Ed.* **51**, 12005-12008, doi:10.1002/anie.201205243 (2012).

81 Goor, O. J. G. M. *et al.* Efficient functionalization of additives at supramolecular material surfaces. *Adv. Mater. (Weinheim, Ger.)* **29**, 1604652, doi:10.1002/adma.201604652 (2017).

82 Wang, S., Lv, J., Ma, J. & Zhang, S. Cellular internalization and intracellular biotransformation of silver nanoparticles in Chlamydomonas reinhardtii. *Nanotoxicology* **10**, 1129-1135, doi:10.1080/17435390.2016.1179809 (2016).

83 Kollmer, F., Paul, W., Krehl, M. & Niehuis, E. Ultra high spatial resolution SIMS with cluster ions - approaching the physical limits. *Surf. Interface Anal.* **45**, 312-314, doi:10.1002/sia.5093 (2013).

84 Hagenhoff, B. *et al.* Detection of micro- and nano-particles in animal cells by ToF-SIMS 3D analysis. *Surf. Interface Anal.* **45**, 315-319, doi:10.1002/sia.5141 (2013).

85 Angerer, T. B. & Fletcher, J. S. 3D Imaging of TiO2 nanoparticle accumulation in Tetrahymena pyriformis. *Surf. Interface Anal.* **46**, 198-203, doi:10.1002/sia.5444 (2014).

86 Kokesch-Himmelreich, J. *et al.* Detection of organic nanoparticles in human bone marrow-derived stromal cells using ToF–SIMS and PCA. *Anal. Bioanal. Chem.* **407**, 4555-4565, doi:10.1007/s00216-015-8647-9 (2015).

87 Barré, F. P. Y., Heeren, R. M. A. & Ogrinc Potočnik, N. Mass spectrometry imaging in nanomedicine: Unraveling the potential of MSI for the detection of nanoparticles in neuroscience. *Curr. Pharm. Des.* **23**, 1-11, doi:10.2174/1381612823666170111112550 (2017).

88 Baer, D. R., Gaspar, D. J., Nachimuthu, P., Techane, S. D. & Castner, D. G. Application of surface chemical analysis tools for characterization of nanoparticles. *Anal. Bioanal. Chem.* **396**, 983-1002, doi:10.1007/s00216-009-3360-1 (2010).

89 Townley, H. E., Kim, J. & Dobson, P. J. In vivo demonstration of enhanced radiotherapy using rare earth doped titania nanoparticles. *Nanoscale* **4**, 5043-5050, doi:10.1039/C2NR30769C (2012).

90 Fernando, I. R. *et al.* Esterase- and pH-responsive poly([small beta]-amino ester)-capped mesoporous silica nanoparticles for drug delivery. *Nanoscale* **7**, 7178-7183, doi:10.1039/C4NR07443B (2015).

91 Moreau, J. W. *et al.* Extracellular proteins limit the dispersal of biogenic nanoparticles. *Science* **316**, 1600-1603, doi:10.1126/science.1141064 (2007).

92 Piret, J.-P. *et al.* Copper(ii) oxide nanoparticles penetrate into HepG2 cells, exert cytotoxicity via oxidative stress and induce pro-inflammatory response. *Nanoscale* **4**, 7168-7184, doi:10.1039/C2NR31785K (2012).

93 Kim, Y. P., Shon, H. K., Shin, S. K. & Lee, T. G. Probing nanoparticles and nanoparticle-conjugated biomolecules using time-of-flight secondary ion mass spectrometry. *Mass Spectrom. Rev.* **34**, 237-247, doi:10.1002/mas.21437 (2015).

94 Hua, X. *et al.* Chemical imaging of molecular changes in a hydrated single cell by dynamic secondary ion mass spectrometry and super-resolution microscopy. *Integr. Biol.* **8**, 635-644, doi:10.1039/C5IB00308C (2016).

95 Rafati, A. *et al.* Chemical and spatial analysis of protein loaded PLGA microspheres for drug delivery applications. *J. Controlled Release* **162**, 321-329, doi:10.1016/j.jconrel.2012.05.008 (2012).

96 Lee, C.-Y., Harbers, G. M., Grainger, D. W., Gamble, L. J. & Castner, D. G. Fluorescence, XPS, and TOF-SIMS surface chemical state image analysis of DNA microarrays. *J. Am. Chem. Soc.* **129**, 9429-9438, doi:10.1021/ja071879m (2007).

97 Shon, H. K. *et al.* Mass imaging of iron oxide nanoparticles inside cells for in vitro cytotoxicity. *J. Nanosci. Nanotechnol.* **11**, 638-641, doi:10.1166/jnn.2011.3273 (2011).

98 Graham, D. J., Wilson, J. T., Lai, J. J., Stayton, P. S. & Castner, D. G. Three-dimensional localization of polymer nanoparticles in cells using ToF-SIMS. *Biointerphases* **11**, 02A304, doi:10.1116/1.4934795 (2016).

99 Proetto, M. T. *et al.* Cellular delivery of nanoparticles revealed with combined optical and isotopic nanoscopy. *ACS Nano* **10**, 4046-4054, doi:10.1021/acsnano.5b06477 (2016).

100 Barnes, C. A. *et al.* Identifying individual cell types in heterogeneous cultures using secondary ion mass spectrometry imaging with C60 etching and multivariate analysis. *Anal. Chem.* **84**, 893-900, doi:10.1021/ac201179t (2012).

101 Georgi, N. *et al.* Differentiation of mesenchymal stem cells under hypoxia and normoxia: lipid profiles revealed by time-of-flight secondary ion mass spectrometry and multivariate analysis. *Anal. Chem.* **87**, 3981-3988, doi:10.1021/acs.analchem.5b00114 (2015).

102 de Peppo, G. M. *et al.* Osteogenic potential of human mesenchymal stem cells and human embryonic stem cell-derived mesodermal progenitors: a tissue engineering perspective. *Tissue Eng. Part A* **16**, 3413-3426, doi:10.1089/ten.TEA.2010.0052 (2010).

103 de Peppo, G. M. *et al.* Free-form-fabricated commercially pure Ti and Ti6Al4V porous scaffolds support the growth of human embryonic stem cell-derived mesodermal progenitors. *Sci. World J.* **2012**, 646417, doi:10.1100/2012/646417 (2012).

104 de Peppo, G. M. & Marolt, D. State of the art in stem cell research: human embryonic stem cells, induced pluripotent stem cells, and transdifferentiation. *J. Blood Transfus.* **2012**, 317632, doi:10.1155/2012/317632 (2012).

105 de Peppo, G. M. *et al.* Human embryonic stem cell-derived mesodermal progenitors display substantially increased tissue formation compared to human mesenchymal stem cells under dynamic culture conditions in a packed bed/column bioreactor. *Tissue Eng. Part A* **19**, 175-187, doi:10.1089/ten.TEA.2011.0412 (2013).

106 Chilkoti, A., Schmierer, A. E., Perezluna, V. & Ratner, B. D. Investigating the Relationship between Surface-Chemistry and Endothelial-Cell Growth - Partial Least-Squares Regression of the Static Secondary-Ion Mass-Spectra of Oxygen-Containing Plasma-Deposited Films. *Anal. Chem.* **67**, 2883-2891, doi:10.1021/ac00113a024 (1995).

107 Mei, Y. *et al.* Combinatorial development of biomaterials for clonal growth of human pluripotent stem cells. *Nat. Mater.* **9**, 768-778, doi:10.1038/nmat2812 (2010).

108 Saha, K. *et al.* Surface-engineered substrates for improved human pluripotent stem cell culture under fully defined conditions. *Proc. Natl. Acad. Sci. U. S. A.* **108**, 18714-18719, doi:10.1073/pnas.1114854108 (2011).

109 Pasqui, D., Torricelli, P., De Cagna, M., Fini, M. & Barbucci, R. Carboxymethyl cellulose-hydroxyapatite hybrid hydrogel as a composite material for bone tissue engineering applications. *J. Biomed. Mater. Res., Part A* **102**, 1568-1579, doi:10.1002/jbm.a.34810 (2014).

110 Ulrich, T. A., Lee, T. G., Shon, H. K., Moon, D. W. & Kumar, S. Microscale mechanisms of agarose-induced disruption of collagen remodeling. *Biomaterials* **32**, 5633-5642, doi:10.1016/j.biomaterials.2011.04.045 (2011).

111 DeQuach, J. A. *et al.* Simple and high yielding method for preparing tissue specific extracellular matrix coatings for cell culture. *PLoS One* **5**, e13039, doi:10.1371/journal.pone.0013039 (2010).

112 Brown, B. N. *et al.* Surface characterization of extracellular matrix scaffolds. *Biomaterials* **31**, 428-437, doi:10.1016/j.biomaterials.2009.09.061 (2010).

113 Barnes, C. A. *et al.* The surface molecular functionality of decellularized extracellular matrices. *Biomaterials* **32**, 137-143, doi:10.1016/j.biomaterials.2010.09.007 (2011).

114 Park, J. *et al.* Synergistic control of mesenchymal stem cell differentiation by nanoscale surface geometry and immobilized growth factors on TiO2 nanotubes. *Small* **8**, 98-107, doi:10.1002/smll.201100790 (2012).

115 Bongo, M. *et al.* PEDOT:gelatin composites mediate brain endothelial cell adhesion. *J. Mater. Chem. B* **1**, 3860-3867, doi:10.1039/C3TB20374C (2013).

116 Lodding, A. R. *et al.* Secondary ion mass spectrometry in the study of biomineralizations and biomaterials. *Anal. Chim. Acta* **241**, 299-314, doi:10.1016/S0003-2670(00)83660-0 (1990).

117 Eriksson, C., Malmberg, P. & Nygren, H. Time-of-flight secondary ion mass spectrometric analysis of the interface between bone and titanium implants. *Rapid Commun. Mass Spectrom.* **22**, 943-949, doi:10.1002/rcm.3445 (2008).

118 Fisher, G. L., Belu, A. M., Mahoney, C. M., Wormuth, K. & Sanada, N. Three-dimensional time-of-flight secondary ion mass spectrometry imaging of a pharmaceutical in a coronary stent coating as a function of elution time. *Anal. Chem.* **81**, 9930-9940, doi:10.1021/ac901587k (2009).

119 Klerk, L. A. *et al.* TOF-secondary ion mass spectrometry imaging of polymeric scaffolds with surrounding tissue after in vivo implantation. *Anal. Chem.* **82**, 4337-4343, doi:10.1021/ac100837n (2010).

120 Fletcher, J. S. *et al.* A new dynamic in mass spectral imaging of single biological cells. *Anal. Chem.* **80**, 9058-9064, doi:10.1021/ac8015278 (2008).

121 Hill, R., Blenkinsopp, P., Thompson, S., Vickerman, J. & Fletcher, J. S. A new time-of-flight SIMS instrument for 3D imaging and analysis. *Surf. Interface Anal.* **43**, 506-509, doi:10.1002/sia.3562 (2011).

122 Carado, A. *et al.* C60 secondary ion mass spectrometry with a hybrid-quadrupole orthogonal time-of-flight mass spectrometer. *Anal. Chem.* **80**, 7921-7929, doi:10.1021/ac801712s (2008).

123 Fisher, G. L. *et al.* A new method and mass spectrometer design for TOF-SIMS parallel imaging MS/MS. *Anal. Chem.* **88**, 6433-6440, doi:10.1021/acs.analchem.6b01022 (2016).

124 Carado, A. *et al.* Biological tissue imaging with a hybrid cluster SIMS quadrupole time-of-flight mass spectrometer. *Appl. Surf. Sci.* **255**, 1572-1575, doi:10.1016/j.apsusc.2008.05.150 (2008).

125 Fisher, G. L., Hammond, J. S., Larson, P. E., Bryan, S. R. & Heeren, R. M. Parallel imaging MS/MS TOF-SIMS instrument. *J. Vac. Sci. Technol., B: Microelectron. Nanometer Struct.--Process., Meas., Phenom.* **34**, 03H126, doi:10.1116/1.4943568 (2016).

126 Fisher, G. L., Hammond, J. S., Bryan, S. R., Larson, P. E. & Heeren, R. M. A. The composition of poly(ethylene terephthalate) (PET) surface precipitates determined at high resolving power by tandem mass spectrometry imaging. *Microsc. Microanal.*, 1-6, doi:10.1017/S1431927617000654 (2017).

127 Smith, D. F. *et al.* High mass accuracy and high mass resolving power FT-ICR secondary ion mass spectrometry for biological tissue imaging. *Anal. Bioanal. Chem.* **405**, 6069-6076, doi:10.1007/s00216-013-7048-1 (2013).

128 DeBord, J. D. *et al.* Secondary ion mass spectrometry imaging of Dictyostelium discoideum aggregation streams. *PLoS One* **9**, e99319, doi:10.1371/journal.pone.0099319 (2014).

129 Pirkl, A. *et al.* in *10th World Biomaterials Congress.* (ed Frontiers in Bioengineering and Biotechnology).

130 Passarelli, M. K. *et al.* The 3D OrbiSIMS—label-free metabolic imaging with subcellular lateral resolution and high mass-resolving power. *Nat. Methods* **14**, 1175, doi:10.1038/nmeth.4504 (2017).

131 Karas, M., Bachmann, D. & Hillenkamp, F. Influence of the wavelength in high-irradiance ultraviolet laser desorption mass spectrometry of organic molecules. *Anal. Chem.* **57**, 2935-2939, doi:10.1021/ac00291a042 (1985).

132 Karas, M., Bachmann, D., Bahr, U. & Hillenkamp, F. Matrix-assisted ultraviolet laser desorption of non-volatile compounds. *Int. J. Mass Spectrom. Ion Processes* **78**, 53-68, doi:10.1016/0168-1176(87)87041-6 (1987).

133 Tanaka, K. *et al.* Protein and polymer analyses up to *m/z* 100 000 by laser ionization time-of-flight mass spectrometry. *Rapid Commun. Mass Spectrom.* **2**, 151-153, doi:10.1002/rcm.1290020802 (1988).

134 Dass, A., Stevenson, A., Dubay, G. R., Tracy, J. B. & Murray, R. W. Nanoparticle MALDI-TOF mass spectrometry without fragmentation: Au25(SCH2CH2Ph)18 and mixed monolayer Au25(SCH2CH2Ph)18−x(L)x. *J. Am. Chem. Soc.* **130**, 5940-5946, doi:10.1021/ja710323t (2008).

135 Dopke, N. C., Treichel, P. M. & Vestling, M. M. Matrix-assisted laser desorption/ionization time-of-flight mass spectrometry (MALDI-TOF MS) of Rhenium(III) halides: a characterization tool for metal atom clusters. *Inorg. Chem.* **37**, 1272-1277, doi:10.1021/ic971220p (1998).

136 Shi, C. Y. & Deng, C. H. Recent advances in inorganic materials for LDI-MS analysis of small molecules. *Analyst* **141**, 2816-2826, doi:10.1039/C6AN00220J (2016).

137 Laiko, V. V., Baldwin, M. A. & Burlingame, A. L. Atmospheric pressure matrix-assisted laser desorption/ionization mass spectrometry. *Anal. Chem.* **72**, 652-657, doi:10.1021/ac990998k (2000).

138 Römpp, A. & Spengler, B. Mass spectrometry imaging with high resolution in mass and space. *Histochem. Cell Biol.* **139**, 759-783, doi:10.1007/s00418-013-1097-6 (2013).

139 Heeren, R. M. A. *et al.* Why don't biologists use SIMS?: A critical evaluation of imaging MS. *Appl. Surf. Sci.* **252**, 6827-6835, doi:10.1016/j.apsusc.2006.02.134 (2006).

140 MacAleese, L., Duursma, M. C., Klerk, L. A., Fisher, G. & Heeren, R. M. A. Protein identification with liquid chromatography and matrix enhanced secondary ion mass spectrometry (LC-ME-SIMS). *J. Proteom.* **74**, 993-1001, doi:10.1016/j.jprot.2011.02.009 (2011).

141 Caprioli, R. M., Farmer, T. B. & Gile, J. Molecular imaging of biological samples: Localization of peptides and proteins using MALDI-TOF MS. *Anal. Chem.* **69**, 4751-4760, doi:10.1021/ac970888i (1997).

142 Schwamborn, K. & Caprioli, R. M. Molecular imaging by mass spectrometry — looking beyond classical histology. *Nat. Rev. Cancer* **10**, 639-646, doi:10.1038/nrc2917 (2010).

143 Zemski Berry, K. A. *et al.* MALDI imaging of lipid biochemistry in tissues by mass spectrometry. *Chem. Rev.* **111**, 6491-6512, doi:10.1021/cr200280p (2011).

144 McDonnell, L. A. & Heeren, R. M. A. Imaging mass spectrometry. *Mass Spectrom. Rev.* **26**, 606-643, doi:10.1002/mas.20124 (2007).

145 Ogrinc Potočnik, N., Porta, T., Becker, M., Heeren, R. M. A. & Ellis, S. R. Use of advantageous, volatile matrices enabled by next-generation high-speed matrix-assisted laser desorption/ionization time-of-flight imaging employing a scanning laser beam. *Rapid Commun. Mass Spectrom.* **29**, 2195-2203, doi:10.1002/rcm.7379 (2015).

146 Zavalin, A., Yang, J., Hayden, K., Vestal, M. & Caprioli, R. M. Tissue protein imaging at 1 μm laser spot diameter for high spatial resolution and high imaging speed using transmission geometry MALDI TOF MS. *Anal. Bioanal. Chem.* **407**, 2337-2342, doi:10.1007/s00216-015-8532-6 (2015).

147 Kompauer, M., Heiles, S. & Spengler, B. Atmospheric pressure MALDI mass spectrometry imaging of tissues and cells at 1.4-μm lateral resolution. *Nat. Methods* **14**, 90-96, doi:10.1038/nmeth.4071 (2017).

148 Addie, R. D., Balluff, B., Bovée, J. V. M. G., Morreau, H. & McDonnell, L. A. Current state and future challenges of mass spectrometry imaging for clinical research. *Anal. Chem.* **87**, 6426-6433, doi:10.1021/acs.analchem.5b00416 (2015).

149 Crecelius, A. C., Alexandrov, T. & Schubert, U. S. Application of matrix-assisted laser desorption/ionization mass spectrometric imaging to monitor surface changes of UV-irradiated poly(styrene) films. *Rapid Commun. Mass Spectrom.* **25**, 2809-2814, doi:10.1002/rcm.5164 (2011).

150 Crecelius, A. C. *et al.* Application of matrix-assisted laser desorption/ionization mass spectrometric imaging for photolithographic structuring. *Anal. Chem.* **84**, 6921-6925, doi:10.1021/ac301616v (2012).

151 Rivas, D., Ginebreda, A., Pérez, S., Quero, C. & Barceló, D. MALDI-TOF MS imaging evidences spatial differences in the degradation of solid polycaprolactone diol in water under aerobic and denitrifying conditions. *Sci. Total Environ.* **566–567**, 27-33, doi:10.1016/j.scitotenv.2016.05.090 (2016).

152 Kurth, M., Eyerer, P., Ascherl, R., Dittel, K. & Holz, U. An evaluation of retrieved UHMWPE hip joint cups. *J. Biomater. Appl.* **3**, 33-51, doi:10.1177/088532828800300102 (1988).

153 Eyerer, P., Kurth, M., McKellup, H. A. & Mittlmeier, T. Characterization of UHMWPE hip cups run on joint simulators. *J. Biomed. Mater. Res.* **21**, 275-291, doi:10.1002/jbm.820210302 (1987).

154 Fröhlich, S. M., Dorrer, V., Archodoulaki, V.-M., Allmaier, G. & Marchetti-Deschmann, M. Synovial fluid protein adsorption on polymer-based artificial hip joint material investigated by MALDI-TOF mass spectrometry imaging. *EuPA Open Proteom.* **4**, 70-80, doi:10.1016/j.euprot.2014.05.001 (2014).

155 Bergmeister, H. *et al.* Biodegradable, thermoplastic polyurethane grafts for small diameter vascular replacements. *Acta Biomater.* **11**, 104-113, doi:10.1016/j.actbio.2014.09.003 (2015).

156 Frohlich, S. M. *et al.* Mass spectrometric imaging of in vivo protein and lipid adsorption on biodegradable vascular replacement systems. *Analyst* **140**, 6089-6099, doi:10.1039/C5AN00921A (2015).

157 Medini, K., West, B., Williams, D. E., Brimble, M. A. & Gerrard, J. A. MALDI-imaging enables direct observation of kinetic and thermodynamic products of mixed peptide fiber assembly. *Chem. Commun. (Cambridge, U. K.)* **53**, 1715-1718, doi:10.1039/C6CC10146A (2017).

158 Chen, S. *et al.* Mass spectrometry imaging reveals the sub-organ distribution of carbon nanomaterials. *Nat. Nanotechnol.* **10**, 176-182, doi:10.1038/nnano.2014.282 (2015).

159 Creran, B. *et al.* Laser desorption ionization mass spectrometric imaging of mass barcoded gold nanoparticles for security applications. *Chem. Commun. (Cambridge, U. K.)* **48**, 4543-4545, doi:10.1039/C2CC30499F (2012).

160 Cooks, R. G., Ouyang, Z., Takats, Z. & Wiseman, J. M. Ambient Mass Spectrometry. *Science* **311**, 1566-1570, doi:10.1126/science.1119426 (2006).

161 Weston, D. J. Ambient ionization mass spectrometry: current understanding of mechanistic theory; analytical performance and application areas. *Analyst* **135**, 661-668, doi:10.1039/b925579f (2010).

162 Harris, G. A., Galhena, A. S. & Fernandez, F. M. Ambient sampling/ionization mass spectrometry: applications and current trends. *Anal. Chem.* **83**, 4508-4538, doi:10.1021/ac200918u (2011).

163 Wu, C., Dill, A. L., Eberlin, L. S., Cooks, R. G. & Ifa, D. R. Mass spectrometry imaging under ambient conditions. *Mass Spectrom. Rev.* **32**, 218-243, doi:10.1002/mas.21360 (2013).

164 Paine, M. R. L., Barker, P. J. & Blanksby, S. J. Ambient ionisation mass spectrometry for the characterisation of polymers and polymer additives: A review. *Anal. Chim. Acta* **808**, 70-82, doi:10.1016/j.aca.2013.10.001 (2014).

165 Monge, M. E., Harris, G. A., Dwivedi, P. & Fernández, F. M. Mass spectrometry: recent advances in direct open air surface sampling/ionization. *Chem. Rev.* **113**, 2269-2308, doi:10.1021/cr300309q (2013).

166 Nemes, P. & Vertes, A. Ambient mass spectrometry for in vivo local analysis and in situ molecular tissue imaging. *Trends Anal. Chem.* **34**, 22-34, doi:10.1016/j.trac.2011.11.006 (2012).

167 Huang, M. Z., Yuan, C. H., Cheng, S. C., Cho, Y. T. & Shiea, J. Ambient ionization mass spectrometry. *Annu. Rev. Anal. Chem.* **3**, 43-65, doi:10.1146/annurev.anchem.111808.073702 (2010).

168 Laskin, J. & Lanekoff, I. Ambient mass spectrometry imaging using direct liquid extraction techniques. *Anal. Chem.* **88**, 52-73, doi:10.1021/acs.analchem.5b04188 (2016).

169 Venter, A., Sojka, P. E. & Cooks, R. G. Droplet dynamics and ionization mechanisms in desorption electrospray ionization mass spectrometry. *Anal. Chem.* **78**, 8549-8555, doi:10.1021/ac0615807 (2006).

170 Kertesz, V. *et al.* Comparison of drug distribution images from whole-body thin tissue sections obtained using desorption electrospray ionization tandem mass spectrometry and autoradiography. *Anal. Chem.* **80**, 5168-5177, doi:10.1021/ac800546a (2008).

171 Kertesz, V. & Van Berkel, G. J. Scanning and surface alignment considerations in chemical imaging with desorption electrospray mass spectrometry. *Anal. Chem.* **80**, 1027-1032, doi:10.1021/ac701947d (2008).

172 Kertesz, V. & Van Berkel, G. J. Improved imaging resolution in desorption electrospray ionization mass spectrometry. *Rapid Commun. Mass Spectrom.* **22**, 2639-2644, doi:10.1002/rcm.3662 (2008).

173 Reiter, S. M., Buchberger, W. & Klampfl, C. W. Rapid identification and semi-quantitative determination of polymer additives by desorption electrospray ionization/time-of-flight mass spectrometry. *Anal. Bioanal. Chem.* **400**, 2317-2322, doi:10.1007/s00216-010-3989-9 (2010).

174 Bennett, R. V. *et al.* Desorption electrospray ionization imaging mass spectrometry as a tool for investigating model prebiotic reactions on mineral surfaces. *Anal. Chem.* **85**, 1276-1279, doi:10.1021/ac303202n (2013).

175 Paine, M. R. L., Barker, P. J. & Blanksby, S. J. Desorption electrospray ionisation mass spectrometry reveals in situ modification of a hindered amine light stabiliser resulting from direct N-OR bond cleavage. *Analyst* **136**, 904-912, doi:10.1039/c0an00656d (2011).

176 Van Berkel, G. J., Sanchez, A. D. & Quirke, J. M. E. Thin-layer chromatography and electrospray mass spectrometry coupled using a surface sampling probe. *Anal. Chem.* **74**, 6216-6223, doi:10.1021/ac020540+ (2002).

177 Van Berkel, G. J. & Kertesz, V. Automated sampling and imaging of analytes separated on thin-layer chromatography plates using desorption electrospray ionization mass spectrometry. *Anal. Chem.* **78**, 4938-4944, doi:10.1021/ac060690a (2006).

178 Van Berkel, G. J., Kertesz, V., Koeplinger, K. A., Vavrek, M. & Kong, A.-N. T. Liquid microjunction surface sampling probe electrospray mass spectrometry for detection of drugs and metabolites in thin tissue sections. *J. Mass Spectrom.* **43**, 500-508, doi:10.1002/jms.1340 (2008).

179 ElNaggar, M. S., Prideaux, B., Dartois, V. & Wiseman, J. S. Metabolic imaging through continuous in situ micro-extractions of tissue samples via flowprobe mass spectrometry. *Curr. Metabolomics* **2**, 122-131, doi:10.2174/2213235x02666141107220920 (2014).

180 Hsu, C.-C. *et al.* Real-time metabolomics on living microorganisms using ambient electrospray ionization flow-probe. *Anal. Chem.* **85**, 7014-7018, doi:10.1021/ac401613x (2013).

181 Eikel, D. & Henion, J. Liquid extraction surface analysis (LESA) of food surfaces employing chip-based nano-electrospray mass spectrometry. *Rapid Commun. Mass Spectrom.* **25**, 2345-2354, doi:10.1002/rcm.5107 (2011).

182 Paine, M. R. L., Barker, P. J., Maclaughlin, S. A., Mitchell, T. W. & Blanksby, S. J. Direct detection of additives and degradation products from polymers by liquid extraction surface analysis employing chip-based nanospray mass spectrometry. *Rapid Commun. Mass Spectrom.* **26**, 412-418, doi:10.1002/rcm.6116 (2012).

183 Eikel, D. *et al.* Liquid extraction surface analysis mass spectrometry (LESA-MS) as a novel profiling tool for drug distribution and metabolism analysis: the terfenadine example. *Rapid Commun. Mass Spectrom.* **25**, 3587-3596, doi:10.1002/rcm.5274 (2011).

184 Tomlinson, L. *et al.* Using a single, high mass resolution mass spectrometry platform to investigate ion suppression effects observed during tissue imaging. *Rapid Commun. Mass Spectrom.* **28**, 995-1003, doi:10.1002/rcm.6869 (2014).

185 Brown, S. H. J., Huxtable, L. H., Willcox, M. D. P., Blanksby, S. J. & Mitchell, T. W. Automated surface sampling of lipids from worn contact lenses coupled with tandem mass spectrometry. *Analyst* **138**, 1316-1320, doi:10.1039/C2AN36189B (2013).

186 Nemes, P. & Vertes, A. Laser ablation electrospray ionization for atmospheric pressure, in vivo, and imaging mass spectrometry. *Anal. Chem.* **79**, 8098-8106, doi:10.1021/ac071181r (2007).

187 Shiea, J. *et al.* Electrospray-assisted laser desorption/ionization mass spectrometry for direct ambient analysis of solids. *Rapid Commun. Mass Spectrom.* **19**, 3701-3704, doi:10.1002/rcm.2243 (2005).

188 Judge, E. J., Brady, J. J., Dalton, D. & Levis, R. J. Analysis of pharmaceutical compounds from glass, fabric, steel, and wood surfaces at atmospheric pressure using spatially resolved, nonresonant femtosecond laser vaporization electrospray mass spectrometry. *Anal. Chem.* **82**, 3231-3238, doi:10.1021/ac902880q (2010).

189 Nemes, P., Barton, A. A. & Vertes, A. Three-dimensional imaging of metabolites in tissues under ambient conditions by laser ablation electrospray ionization mass spectrometry. *Anal. Chem.* **81**, 6668-6675, doi:10.1021/ac900745e (2009).

190 Lin, S.-Y., Huang, M.-Z., Chang, H.-C. & Shiea, J. Using electrospray-assisted laser desorption/ionization mass spectrometry to characterize organic compounds separated on thin-layer chromatography plates. *Anal. Chem.* **79**, 8789-8795, doi:10.1021/ac070590k (2007).

191 Ovchinnikova, O. S., Lorenz, M., Kertesz, V. & Van Berkel, G. J. Laser ablation sampling of materials directly into the formed liquid microjunction of a continuous flow surface sampling probe/electrospray ionization emitter for mass spectral analysis and imaging. *Anal. Chem.* **85**, 10211-10217, doi:10.1021/ac4018499 (2013).

192 Galhena, A. S., Harris, G. A., Nyadong, L., Murray, K. K. & Fernández, F. M. Small molecule ambient mass spectrometry imaging by infrared laser ablation metastable-induced chemical ionization. *Anal. Chem.* **82**, 2178-2181, doi:10.1021/ac902905v (2010).

193 Shelley, J. T., Ray, S. J. & Hieftje, G. M. Laser ablation coupled to a flowing atmospheric pressure afterglow for ambient mass spectral imaging. *Anal. Chem.* **80**, 8308-8313, doi:10.1021/ac801594u (2008).

194 Liu, Y. *et al.* Imaging mass spectrometry with a low-temperature plasma probe for the analysis of works of art. *Angew. Chem., Int. Ed.* **49**, 4435-4437, doi:10.1002/anie.200906975 (2010).

195 Feng, B. *et al.* Ambient mass spectrometry imaging: plasma assisted laser desorption ionization mass spectrometry imaging and its applications. *Anal. Chem.* **86**, 4164-4169, doi:10.1021/ac403310k (2014).

196 Ovchinnikova, O. S. & Van Berkel, G. J. Thin-layer chromatography and mass spectrometry coupled using proximal probe thermal desorption with electrospray or atmospheric pressure chemical ionization. *Rapid Commun. Mass Spectrom.* **24**, 1721-1729, doi:10.1002/rcm.4551 (2010).

197 Ovchinnikova, O. S., Kertesz, V. & Van Berkel, G. J. Molecular surface sampling and chemical imaging using proximal probe thermal desorption/secondary ionization mass spectrometry. *Anal. Chem.* **83**, 598-603, doi:10.1021/ac102766w (2011).

198 Jesse, S. *et al.* Band excitation in scanning probe microscopy: recognition and functional imaging. *Annu. Rev. Phys. Chem.* **65**, 519-536, doi:10.1146/annurev-physchem-040513-103609 (2014).

199 Ovchinnikova, O. S., Nikiforov, M. P., Bradshaw, J. A., Jesse, S. & Van Berkel, G. J. Combined atomic force microscope-based topographical imaging and nanometer-scale resolved proximal probe thermal desorption/electrospray ionization–mass spectrometry. *ACS Nano* **5**, 5526-5531, doi:10.1021/nn200939e (2011).

200 Ovchinnikova, O. S., Kjoller, K., Hurst, G. B., Pelletier, D. A. & Van Berkel, G. J. Atomic force microscope controlled topographical imaging and proximal probe thermal desorption/ionization mass spectrometry imaging. *Anal. Chem.* **86**, 1083-1090, doi:10.1021/ac4026576 (2014).

201 Ovchinnikova, O. S. *et al.* Co-registered topographical, band excitation nanomechanical, and mass spectral imaging using a combined atomic force microscopy/mass spectrometry platform. *ACS Nano* **9**, 4260-4269, doi:10.1021/acsnano.5b00659 (2015).

202 Altelaar, A. F. M. *et al.* Gold-enhanced biomolecular surface imaging of cells and tissue by SIMS and MALDI mass spectrometry. *Anal. Chem.* **78**, 734-742, doi:10.1021/ac0513111 (2006).

203 Svara, F. N., Kiss, A., Jaskolla, T. W., Karas, M. & Heeren, R. M. A. High-reactivity matrices increase the sensitivity of matrix enhanced secondary ion mass spectrometry. *Anal. Chem.* **83**, 8308-8313, doi:10.1021/ac202222h (2011).

204 Soltwisch, J. *et al.* Mass spectrometry imaging with laser-induced postionization. *Science* **348**, 211, doi:10.1126/science.aaa1051 (2015).

205 Zavalin, A. *et al.* Direct imaging of single cells and tissue at sub-cellular spatial resolution using transmission geometry MALDI MS. *J. Mass Spectrom.* **47**, i-i, doi:10.1002/jms.3132 (2012).

206 Ellis, S. R., Bruinen, A. L. & Heeren, R. M. A critical evaluation of the current state-of-the-art in quantitative imaging mass spectrometry. *Anal. Bioanal. Chem.* **406**, 1275-1289, doi:10.1007/s00216-013-7478-9 (2014).

207 Giesen, C. *et al.* Highly multiplexed imaging of tumor tissues with subcellular resolution by mass cytometry. *Nat. Methods* **11**, 417-422, doi:10.1038/nmeth.2869 (2014).

208 Angelo, M. *et al.* Multiplexed ion beam imaging of human breast tumors. *Nat. Med. (N. Y., NY, U. S.)*, 436-442, doi:10.1038/nm.3488 (2014).

209 Barre, F. P. *et al.* Derivatization strategies for the detection of triamcinolone acetonide in cartilage by using matrix-assisted laser desorption/ionization mass spectrometry imaging. *Anal. Chem.* **88**, 12051-12059, doi:10.1021/acs.analchem.6b02491 (2016).

210 Balluff, B., Hanselmann, M. & Heeren, R. M. Mass spectrometry imaging for the investigation of intratumor heterogeneity. *Adv. Cancer Res.* **134**, 201-230, doi:10.1016/bs.acr.2016.11.008 (2017).

211 Heijs, B. *et al.* Multimodal mass spectrometry imaging of N-Glycans and proteins from the same tissue section. *Anal. Chem.* **88**, 7745-7753, doi:10.1021/acs.analchem.6b01739 (2016).

212 Spraggins, J. M. *et al.* MALDI FTICR IMS of intact proteins: using mass accuracy to link protein images with proteomics data. *J. Am. Soc. Mass Spectrom.* **26**, 974-985, doi:10.1007/s13361-015-1147-5 (2015).

213 Ellis, S. R. *et al.* Automated, parallel mass spectrometry imaging and structural identification of lipids. *Nat. Methods* **15**, 515-518, doi:10.1038/s41592-018-0010-6 (2018).

214 Stoeckli, M., Farmer, T. B. & Caprioli, R. M. Automated mass spectrometry imaging with a matrix-assisted laser desorption ionization time-of-flight instrument. *J. Am. Soc. Mass Spectrom.* **10**, 67-71, doi:10.1016/S1044-0305(98)00126-3 (1999).

215 Spengler, B. & Hubert, M. Scanning microprobe matrix-assisted laser desorption ionization (SMALDI) mass spectrometry: instrumentation for sub-micrometer resolved LDI and MALDI surface analysis. *J. Am. Soc. Mass Spectrom.* **13**, 735-748, doi:10.1016/S1044-0305(02)00376-8 (2002).

216 Dewez, F. *et al.* Precise co-registration of mass spectrometry imaging, histology, and laser microdissection-based omics. *Anal. Bioanal. Chem.* **411**, 5647-5653, doi:10.1007/s00216-019-01983-z (2019).

217 Janfelt, C. in *Mass spectrometry Imaging of Small Molecules* Vol. 1203 *Methods in Molecular Biology* (ed Lin He) 91-97 (Humana Press, 2015).

218 Robichaud, G., Barry, J. A. & Muddiman, D. C. IR-MALDESI mass spectrometry imaging of biological tissue sections using ice as a matrix. *J. Am. Soc. Mass Spectrom.* **25**, 319-328, doi:10.1007/s13361-013-0787-6 (2014).

219 Kiss, A., Smith, D. F., Reschke, B. R., Powell, M. J. & Heeren, R. M. Top-down mass spectrometry imaging of intact proteins by laser ablation ESI FT-ICR MS. *Proteomics* **14**, 1283-1289, doi:10.1002/pmic.201300306 (2014).

220 Bacon, C. W., Hinton, D. M., Mitchell, T. R. & Palencia, E. R. In situ ergot alkaloid detection in three Balansia epichloe-infected grass species. *J. Appl. Microbiol.* **125**, 976-985, doi:10.1111/jam.13941 (2018).

221 Stopka, S. A. *et al.* Metabolic noise and distinct subpopulations observed by single cell LAESI mass spectrometry of plant cells in situ. *Front. Plant Sci.* **9**, 1646, doi:10.3389/fpls.2018.01646 (2018).

222 Barry, J. A. *et al.* Mapping antiretroviral drugs in tissue by IR-MALDESI MSI coupled to the Q Exactive and comparison with LC-MS/MS SRM assay. *J. Am. Soc. Mass Spectrom.* **25**, 2038-2047, doi:10.1007/s13361-014-0884-1 (2014).

223 Bacon, C. W., Hinton, D. M. & Mitchell, T. R. Screening of Bacillus mojavensis biofilms and biosurfactants using laser ablation electrospray ionization mass spectroscopy. *J. Appl. Microbiol.* **125**, 867-875, doi:10.1111/jam.13905 (2018).

224 Stopka, S. A. *et al.* Ambient metabolic profiling and imaging of biological samples with ultrahigh molecular resolution using laser ablation electrospray ionization 21 Tesla FTICR mass spectrometry. *Anal. Chem.* **91**, 5028-5035, doi:10.1021/acs.analchem.8b05084 (2019).

225 Nazari, M. & Muddiman, D. C. Cellular-level mass spectrometry imaging using infrared matrix-assisted laser desorption electrospray ionization (IR-MALDESI) by oversampling. *Anal. Bioanal. Chem.* **407**, 2265-2271, doi:10.1007/s00216-014-8376-5 (2015).

226 Bokhart, M. T. *et al.* IR-MALDESI mass spectrometry imaging at 50 micron spatial resolution. *J. Am. Soc. Mass Spectrom.* **28**, 2099-2007, doi:10.1007/s13361-017-1740-x (2017).

227 Albert, A. & Engelhard, C. Characteristics of low-temperature plasma ionization for ambient mass spectrometry compared to electrospray ionization and atmospheric pressure chemical ionization. *Anal. Chem.* **84**, 10657-10664, doi:10.1021/ac302287x (2012).

228 Imbert, L. *et al.* Comparison of electrospray ionization, atmospheric pressure chemical ionization and atmospheric pressure photoionization for a lipidomic analysis of Leishmania donovani. *J. Chromatogr. A* **1242**, 75-83, doi:10.1016/j.chroma.2012.04.035 (2012).

229 Bartels, B. *et al.* Mapping metabolites from rough terrain: laser ablation electrospray ionization on non-flat samples. *RSC Adv.* **7**, 9045-9050, doi:10.1039/C6RA26854D (2017).

230 Barry, J. A. & Muddiman, D. C. Global optimization of the infrared matrix-assisted laser desorption electrospray ionization (IR MALDESI) source for mass spectrometry using statistical design of experiments. *Rapid Commun. Mass Spectrom.* **25**, 3527-3536, doi:10.1002/rcm.5262 (2011).

231 Cheng, S. C., Jhang, S. S., Huang, M. Z. & Shiea, J. Simultaneous detection of polar and nonpolar compounds by ambient mass spectrometry with a dual electrospray and atmospheric pressure chemical ionization source. *Anal. Chem.* **87**, 1743-1748, doi:10.1021/ac503625m (2015).

232 Ogawa, M., Kadowaki, A., Yamada, T. & Kadooka, O. Applied development of a novel fungicide isotianil (Stout). 1-15 (2011).

233 (EPA), E. P. A. Vol. 84 FR 58623 (ed Environmental Protection Agency (EPA)) 58623-58627 (Federal Register, Washington, DC, US, 2019).

234 Nakanishi, T. M. What you can see by developing real-time radioisotope imaging system for plants: from water to element and CO2 gas imaging. *J. Radioanal. Nucl. Chem.* **318**, 1689-1695, doi:10.1007/s10967-018-6324-0 (2018).

235 Nemes, P., Woods, A. S. & Vertes, A. Simultaneous imaging of small metabolites and lipids in rat brain tissues at atmospheric pressure by laser ablation electrospray ionization mass spectrometry. *Anal. Chem.* **82**, 982-988, doi:10.1021/ac902245p (2010).

236 Fideler, J., Johanningsmeier, S. D., Ekelöf, M. & Muddiman, D. C. Discovery and quantification of bioactive peptides in fermented cucumber by direct analysis IR-MALDESI mass spectrometry and LC-QQQ-MS. *Food Chem.* **271**, 715-723, doi:10.1016/j.foodchem.2018.07.187 (2019).

237 Eijkel, G. B. *et al.* Correlating MALDI and SIMS imaging mass spectrometric datasets of biological tissue surfaces. *Surf. Interface Anal.* **41**, 675-685, doi:10.1002/sia.3088 (2009).

238 Nuñez, J. R., Anderton, C. R. & Renslow, R. S. Optimizing colormaps with consideration for color vision deficiency to enable accurate interpretation of scientific data. *PLoS One* **13**, e0199239, doi:10.1371/journal.pone.0199239 (2018).

239 Stolee, J. A. & Vertes, A. Toward single-cell analysis by plume collimation in laser ablation electrospray ionization mass spectrometry. *Anal. Chem.* **85**, 3592-3598, doi:10.1021/ac303347n (2013).

240 Vaikkinen, A. *et al.* Simultaneous detection of nonpolar and polar compounds by heat-assisted laser ablation electrospray ionization mass spectrometry. *Anal. Chem.* **85**, 177-184, doi:10.1021/ac302432h (2013).

241 Carrari, F. *et al.* Integrated analysis of metabolite and transcript levels reveals the metabolic shifts that underlie tomato fruit development and highlight regulatory aspects of metabolic network behavior. *Plant Physiol.* **142**, 1380-1396, doi:10.1104/pp.106.088534 (2006).

242 Watrous, J. D. *et al.* Microbial metabolic exchange in 3D. *ISME J.* **7**, 770-780, doi:10.1038/ismej.2012.155 (2013).

243 Leney, A. C. & Heck, A. J. R. Native mass spectrometry: what is in the name? *J. Am. Soc. Mass Spectrom.* **28**, 5-13, doi:10.1007/s13361-016-1545-3 (2017).

244 Mehmood, S., Allison, T. M. & Robinson, C. V. Mass spectrometry of protein complexes: from origins to applications. *Annu. Rev. Phys. Chem.* **66**, 453-474, doi:10.1146/annurev-physchem-040214-121732 (2015).

245 Zhou, M. *et al.* Mass spectrometry of intact V-Type ATPases reveals bound lipids and the effects of nucleotide binding. *Science* **334**, 380-385, doi:10.1126/science.1210148 (2011).

246 Gold, M. G. *et al.* Architecture and dynamics of an A-kinase anchoring protein 79 (AKAP79) signaling complex. *Proc. Natl. Acad. Sci. U. S. A.* **108**, 6426-6431, doi:10.1073/pnas.1014400108 (2011).

247 von Kügelgen, A. *et al.* In situ structure of an intact lipopolysaccharide-bound bacterial surface layer. *Cell* **180**, 348-358.e315, doi:10.1016/j.cell.2019.12.006 (2020).

248 Bolla, J. R., Agasid, M. T., Mehmood, S. & Robinson, C. V. Membrane protein–lipid interactions probed using mass spectrometry. *Annu. Rev. Biochem.* **88**, 85-111, doi:10.1146/annurev-biochem-013118-111508 (2019).

249 Snijder, J., Rose, R. J., Veesler, D., Johnson, J. E. & Heck, A. J. R. Studying 18 MDa virus assemblies with native mass spectrometry. *Angew. Chem., Int. Ed.* **52**, 4020-4023, doi:10.1002/anie.201210197 (2013).

250 Renaud, J.-P. *et al.* Biophysics in drug discovery: impact, challenges and opportunities. *Nat. Rev. Drug Discov.* **15**, 679, doi:10.1038/nrd.2016.123 (2016).

251 Lin, S. *et al.* Mapping the dark space of chemical reactions with extended nanomole synthesis and MALDI-TOF MS. *Science* **361**, eaar6236, doi:10.1126/science.aar6236 (2018).

252 Lemaire, R. *et al.* Direct analysis and MALDI imaging of formalin-fixed, paraffin-embedded tissue sections. *J. Proteome Res.* **6**, 1295–1305, doi:10.1021/pr060549i (2007).

253 Horneffer, V., Strupat, K. & Hillenkamp, F. Localization of noncovalent complexes in MALDI-preparations by CLSM. *J. Am. Soc. Mass Spectrom.* **17**, 1599-1604, doi:10.1016/j.jasms.2006.06.028 (2006).

254 Beaufour, M., Ginguené, D., Le Meur, R., Castaing, B. & Cadene, M. Liquid native MALDI mass spectrometry for the detection of protein-protein complexes. *J. Am. Soc. Mass Spectrom.* **29**, 1981-1994, doi:10.1007/s13361-018-2015-x (2018).

255 Song, F. A study of noncovalent protein complexes by matrix-assisted laser desorption/ionization. *J. Am. Soc. Mass Spectrom.* **18**, 1286-1290, doi:10.1016/j.jasms.2007.03.026 (2007).

256 Rosinke, B. *et al.* Matrix-assisted laser desorption/ionization mass spectrometry (MALDI-MS) of membrane proteins and non-covalent complexes. *J. Mass Spectrom.* **30**, 1462-1468, doi:10.1002/jms.1190301012 (1995).

257 Trimpin, S., Inutan, E. D., Herath, T. N. & McEwen, C. N. Laserspray ionization, a new atmospheric pressure MALDI method for producing highly charged gas-phase ions of peptides and proteins directly from solid solutions. *Mol. Cell. Proteomics* **9**, 362-367, doi:10.1074/mcp.M900527-MCP200 (2010).

258 Peetz, O. *et al.* LILBID and nESI: different native mass spectrometry techniques as tools in structural biology. *J. Am. Soc. Mass Spectrom.* **30**, 181-191, doi:10.1007/s13361-018-2061-4 (2019).

259 Ambrose, S. *et al.* Native desorption electrospray ionization liberates soluble and membrane protein complexes from surfaces. *Angew. Chem.* **129**, 14655-14660, doi:10.1002/anie.201704849 (2017).

260 Griffiths, R. L. *et al.* Native mass spectrometry imaging of intact proteins and protein complexes in thin tissue sections. *Int. J. Mass Spectrom.* **437**, 23-29, doi:10.1016/j.ijms.2017.10.009 (2019).

261 Shiea, J. *et al.* Detection of native protein ions in aqueous solution under ambient conditions by electrospray laser desorption/ionization mass spectrometry. *Anal. Chem.* **80**, 4845-4852, doi:10.1021/ac702108t (2008).

262 Cho, Y. T. *et al.* Using electrospray laser desorption ionization mass spectrometry to rapidly examine the integrity of proteins stored in various solutions. *Anal. Bioanal. Chem.* **406**, 577-586, doi:10.1007/s00216-013-7491-z (2014).

263 Judge, E. J., Brady, J. J. & Levis, R. J. Mass analysis of biological macromolecules at atmospheric pressure using nonresonant femtosecond laser vaporization and electrospray ionization. *Anal. Chem.* **82**, 10203-10207, doi:10.1021/ac102409k (2010).

264 van de Waterbeemd, M. *et al.* High-fidelity mass analysis unveils heterogeneity in intact ribosomal particles. *Nat. Methods* **14**, 283-286, doi:10.1038/nmeth.4147 (2017).

265 Lössl, P., Snijder, J. & Heck, A. J. R. Boundaries of mass resolution in native mass spectrometry. *J. Am. Soc. Mass Spectrom.* **25**, 906-917, doi:10.1007/s13361-014-0874-3 (2014).

266 Konermann, L., Rodriguez, A. D. & Liu, J. On the formation of highly charged gaseous ions from unfolded proteins by electrospray ionization. *Anal. Chem.* **84**, 6798-6804, doi:10.1021/ac301298g (2012).

267 Perutz, M. F. & Lehmann, H. Molecular pathology of human haemoglobin. *Nature* **219**, 902-909, doi:10.1038/219902a0 (1968).

268 Uetrecht, C., Rose, R. J., van Duijn, E., Lorenzen, K. & Heck, A. J. Ion mobility mass spectrometry of proteins and protein assemblies. *Chem. Soc. Rev.* **39**, 1633-1655, doi:10.1039/b914002f (2010).

269 Breuker, K. & McLafferty, F. W. The thermal unfolding of native cytochrome C in the transition from solution to gas phase probed by native electron capture dissociation. *Angew. Chem., Int. Ed.* **44**, 4911-4914, doi:10.1002/anie.200500668 (2005).

270 Nemes, P., Huang, H. & Vertes, A. Internal energy deposition and ion fragmentation in atmospheric-pressure mid-infrared laser ablation electrospray ionization. *Phys. Chem. Chem. Phys.* **14**, 2501-2507, doi:10.1039/c2cp23411d (2012).

271 Marty, M. T. *et al.* Bayesian deconvolution of mass and ion mobility spectra: from binary interactions to polydisperse ensembles. *Anal. Chem.* **87**, 4370-4376, doi:10.1021/acs.analchem.5b00140 (2015).

272 Monge, M. E., Harris, G. A., Dwivedi, P. & Fernandez, F. M. Mass spectrometry: recent advances in direct open air surface sampling/ionization. *Chem. Rev.* **113**, 2269-2308, doi:10.1021/cr300309q (2013).

273 Morelato, M., Beavis, A., Kirkbride, P. & Roux, C. Forensic applications of desorption electrospray ionisation mass spectrometry (DESI-MS). *Forensic Sci. Int.* **226**, 10-21, doi:10.1016/j.forsciint.2013.01.011 (2013).

274 Green, F. M., Salter, T. L., Stokes, P., Gilmore, I. S. & O'Connor, G. Ambient mass spectrometry: advances and applications in forensics. *Surf. Interface Anal.* **42**, 347-357, doi:10.1002/sia.3131 (2010).

275 Takats, Z., Cotte-Rodriguez, I., Talaty, N., Chen, H. & Cooks, R. G. Direct, trace level detection of explosives on ambient surfaces by desorption electrospray ionization mass spectrometry. *Chem. Commun. (Cambridge, U. K.)* **0**, 1950-1952, doi:10.1039/B418697D (2005).

276 Talaty, N. *et al.* Fabric analysis by ambient mass spectrometry for explosives and drugs. *Analyst* **133**, 1532-1540, doi:10.1039/b807934j (2008).

277 Cajka, T., Riddellova, K., Tomaniova, M. & Hajslova, J. Ambient mass spectrometry employing a DART ion source for metabolomic fingerprinting/profiling: a powerful tool for beer origin recognition. *Metabolomics* **7**, 500-508, doi:10.1007/s11306-010-0266-z (2011).

278 García-Reyes, J. F., Jackson, A. U., Molina-Díaz, A. & Cooks, R. G. Desorption electrospray ionization mass spectrometry for trace analysis of agrochemicals in food. *Anal. Chem.* **81**, 820-829, doi:10.1021/ac802166v (2008).

279 Angel, P. M., Spraggins, J. M., Baldwin, H. S. & Caprioli, R. Enhanced sensitivity for high spatial resolution lipid analysis by negative ion mode matrix assisted laser desorption ionization imaging mass spectrometry. *Anal. Chem.* **84**, 1557-1564, doi:10.1021/ac202383m (2012).

280 Wang, H. Y., Liu, C. B. & Wu, H. W. A simple desalting method for direct MALDI mass spectrometry profiling of tissue lipids. *J. Lipid Res.* **52**, 840-849, doi:10.1194/jlr.D013060 (2011).

281 Dilillo, M. *et al.* Ultra-high mass resolution MALDI imaging mass spectrometry of proteins and metabolites in a mouse model of glioblastoma. *Sci. Rep.* **7**, 603, doi:10.1038/s41598-017-00703-w (2017).

282 Cornett, D. S., Frappier, S. L. & Caprioli, R. M. MALDI-FTICR imaging mass spectrometry of drugs and metabolites in tissue. *Anal. Chem.* **80**, 5648-5653, doi:10.1021/ac800617s (2008).

283 Doria, M. L. *et al.* Epithelial ovarian carcinoma diagnosis by desorption electrospray ionization mass spectrometry imaging. *Sci. Rep.* **6**, 39219, doi:10.1038/srep39219 (2016).

284 Manicke, N. E., Dill, A. L., Ifa, D. R. & Cooks, R. G. High resolution tissue imaging on an orbitrap mass spectrometer by desorption electro-spray ionization mass spectrometry. *J. Mass Spectrom.* **45**, 223-226, doi:10.1002/jms.1707 (2010).

285 Pol, J. *et al.* Automated ambient desorption–ionization platform for surface imaging integrated with a commercial Fourier transform ion cyclotron resonance mass spectrometer. *Anal. Chem.* **81**, 8479-8487, doi:10.1021/ac901368q (2009).

286 Takats, Z., Wiseman, J. M., Gologan, B. & Cooks, R. G. Mass spectrometry sampling under ambient conditions with desorption electrospray ionization. *Science* **306**, 471-473, doi:10.1126/science.1104404 (2004).

287 Robichaud, G., Barry, J. A., Garrard, K. P. & Muddiman, D. C. Infrared matrix-assisted laser desorption electrospray ionization (IR-MALDESI) imaging source coupled to a FT-ICR mass spectrometer. *J. Am. Soc. Mass Spectrom.* **24**, 92-100, doi:10.1007/s13361-012-0505-9 (2013).

288 Cochran, K. H., Barry, J. A., Robichaud, G. & Muddiman, D. C. Analysis of trace fibers by IR-MALDESI imaging coupled with high resolving power MS. *Anal. Bioanal. Chem.* **407**, 813-820, doi:10.1007/s00216-014-8042-y (2015).

289 Arts, M. *et al.* Detection of localized hepatocellular amino acid kinetics by using mass spectrometry imaging of stable isotopes. *Angew. Chem., Int. Ed.* **56**, 7146-7150, doi:10.1002/anie.201702669 (2017).

290 Almeida, R., Pauling, J. K., Sokol, E., Hannibal-Bach, H. K. & Ejsing, C. S. Comprehensive lipidome analysis by shotgun lipidomics on a hybrid quadrupole-orbitrap-linear ion trap mass spectrometer. *J. Am. Soc. Mass Spectrom.* **26**, 133-148, doi:10.1007/s13361-014-1013-x (2015).

291 Schuhmann, K. *et al.* Monitoring membrane lipidome turnover by metabolic 15N labeling and shotgun ultra-high-resolution orbitrap fourier transform mass spectrometry. *Anal. Chem.* **89**, 12857-12865, doi:10.1021/acs.analchem.7b03437 (2017).

292 Douglass, K. A., Ifa, D. R. & Venter, A. R. in *Pharmaco-Imaging in Drug and Biologics Development AAPS Advances in the Pharmaceutical Sciences Series* 327-353 (Springer, New York, NY, 2014).

293 Gorshkov, M. V., Pasa-Tolic, L., Bruce, J. E., Anderson, G. A. & Smith, R. D. A dual-trap design and its applications in electrospray ionization FTICR mass spectrometry. *Anal. Chem.* **69**, 1307-1314, doi:10.1021/ac960941n (1997).

294 Park, S. G., Anderson, G. A., Navare, A. T. & Bruce, J. E. Parallel spectral acquisition with an ion cyclotron resonance cell array. *Anal. Chem.* **88**, 1162-1168, doi:10.1021/acs.analchem.5b02987 (2015).

295 Senko, M. W., Hendrickson, C. L., Emmett, M. R., Shi, S. D. H. & Marshall, A. G. External accumulation of ions for enhanced electrospray ionization Fourier transform ion cyclotron resonance mass spectrometry. *J. Am. Soc. Mass Spectrom.* **8**, 970-976, doi:10.1016/s1044-0305(97)00126-8 (1997).

296 Blakney, G. T., Hendrickson, C. L. & Marshall, A. G. Predator data station: a fast data acquisition system for advanced FT-ICR MS experiments. *Int. J. Mass Spectrom.* **306**, 246-252, doi:10.1016/j.ijms.2011.03.009 (2011).

297 Kaiser, N. K., Quinn, J. P., Blakney, G. T., Hendrickson, C. L. & Marshall, A. G. A novel 9.4 tesla FTICR mass spectrometer with improved sensitivity, mass resolution, and mass range. *J. Am. Soc. Mass Spectrom.* **22**, 1343-1351, doi:10.1007/s13361-011-0141-9 (2011).

298 Ridgeway, M. E., Lubeck, M., Jordens, J., Mann, M. & Park, M. A. Trapped ion mobility spectrometry: A short review. *Int. J. Mass Spectrom.* **425**, 22-35, doi:10.1016/j.ijms.2018.01.006 (2018).

299 Kozhinov, A. N., Tsybin, Y. O. & Nagornov, K. O. Data acquisition apparatus and methods for mass spectrometry. International patent WO2017168389A1 (2016).

300 Hendrickson, C. L. *et al.* 21 Tesla Fourier transform ion cyclotron resonance mass spectrometer: a national resource for ultrahigh resolution mass analysis. *J. Am. Soc. Mass Spectrom.* **26**, 1626-1632, doi:10.1007/s13361-015-1182-2 (2015).

301 Nagornov, K. O., Gorshkov, M. V., Kozhinov, A. N. & Tsybin, Y. O. High-resolution Fourier transform ion cyclotron resonance mass spectrometry with increased throughput for biomolecular analysis. *Anal. Chem.* **86**, 9020-9028, doi:10.1021/ac501579h (2014).

302 Shaw, J. B., Gorshkov, M. V., Wu, Q. & Pasa-Tolic, L. High speed intact protein characterization using 4X frequency multiplication, ion trap harmonization, and 21 Tesla FTICR-MS. *Anal. Chem.* **90**, 5557-5562, doi:10.1021/acs.analchem.7b04606 (2018).

303 Comisarow, M. B. & Marshall, A. G. Selective-phase ion cyclotron resonance spectroscopy. *Can. J. Chem.* **52**, 1997-1999, doi:10.1139/v74-288 (1974).

304 Comisarow, M. B. Comprehensive theory for ion cyclotron resonance power absorption: application to line shapes for reactive and nonreactive ions. *J. Chem. Phys.* **55**, 205-217, doi:10.1063/1.1675510 (1971).

305 Marshall, A. G. Theory for ion cyclotron resonance absorption line shapes. *J. Chem. Phys.* **55**, 1343-1354, doi:10.1063/1.1676226 (1971).

306 Qi, Y. *et al.* Absorption-mode: the next generation of Fourier transform mass spectra. *Anal. Chem.* **84**, 2923-2929, doi:10.1021/ac3000122 (2012).

307 Qi, Y., Thompson, C. J., Van Orden, S. L. & O'Connor, P. B. Phase correction of Fourier transform ion cyclotron resonance mass spectra using MATLAB. *J. Am. Soc. Mass Spectrom.* **22**, 138-147, doi:10.1007/s13361-010-0006-7 (2011).

308 Smith, D. F., Kilgour, D. P., Konijnenburg, M., O'Connor, P. B. & Heeren, R. M. Absorption mode FTICR mass spectrometry imaging. *Anal. Chem.* **85**, 11180-11184, doi:10.1021/ac403039t (2013).

309 Smith, D. F. *et al.* Advanced mass calibration and visualization for FT-ICR mass spectrometry imaging. *J. Am. Soc. Mass Spectrom.* **23**, 1865-1872, doi:10.1007/s13361-012-0464-1 (2012).

310 Barry, J. A., Robichaud, G. & Muddiman, D. C. Mass recalibration of FT-ICR mass spectrometry imaging data using the average frequency shift of ambient ions. *J. Am. Soc. Mass Spectrom.* **24**, 1137-1145, doi:10.1007/s13361-013-0659-0 (2013).

311 Savory, J. J. *et al.* Parts-per-billion Fourier transform ion cyclotron resonance mass measurement accuracy with a "walking" calibration equation. *Anal. Chem.* **83**, 1732-1736, doi:10.1021/ac102943z (2011).

312 Wong, R. L. & Amster, I. J. Sub part-per-million mass accuracy by using stepwise-external calibration in fourier transform ion cyclotron resonance mass spectrometry. *J. Am. Soc. Mass Spectrom.* **17**, 1681-1691, doi:10.1016/j.jasms.2006.07.019 (2006).

313 Kozhinov, A. N., Zhurov, K. O. & Tsybin, Y. O. Iterative method for mass spectra recalibration via empirical estimation of the mass calibration function for Fourier transform mass spectrometry-based petroleomics. *Anal. Chem.* **85**, 6437-6445, doi:10.1021/ac400972y (2013).

314 Scigelova, M., Hornshaw, M., Giannakopulos, A. & Makarov, A. Fourier transform mass spectrometry. *Mol. Cell. Proteomics* **10**, M111 009431, doi:10.1074/mcp.M111.009431 (2011).

315 Francl, T. J. *et al.* Experimental determination of the effects of space charge on ion cyclotron resonance frequencies. *Int. J. Mass Spectrom. Ion Processes* **54**, 189-199, doi:10.1016/0168-1176(83)85017-4 (1983).

316 Palmer, A. *et al.* FDR-controlled metabolite annotation for high-resolution imaging mass spectrometry. *Nat. Methods* **14**, 57-60, doi:10.1038/nmeth.4072 (2017).

317 Kooijman, P. C. & Nagornov, K. O. (METASPACE, 2018).

318 Kooijman, P. C. & Nagornov, K. O. (METASPACE, 2018).

319 Hankin, J. A. *et al.* MALDI mass spectrometric imaging of lipids in rat brain injury models. *J. Am. Soc. Mass Spectrom.* **22**, 1014-1021, doi:10.1007/s13361-011-0122-z (2011).

320 Kilgour, D. P., Van Orden, S. L., Tran, B. Q., Goo, Y. A. & Goodlett, D. R. Producing isotopic distribution models for fully apodized absorption mode FT-MS. *Anal. Chem.* **87**, 5797-5801, doi:10.1021/acs.analchem.5b01032 (2015).

321 Koelmel, J. P., Ulmer, C. Z., Jones, C. M., Yost, R. A. & Bowden, J. A. Common cases of improper lipid annotation using high-resolution tandem mass spectrometry data and corresponding limitations in biological interpretation. *Biochim. Biophys. Acta* **1862**, 766-770, doi:10.1016/j.bbalip.2017.02.016 (2017).

322 Garza, K. Y. *et al.* Desorption electrospray ionization mass spectrometry imaging of proteins directly from biological tissue sections. *Anal. Chem.* **90**, 7785-7789, doi:10.1021/acs.analchem.8b00967 (2018).

323 Kilgour, D. P. & Van Orden, S. L. Absorption mode Fourier transform mass spectrometry with no baseline correction using a novel asymmetric apodization function. *Rapid Commun. Mass Spectrom.* **29**, 1009-1018, doi:10.1002/rcm.7190 (2015).

324 Zhurov, K. O., Kozhinov, A. N., Fornelli, L. & Tsybin, Y. O. Distinguishing analyte from noise components in mass spectra of complex samples: where to cut the noise? *Anal. Chem.* **86**, 3308-3316, doi:10.1021/ac403278t (2014).

325 Yan, B. & Bunch, J. Probing folded proteins and intact protein complexes by desorption electrospray ionization mass spectrometry. *J. Am. Soc. Mass Spectrom.* **32**, 690-699, doi:10.1021/jasms.0c00417 (2021).

326 Unsihuay, D. *et al.* Imaging of triglycerides in tissues using nanospray desorption electrospray ionization (Nano-DESI) mass spectrometry. *Int. J. Mass Spectrom.* **448**, 116269, doi:10.1016/j.ijms.2019.116269 (2020).

327 Nagornov, K. O., Kozhinov, A. N., III, F. E. L. & Tsybin, Y. O. in *Proceedings of the 68th ASMS Conference on Mass Spectrometry and Allied Topics.* 305176 (ASMS Reboot 2020).

328 Brown, H. *et al.* Mass spectrometry imaging of diclofenac and its metabolites in tissues using nanospray desorption electrospray ionization. *ChemRxiv*, Medium: X; Size: null; Quantity: null; OS: null; Compatibility: null; Other: null, doi:10.26434/chemrxiv.13194422 (2020).

329 Loo, J. A. Studying noncovalent protein complexes by electrospray ionization mass spectrometry. *Mass Spectrom. Rev.* **16**, 1-23, doi:10.1002/(SICI)1098-2787(1997)16:1<1::AID-MAS1>3.0.CO;2-L (1997).

8.2. PUBLICATIONS CONTAINED IN THIS THESIS

Visualizing molecular distributions for biomaterials applications with mass spectrometry imaging: a review
M.R.L. Paine[¥], Pieter C. Kooijman[¥], G.L. Fisher, R.M.A. Heeren, F. Fernandez and S.R. Ellis
Journal of Materials Chemistry B. **2017** 5 (36): 7444-60

Increased throughput and ultra-high mass resolution in DESI FT-ICR MS imaging through new-generation external data acquisition system and advanced data processing approaches
Pieter C. Kooijman, K.O. Nagornov, A.N. Kozhinov, D.P.A. Kilgour, T.O. Tsybin, R.M.A. Heeren and S.R. Ellis
Scientific Reports **2019** 9 (1): 8

Infrared laser desorption and mass spectrometry analysis of non-covalent protein complexes
Pieter C. Kooijman, A. Mathew, S.R. Ellis and R.M.A. Heeren
Analysis & Sensing **2021**, 1: 44-7

A novel dual ionization modality source for infrared laser ablation post-ionization mass spectrometry imaging to study fungicide metabolism and transport
Pieter C. Kooijman, S. Lamprecht, B. Beine, M. Lamshoeft, B.J.H.T. Verhoeven, S.R. Ellis and R.M.A. Heeren
International Journal of Mass Spectrometry **2021**,465: 116602

[¥]*Shared first authorship*

8.3. PUBLICATIONS NOT PART OF THIS THESIS

On-Line electrochemical reduction of disulfide bonds: improved FTICR-CID and -ETD coverage of oxytocin and hepcidin
S. Nicolardi, M. Giera, Pieter C. Kooijman, A. Kraj, J-P. Chervet, A.M. Deelder and Y.E.M. van der Burgt
Journal of the American Society of Mass Spectrometry **2013** 24 (12): 1980-7

Fluorescence behavior of (selected) flavonols: a combined experimental and computational study
S. Hofener, Pieter C. Kooijman, J. Groen, F. Ariese and L. Visscher
Physical Chemistry Chemical Physics **2013** 15 (30): 12572-81

Independent assessment of matrix-assisted laser desorption/ionization mass spectrometry (MALDI-MS) sample preparation quality: A novel statistical approach for quality scoring
Pieter C. Kooijman, S.J. Kok SJ, J.J.A.M. Weusten and M. Honing
Analytica Chimica Acta **2016** 919: 1-10

Independent assessment of matrix-assisted laser desorption/ionization mass spectrometry (MALDI-MS) sample preparation quality: Effect of sample preparation on MALDI-MS of synthetic polymers
Pieter C. Kooijman, S. Kok and M. Honing
Rapid Communications in Mass Spectrometry **2017** 31 (4): 362-70

8.4. ACKNOWLEDGEMENTS

Ron, bedankt voor jouw eindeloze barrage aan ideeën, waaruit ik langzaamaan heb geleerd de diamantjes te filteren. Je wist de balans te bewaren tussen het geven van ruimte en het opporren van inactiviteit. Je hebt altijd geleid door voorbeeld, wat op zichzelf weer een voorbeeld voor mij is. We hebben het gehad over jouw curieuze dwaaltocht door de wetenschap en ik zal met veel interesse volgen waar deze tocht eindigt.

Shane, I know I've not been the easiest first PhD to supervise, but I hope it didn't cause any headaches. Your awe-inspiring knowledge and focus were truly motivating and called for me to raise my game. I'm sure you'll do a lot more amazing stuff, now that you're back on home soil.

Lieke, bedankt voor het zijn van de lijm die de groep (en mijzelf) zo vaak bij elkaar heeft gehouden. Ik mis onze koffie en thee pauzes. Thank you Tiffany, for the cleansing talks and good food we shared. Bedankt Brenda, omdat je mij dwong altijd mijn niveau op peil te houden, zowel op de fiets als in het lab.

Bedankt Frans, omdat je er altijd was, voor al het gemopper en gegrap. De trots die jij in jouw fabricage legt is nog steeds een bron van inspiratie. Bedankt Gert, voor alle vruchtbare discussies en alle trucjes die je mij geleerd hebt. Bedankt Anne, voor het vormen van het High Resolution-duo, mijn respect voor jou is niet-aflatend gegroeid over de jaren. En dank jullie alledrie voor de slappe verhalen die een tegenvallende dag altijd weer opfleurden.

Thank you Nina, for always being a friend when I needed one. Thanks to P-Max for always putting a smile on my face, whether you meant to or not. Thanks to Bryn and Jo for being the best office mates I could ask for, brightening my days and introducing me to the finer British traditions. Thank you Anjusha for sitting through the pain of writing with me. And Marty, I'll always remember you.

Lennart, Frederic, Britt, Jian-Hua, Andrew, Florian, Benjamin, Naomi, Beatriz, Berta, Darya, Klara, Livia, Marta, Michele, Maxime, Naomi, Ronny, Sylvia and so many others: merci, grazie, gracias, هزاریش, bedankt, 谢谢 , děkuji vám, thank you for making M4I such a wonderful place to spend my days.

Birte, Marc, Sybille, Maarten and the others at Bayer and DSM, thank you for your willingness to invest your time and effort in novel, different analysis techniques. I learned so much from our conversation and without your challenging research questions this thesis would not be what it is today.

Yuri, Anton and Konstantin, thank you for a wonderful chapter of this thesis. Just trying to keep up with your amazing work pushed me to increase my understanding of mathematics, physics and programming, which I'll always be grateful.

Fred and Ben, thank you for the valuable discussions on LAESI. Despite the physical and organisational distance between us, I felt us three formed the "European LAESI-development center".

Vincent, dankzij jouw miraculeuze timing hebben wij samen prachtige dingen beleefd in Maastricht. Je hebt me uit dat hopeloze studentkamertje gesleept en een echt thuis gegeven om na een lange dag (of nacht) werken naar terug te keren. Jouw eeuwige AVGtjes en die belachelijke kop-over-kop trainingen door het heuvelland hebben dit hoofdstuk van mijn leven extra memorabel gemaakt. Jouw niveau van werkdiscipline is de lat die ik nog steeds nastreef.

Bedankt Thomas, Tom, Job, Bas, Niek, Remco, Sarissa, Thara en alle andere leden van de Ferro Mosae triathlonvereniging voor de mooie momenten op de fiets en in het water. Dankzij jullie verlaat ik Maastricht met - naast dit proefschrift - iets onbetaalbaars: een hobby voor het leven.

Pap, mam, Mark en Robert, bedankt voor de steun. Ik weet dat jullie nog steeds niet echt snappen wat ik in Maastricht gedaan heb - of waarom - maar jullie hebben mij altijd met de voeten op de grond gehouden. Jullie hebben mij geleerd alles in perspectief te zien en op waarde te schatten.

En boven alles: dankjewel Anna. Zonder jou had ik het nooit volgehouden. Of het nu gaat om m'n scriptie, proefschrift, Afrika droom of gewoon mijn persoon: vanwege jou wil ik altijd mijn beste zelf zijn. Dank daarvoor.

8.5. CURRICULUM VITAE

Petrus (Pieter) Christian Kooijman was born on September 1st 1989 in Woerden (the Netherlands). In June 2007 he completed secondary school at the Alkwin Kollege in Uithoorn with a VWO-degree in the Nature and Health track. He obtained a Bachelor's degree in Pharmaceutical Sciences from the Vrije Universiteit in Amsterdam in 2013. During his Bachelor's he contributed to a fluorescence spectrometry project of the Laser Lab at the Vrije Universiteit. His Bachelor's internship took him to the Leiden University Medical Center, where he analysed peptides via electrochemistry and mass spectrometry in the Center for Proteomics and Metabolomics.

He obtained his Master's degree in Chemistry (Analytical Sciences track) at the Vrije Universiteit in November 2015. The Master's programme included a 10-month corporate internship at DSM Resolve (Geleen, the Netherlands), where he developed an automated optimization method for MALDI-MS sample preparation of synthetic polymers based on MSI. Alongside his Master's, Pieter participated in the TI-COAST MSc+ honours programme, which extends the range of subjects covered by analytical chemistry Master programmes (incl. advanced chemometrics, separation techniques and clinical applications), and provides access to an extensive corporate network.

Pieter started his PhD research in the M4I institute at Maastricht University under the supervision of Prof. dr. Ron Heeren and dr. Shane Ellis in 2015. Here, he helped the recently relocated research group to set up, and developed the research described in this thesis. Parts of this research he presented at national (NVMS, CHAINS, FAST, TAC) and international conferences (OurCon, EMIM, ASMS). In 2017, he chaired the organising committee for the international mass spectrometry imaging conference OurCon V in Doorn, the Netherlands.

In January 2021 Pieter started as researcher in the HFML-FELIX Laboratory at Radboud University in Nijmegen working with infrared ion spectroscopy technology to structurally identify disease-related metabolites in collaboration with the RadboudUMC.


8